Serotonin Transporter Ligands: CoMFA and CoMSIA Studies for the Prediction of New PET Radiotracers

Serotonin-Transporter-Liganden: CoMFA und CoMSIA Studien zur Vorhersage neuer PET-Radiotracer

DISSERTATION

der Fakultät für Chemie und Pharmazie der
Eberhard-Karls-Universität Tübingen

zu Erlangung des Grades eines Doktors
der Naturwissenschaften

2002

vorgelegt von
Julia Wellsow

Tag der mündlichen Prüfung:	29. November 2002
Dekan:	Prof. Dr. Hansgeorg Probst
Erster Berichterstatter:	Prof. Dr. Karl-Artur Kovar
Zweiter Berichterstatter:	Prof. Dr. Hans-Jürgen Machulla
Dritter Berichterstatter:	Prof. Dr. Gerd Folkers

Die vorliegende Arbeit wurde unter Leitung von Herrn Prof. Dr. Karl-Artur Kovar in der Zeit von Januar 1999 bis September 2002 am Pharmazeutischen Institut der Eberhard-Karls-Universität Tübingen angefertigt.

The present thesis was carried out under the supervision of Prof. Dr. Karl-Artur Kovar during the time period from January 1999 to September 2002 at the Pharmaceutical Institute of Tübingen University.

I wish to express my gratitude to my supervisor Prof. Dr. Karl-Artur Kovar for providing the opportunity to undertake this work and for guidance. I particularly want to thank him for his constant support one could always rely on, for his most valuable advice and suggestions, and for his cheerful way of looking at things.

I would like to extend my sincere thanks to Prof. Dr. Hans-Jürgen Machulla (PET Center Tübingen) for most helpful discussions and the interest with which he followed the progress of the work.

Special thanks go to all present and former working group colleagues for their constant and reliable willingness to help, for their patience, and for providing the most friendly working atmosphere one can possibly imagine.

I also want to thank everyone from the PET Center Tübingen for their help and the most friendly welcome.

Financial support from the *f*ortüne research programme of the University Hospital of Tübingen (732-0-0) is gratefully acknowledged.

I am indebted to everyone from Tripos GmbH, Munich for much appreciated help.

I would also like to include the invaluable help I received from Silicon Graphics Inc., Munich.

I am most grateful to Kristina Nielsen, Gerd Wagner, and my uncle Derek Wareham for thoroughly proof-reading the manuscript.

I want to thank my parents for their confidence, their consideration, and their support whenever this was needed.

Parts of this work have been published and presented.

Wellsow J, Machulla HJ, Kovar KA. 3D QSAR of Serotonin Transporter Ligands: CoMFA and CoMSIA Studies. Quant Struct-Act Relat 2002. In Print.

Wellsow J, Machulla HJ, Kovar KA. Molecular Modeling of Potential New and Selective PET Radiotracers for the Serotonin Transporter. J Pharm Pharmaceut Sci (www.ualberta.ca/~csps) 5(3):245-257, 2002.

Wellsow J, Machulla HJ, Kovar KA. 3D QSAR of Serotonin Transporter Ligands. Poster presentation at the Third European Workshop in Drug Design, University of Siena, Certosa di Pontignano, Italy, June 17–24, 2001

Wellsow J, Machulla HJ, Kovar KA. Entwicklung eines selektiven Radiotracers für den Serotonintransporter – Eine Molecular Modelling Studie. Poster presentation at the *f*ortüne and AKF Kolloquium, University Hospital of Tübingen, Tübingen, 12 October 2001

Poster presentation at the 14th European Symposium on Quantitative Structure-Activity Relationships, Bournemouth, UK, 8–13 September 2002

Wellsow J, Machulla HJ, Kovar KA. Molecular Modelling Studien an Liganden des Serotonintransporters. Talk at the 11. gemeinsame Herbsttagung der Universitätsklinik für Psychiatrie und der Neurologischen Universitätsklinik in Kooperation mit dem Geriatrischen Zentrum am Universitätsklinikum, Tübingen, 9-10 November 2001

Wellsow J, Machulla HJ, Kovar KA. Entwicklung selektiver Radiotracer für den Serotonintransporter – Eine Molecular Modelling Studie. Talk at the 40. Jahrestagung der Deutschen Gesellschaft für Nuklearmedizin, Freiburg, 10–13 April 2002, Nuklearmedizin als Paradigma molekularer Bildgebung, Brink I et al. (Eds), Berlin: Blackwell, 2002 (Abstractband der Jahrestagung der DGN; 40), pp. 16–17

Contents

Abbreviations

3D QSAR	Three-Dimensional Quantitative Structure-Activity Relationship
5-HT_{1A}-receptor	$Serotonin_{1A}$ receptor
5-HT_{2A}-receptor	$Serotonin_{2A}$ receptor
CoMFA	Comparative Molecular Field Analysis
CoMSIA	Comparative Molecular Similarity Indices Analysis
DAT	Dopamine Transporter
F	F-value: ratio of explained to unexplained variance
GA	Genetic Algorithm
GASP	Genetic Algorithm Similarity Program
K_i	Equilibrium inhibition constant
LOO	Leave One Out
NET	Norepinephrine (= Noradrenaline) Transporter
N_{PC}	Number of Principle Components
PC	Principle Component
PET	Positron Emission Tomography
$pK_{i\ exp.}$	Negative logarithm of the experimental equilibrium inhibition constant
$pK_{i\ fit}$	Negative logarithm of the fitted equilibrium inhibition constant
$pK_{i\ pred.}$	Negative logarithm of the predicted equilibrium inhibition constant
PLS	Partial Least Squares
PRESS	Predictive Residual Sum of Squares
q^2	Squared cross-validated correlation coefficient
QSAR	Quantitative Structure-Activity Relationship
r^2	Squared non cross-validated correlation coefficient
RF	Region Focusing
SAR	Structure-Activity Relationship
SE	Standard Error of Estimate
SERT	Serotonin Transporter
SPECT	Single Photon Emission Computerized Tomography
s_{PRESS}	Standard Error of Prediction

SSRI	Selective Serotonin Reuptake Inhibitor
TCA	Tricyclic Antidepressant
DASB	3-Amino-4-[(2-dimethylaminomethyl)-phenylsulfanyl]-benzonitrile
DAPP	N,N-Dimethyl-2-(2-amino-4-methoxyphenylsulfanyl)-benzylamine
ADAM	N,N-Dimethyl-2-(2-amino-4-iodophenylsulfanyl)-benzylamine
MADAM	N,N-Dimethyl-2-(2-amino-4-methylphenylsulfanyl)-benzylamine
MDMA	N-Methyl-3,4-methylenedioxyamphetamine
IDAM	5-Iodo-2-[(2-(dimethylaminomethyl)-phenylsulfanyl]-benzylalcohol
(+)McN5652	*trans*-1,2,3,5,6,10b-Hexahydro-6-(4-methylsulfanyl--phenyl)-pyrrolo[2,1-a]isoquinoline

Abstract

Imaging the serotonin transporter (SERT) with Positron Emission Tomography (PET) provides a useful tool for understanding alterations of the serotonergic system. These alterations are associated with many psychiatric disorders. However, no optimal PET radiotracer for the SERT yet exists as particular demands are made on PET ligands. Both a high binding affinity at the target site and a high selectivity are required, as well as suitable PET kinetics and a straightforward synthetic access.

The purpose of this work was the investigation of quantitative structure-activity relationships (QSAR) of SERT ligands. Distinctive features for high binding affinity at the SERT and at the structurally similar norepinephrine transporter (NET) were to be elucidated. The work was concluded with the design of potential new PET radiotracers for the SERT. Possibilities for radiolabelling were to be considered.

A heterogeneous data set of 19 selective and non-selective SERT ligands was used. Affinity data for both the SERT and the NET was available. As a necessary prerequisite for 3D QSAR studies a reasonable alignment of the compounds was developed using GASP. This was based on an existing pharmacophore model. In addition to the widely used CoMFA method, the CoMSIA method, considered to be an extension of the former, was applied. This permitted the comparison of both methods. Statistically reliable CoMFA models for both the SERT (q^2 = 0.538) and the NET (q^2 = 0.445) were developed, further improving the internal predictability by applying region focusing for the SERT (q^2 = 0.674). The CoMSIA models yielded comparable cross-validated correlation coefficients of q^2 = 0.531 for the SERT, and q^2 = 0.502 for the NET. q^2-Values of above 0.3 to 0.5 are considered to be significant in CoMFA and CoMSIA models. Thus, fully satisfying results were obtained. Certain structural features that are distinctive of each transporter and important for high binding affinity were identified. As highly comparable contour maps were obtained from CoMFA and CoMSIA both methods seem to be equally well suited. Therefore both methods were applied for a selectivity analysis, allowing a clear discrimination between selectivity features for the SERT and for the NET.

The resulting 3D QSAR models provide important information for lead optimisation with respect to selectivity enhancement and offer the opportunity to predict the binding affinity of new substances at both the SERT and the NET. Based on the fact that diphenyl sulphide derivatives such as [^{11}C]DASB have recently proven to be promising PET ligands a rational modification of their N,N-dimethyl-2-phenylsulfanyl-benzylamine scaffold has been performed. A series of 100 compounds were suggested. The novel compounds were predicted to be selective high affinity SERT ligands.

Important new ideas are the introduction of a fluoroethyl-oxycarbonyl group (ester) and a fluoroethyl-carbonyl group (ketone), as well as a formyl group (aldehyde) and the corresponding oxime and imine. Another innovative suggestion is the replacement of the sulphur bridge with a cyanamide group and a fluoroethyl-amino group. The suggested compounds are possessing features providing new possibilities for carbon-11 or fluorine-18 labelling. Synthesis, biological testing, and screening for PET suitability are reasonable further steps.

Zusammenfassung

Veränderungen im serotonergen System stehen im Zusammenhang mit verschiedenen psychischen Erkrankungen. Diese Veränderungen können über eine Visualisierung des Serotonintransporters (SERT) mittels Positronen-Emissions-Tomographie (PET) nachvollzogen werden. Bisher fehlt es jedoch an geeigneten PET-Radiotracern für den SERT, da solche PET-Tracer spezielle Anforderungen erfüllen müssen. Hierzu gehören, neben einer hohen Bindungsaffinität an der Zielstruktur und einer hohen Selektivität, eine geeignete PET-Kinetik und eine unproblematische synthetische Zugänglichkeit.

Das Ziel der vorliegenden Arbeit war eine quantitative Untersuchung der Struktur-Wirkungsbeziehungen (QSAR) von Serotonintransporterliganden. Dabei sollte eine klare Abgrenzung zwischen Struktur-Wirkungsbeziehungen am SERT und Struktur-Wirkungsbeziehungen am strukturell ähnlichen Noradrenalintransporter (NET) erzielt werden. Im Anschluss stand das Design neuer potentieller PET-Liganden für den SERT unter Berücksichtigung der Möglichkeit zur Tracermarkierung.

Es wurde mit einem heterogenen Datensatz bestehend aus 19 selektiven und nicht-selektiven Serotonintransporter-Liganden gearbeitet, für die Bindungsdaten sowohl für den SERT als auch für den NET vorlagen. Grundvoraussetzung einer 3D QSAR Studie ist ein geeignetes Alignment der Substanzen. Dieses basierte für die vorliegende Arbeit auf einem existierenden Pharmakophormodell aus der Literatur. Zur Überlagerung der Substanzen wurde GASP herangezogen. Für die 3D QSAR Studien wurde neben der etablierten CoMFA Methodik die aus letzterer entwickelte CoMSIA Methodik eingesetzt. Dies sollte einen Vergleich der beiden Methoden ermöglichen. Bei CoMFA und CoMSIA spricht man von statistisch signifikanten Modellen bei einem kreuzvaldidierten Korrelationskoeffizienten q^2 oberhalb von 0,3 bis 0,5. Zunächst konnten valide und statistisch signifikante CoMFA Modelle für den SERT (q^2 = 0,538) und den NET (q^2 = 0,445) erstellt werden. Das SERT Modell konnte mittels Region Focusing weiter verbessert werden (q^2 = 0,674). Die erarbeiteten CoMSIA Modelle zeigen vergleichbare kreuzvalidierte Korrelationskoeffizienten mit q^2 = 0,531 für den SERT und q^2 = 0,502 für den NET. Sie beschreiben in ähnlicher Weise wie die entsprechenden CoMFA Modelle die molekularen Voraussetzungen für eine Bindung an den SERT und an den NET. Dies zeigt, dass beide Methoden gleichermaßen eingesetzt werden können. Beide Methoden wurden demnach auch für eine Selektivitätsanalyse verwendet, die deutlich die Kriterien für SERT-Selektivität zeigt. Damit wurde das Ziel erreicht, eine klare Abgrenzung der Struktur-Wirkungsbeziehungen zwischen SERT und NET zu schaffen.

Die vorliegenden 3D QSAR Modelle sind eine geeignete Grundlage für die Konzeption neuer selektiver Radiotracer für den SERT und ermöglichen es außerdem, Bindungsaffinitäten neuer Substanzen am SERT und am NET vorherzusagen. Als Ausgangspunkt für Modifikationen wurde das Grundgerüst der N,N-Dimethyl-2-phenylsulfanyl-benzylamine gewählt. Zu ihnen gehört beispielsweise [^{11}C]DASB, das sich kürzlich als vielversprechender, jedoch noch nicht optimaler PET-Ligand für den SERT erwiesen hat und sich gut in die vorliegenden 3D QSAR Modelle einfügen lässt. Dadurch ergibt sich die Möglichkeit einer Leitstrukturoptimierung. 100 neue Strukturen wurden als selektive SERT-Liganden vorgeschlagen. Wichtige neue Strukturvorschläge sind die Einführung einer Fluorethyl-oxycarbonylgruppe (Ester), einer Fluorethyl-carbonylgruppe (Keton) und einer Formylgruppe (Aldehyd), sowie des entsprechenden Oxims und Imins. Ein weiterer innovativer Vorschlag ist der Ersatz der Schwefelbrücke durch eine Cyanamidgruppe oder eine Fluorethylaminogruppe. Hierbei ergeben sich neue Möglichkeiten zur Kohlenstoff-11- und Fluor-18-Markierung. Als weitere Schritte bieten sich die Synthese der Substanzen und ihre biologische Testung an, sowie die Überprüfung auf ihre Eignung als PET-Liganden.

1 Introduction

1.1 Background

The serotonergic neurotransmission plays an important role in the central nervous system. Alterations of serotonin levels are associated with many psychiatric disorders. The serotonin transporter (SERT), located on presynaptic nerve endings, modulates synaptic serotonin levels and also functions as the primary target site for many antidepressant drugs. Moreover drugs of misuse, such as **MDMA** (N-methyl-3,4-methylenedioxyamphetamine, “ecstasy”) and to some extent cocaine, are known to exert their effect via the serotonin reuptake site. For these reasons, *in vivo* mapping of the SERT in the living human brain by positron emission tomography (PET) is most valuable for understanding alterations of the serotonergic system, and might also prove useful in monitoring antidepressant therapy. However, PET investigations of the SERT have been limited by the small amount of candidate radioligands and their various shortcomings. Consequently there is considerable interest in the development of a suitable PET radioligand for the SERT.

1.2 Positron Emission Tomography (PET)

PET is a molecular imaging technique that uses radiolabelled molecules to image molecular interactions of biological processes *in vivo*. Biochemical processes such as metabolism, and parameters such as receptor densities can be quantified and localised to certain

anatomical structures [1]. Radiotracers are labelled with short-lived positron-emitting radionuclides such as ^{11}C, ^{18}F, ^{15}O, ^{13}N or ^{76}Br. Due to the very high specific radioactivity obtainable by the short-lived radionuclides, minute amounts of radiotracers can be used [1]. These are injected intravenously into experimental animals, human volunteers or patients. A cyclotron is required to generate the radionuclides in close vicinity to the radiochemistry laboratory and the PET camera. This makes the clinical implementation of PET slightly more difficult in comparison with Single Photon Emission Computerized Tomography (SPECT), another molecular imaging technique using short-lived single photon emitting radionuclides such as ^{123}I. However, PET offers several advantages over SPECT. Tracer concentration can be quantitatively measured, PET displays a greater sensitivity and a higher spatial resolution than SPECT, and chemically more diverse radiotracers can be used [1]. Important applications of PET in brain research concern human neuropsychopharmacology and the development of novel drugs to be used in the therapy of neurological and psychiatric disorders.

Necessary requirements for a successful PET radioligand are not only a high binding affinity at the target site, but also a high selectivity, rapid crossing of the blood brain barrier, a high specific-to-nonspecific binding ratio, suitable brain kinetics, and good synthetic availability. PET radioligands are usually labelled with either carbon-11 or fluorine-18. This is preferably done in the last synthetic step. Replacement of carbon-12 with carbon-11 results in compounds which are physiologically indistinguishable from their unlabelled counterparts. Replacement of a hydrogen atom or hydroxy group with fluorine also very often retains or even enhances the biological activity of a molecule [1]. Carbon-11 has got a half-life of 20 min, whereas fluorine-18 has got

a half-life of 110 min. This longer half-life of fluorine-18 can be advantageous when using PET ligands with slow kinetics.

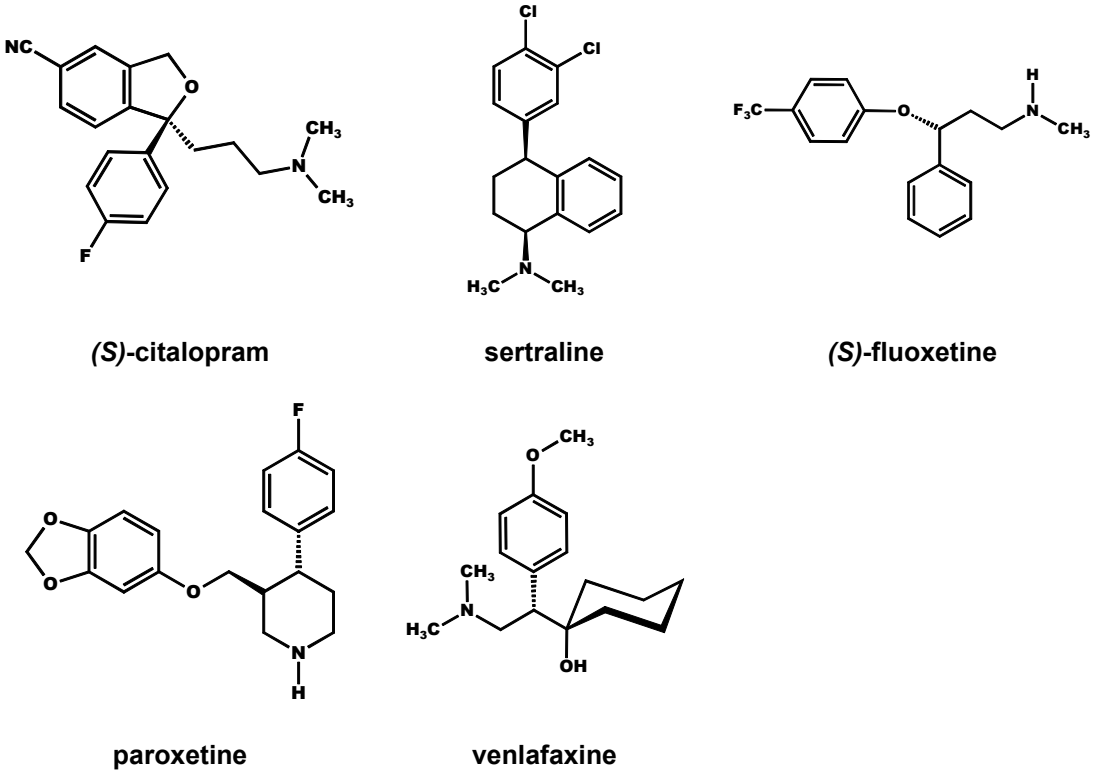

***(S)*-citalopram** **sertraline** ***(S)*-fluoxetine**

paroxetine **venlafaxine**

Figure 1-1: Molecular structures of citalopram, sertraline, fluoxetine, paroxetine and venlafaxine

1.3 PET Radiotracers for the SERT

Several classes of compounds have been screened for their suitability as PET ligands for the SERT. Scheffel et al. [2] give a comprehensive overview of early investigations. Oh et al. [3] and Laakso et al. [4] summarise recent developments. Selective serotonin reuptake inhibitors (SSRIs) such as **citalopram**, **sertraline** and **fluoxetine** have been labelled with carbon-11 but a relatively poor signal-to-noise ratio limited their use *in vivo* for the quantification of the SERT [2, 5-7]. Carbon-11 labelled **venlafaxine** also turned out not to be an ideal PET

ligand [8]. Neither carbon-11 labelling nor fluorine-18 labelling of **paroxetine**, another SSRI with high affinity for the SERT, has been accomplished yet [2].

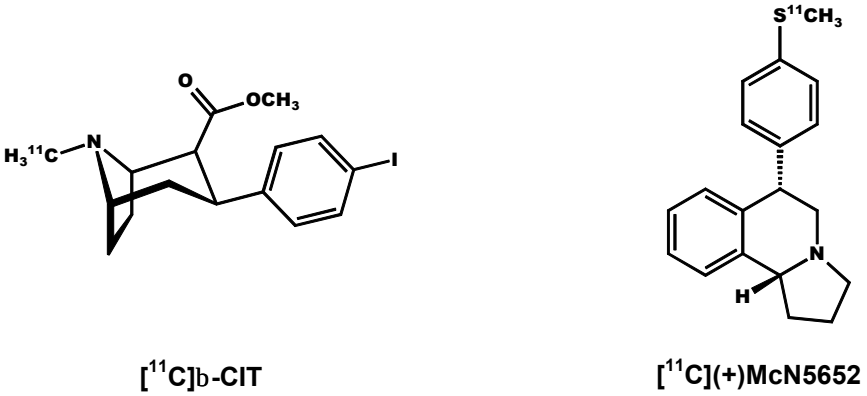

[^{11}C]b-CIT **[^{11}C](+)McN5652**

Figure 1-2: Molecular structures of [^{11}C]β-CIT and [^{11}C](+)McN5652

Many tropane and nortropane analogues have been investigated as PET ligands for the SERT such as **[^{11}C]b-CIT** (2-β-carbomethoxy-3-β-(4-iodophenyl)-tropane) and **[^{11}C]nor-b-CIT** (2-β-carbomethoxy-3-β-(4-iodophenyl)-nortropane [9, 10]. However, one major drawback is their lacking selectivity for the SERT over the dopamine transporter (DAT). Some new derivatives like **ZIENT** (2-β-carbomethoxy-3-β-(4-(*(Z)*-2-iodoethenyl)phenyl)-nortropane) [11] and **FEINT** (2-β-carbomethoxy-3-β-(4-(2-fluoroethyl)-3-iodophenyl)-nortropane) [12] display high specific binding at the SERT and have been proposed as potential PET ligands. The most widely used radiotracer to date for PET imaging of the SERT is **[^{11}C](+)McN5652** (*trans*-1,2,3,5,6,10b-hexahydro-6-(4-methylsulfanyl-phenyl)-pyrrolo[2,1-a]isoquinoline) [13, 14], a potent inhibitor of serotonin reuptake. McCann et al. [15, 16] proved neurotoxic effects of **MDMA** on the serotonergic system in the human brain by using **[^{11}C](+)McN5652** as a radiotracer. However,

[^{11}C](+)McN5652 also displays moderate affinity at the norepinephrine transporter (NET) and at the DAT. The low specific-to-nonspecific binding ratio observed with **[^{11}C](+)McN5652** in humans limits its application as a PET imaging agent *in vivo* [14].

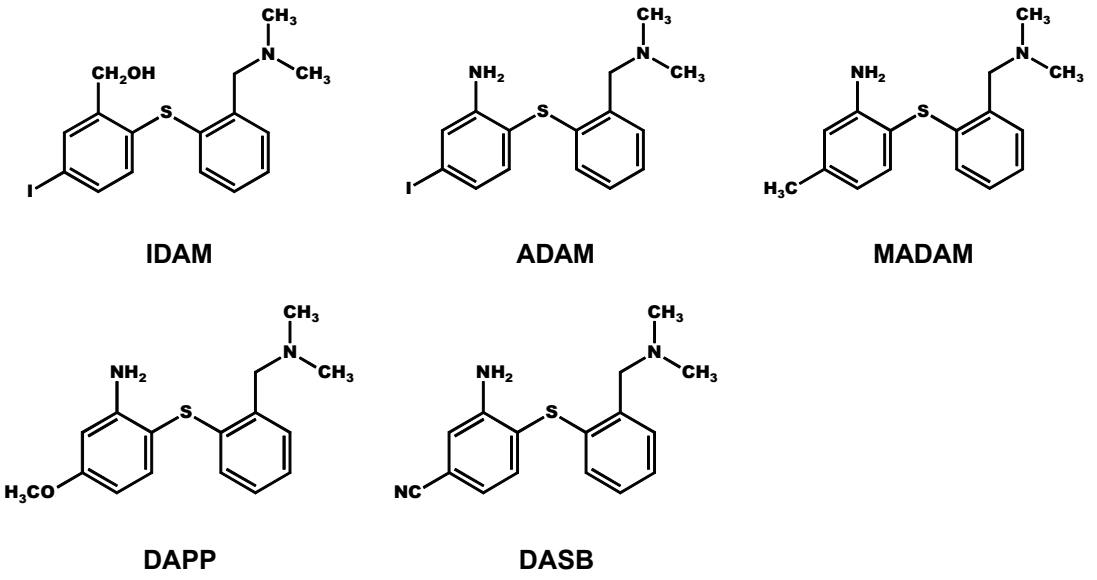

Figure 1-3: Molecular structures of IDAM, ADAM, MADAM, DAPP and DASB

Only recently several substituted diphenyl sulphides such as **IDAM** (5-iodo-2-[(2-(dimethylaminomethyl)-phenylsulfanyl]benzylalcohol) [17], **ADAM** (N,N-dimethyl-2-(2-amino-4-iodophenylsulfanyl)benzylamine) [18], **MADAM** (N,N-dimethyl-2-(2-amino-4-methylphenylsulfanyl)-benzylamine) [19], **DAPP** (N,N-dimethyl-2-(2-amino-4-methoxyphenyl-sulfanyl)benzylamine) [20] and **DASB** (3-amino-4-[(2-dimethylamino-methyl)-phenylsulfanyl)]benzonitrile) [20, 21] have been described as potent and selective SERT ligands.

These investigations were originally based on early studies that described **moxifetin** [22] and **403U76** [23] as novel antidepressants.

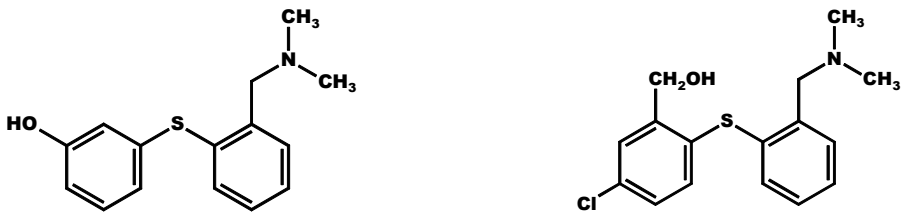

moxifetin **403U76**

Figure 1-4: Molecular structures of moxifetin and 403U76

Whereas iodine-123 labelled **IDAM** and **ADAM** have been described as suitable radioligands for *in vivo* visualisation of the SERT using SPECT in primates [17], carbon-11 labelled **DAPP** and **DASB** have shown favourable PET characteristics in the human brain [24]. Also carbon-11 labelled **MADAM** might prove a suitable PET ligand for imaging the SERT [19, 25]. The studies have shown that these diphenyl sulphides have promising characteristics for imaging the SERT. However, as yet, no optimal PET ligand has been found among them. The slow kinetics preclude **ADAM**, for instance, from being a useful PET tracer, and [^{11}C]**DASB** is not appropriate to detect SERT in the cortex [26]. Thus, further structure-activity relationship (SAR) studies of these diphenyl sulphides are both necessary and warranted, particularly as the lack of an asymmetric centre in these agents makes synthesis comparatively easy.

1.4 Purpose of the Work

PET investigations of the SERT have been limited due to the various shortcomings of the candidate radioligands. Therefore new PET radiotracers for the SERT are needed.

According to a thorough literature search, no 3D QSAR studies on SERT ligands yet exist with the exception of a CoMFA study on tropane analogues [27]. Any other molecular modelling studies regarding SARs of SERT ligands are either of a qualitative nature [28, 29], or are exploring two-dimensional QSARs [30].

The purpose of the present work was to quantitatively investigate SARs of SERT ligands at the SERT and at the structurally similar NET with regard to the development of potential new PET radiotracers. Structural requirements for SERT selectivity were to be elucidated since many known SERT ligands bind to both the SERT and the NET due to the similarity of the monoamine transporters, and selectivity is an important issue with PET ligands. No three-dimensional structure of the SERT was available in literature, thereby excluding receptor based modelling. In addition, the complexity of a transporter protein made homology modelling difficult. Therefore 3D QSAR techniques were limited to ligand based methods such as Comparative Molecular Field Analysis (CoMFA), and Comparative Molecular Similarity Indices Analysis (CoMSIA). Both techniques were chosen for the present work as this permits a comparison of the results. The resulting CoMFA and CoMSIA models were to be used to design potential new and selective PET radiotracers for the SERT and to predict their binding affinity at both the SERT and the NET.

In recent years a new series of different N,N-dimethyl-2-phenylsulfanyl-benzylamines was developed as potential new PET tracers for the SERT [21]. Although some of these diphenyl sulphides, for instance

[^{11}C]**DASB**, displayed promising PET characteristics, no optimal PET tracer was found among them yet. Further investigation of this class of compounds was considered worthwhile. Therefore their N,N-dimethyl-2-phenylsulfanyl-benzylamine scaffold was chosen as lead for structural modification. Possibilities for radiolabelling were to be considered when modifying the structures.

2 Theoretical Background

2.1 Monoamine Transporters

2.1.1 Functions

Monoamine transporters are membrane proteins mainly located on nerve endings of serotonergic, noradrenergic and dopaminergic neurons. Their function is to terminate the action of released neurotransmitter in the synaptic cleft by transporting it back into the neuron, a process known as reuptake. The structures of the chemically related monoaminergic neurotransmitters **serotonin**, **norepinephrine** and **dopamine** are shown in **Figure 2-1**.

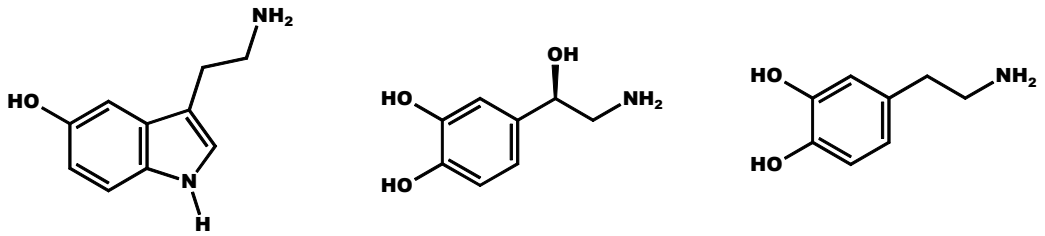

serotonin **norepinephrine** **dopamine**

Figure 2-1: Molecular structures of the monoaminergic neurotransmitters serotonin, norepinephrine and dopamine

These neurotransmitters are important in the regulation of affective states and cognitive functions and also in the development of many neuropsychiatric disorders such as Parkinson´s disease, depression

and substance dependence [4]. Comprehensive overviews of monoamine transporters and their functions are provided by Povlock et al. [31] and Olivier et al. [32].

Blocking the reuptake leads to an increased concentration of transmitters in the synaptic cleft. This is the effect of many antidepressant drugs [33]. Whereas the older tricyclic antidepressants (TCAs) block both the reuptake of serotonin and norepinephrine, the second generation antidepressants, selective serotonin reuptake inhibitors (SSRIs), selectively block the serotonin reuptake. However, the third generation of antidepressants focuses again upon the reuptake of both serotonin and norepinephrine, combined with an antagonism at 5-HT_{2A}-receptors and 5-HT_{1A}-receptors. The mechanism of depression is fairly complex and not wholly understood yet.

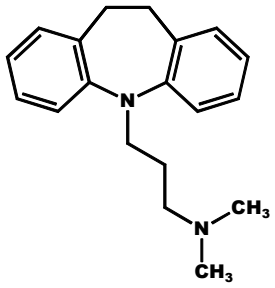

imipramine

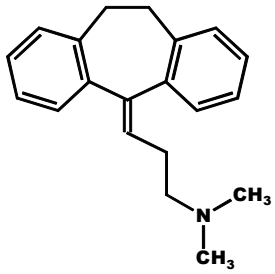

amitriptyline

Figure 2-2: Molecular structures of imipramine and amitriptyline

Imipramine and **amitriptyline** belong to the TCAs. **Fluoxetine**, **paroxetine**, **citalopram** and **sertraline** are SSRIs. **Venlafaxine** is a third generation antidepressant affecting both the SERT and the NET *in vivo*, whereas **nefazodone** and **trazodone** are third generation antidepressants blocking both the serotonin transporter and the 5-HT_{2A}-receptor [34].

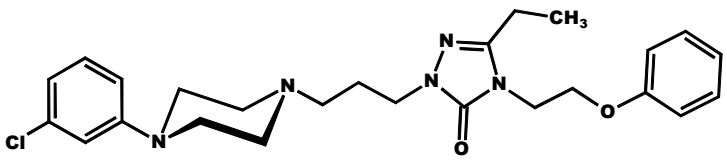

nefazodone

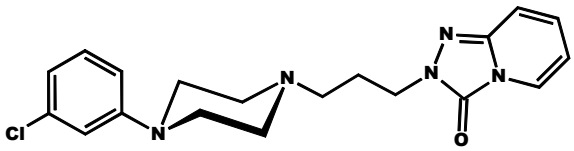

trazodone

Figure 2-3: Molecular structures of nefazodone and trazodone

Also psychostimulants like amphetamine and cocaine block the reuptake of monoamines [35].

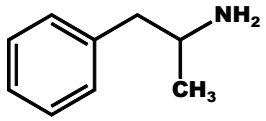

amphetamine

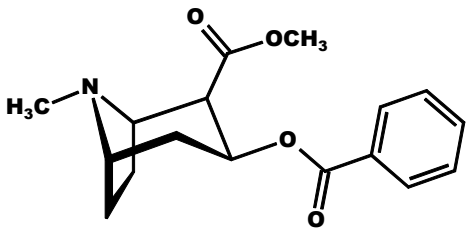

cocaine

Figure 2-4: Molecular structures of amphetamine and cocaine

The increase of dopamine in the synaptic cleft is mainly responsible for the stimulating and rewarding effects of the drugs [35, 36] and enhance the development of addiction and the "addiction memory" [37, 38]. Serotonin is considered to play a role in neuromodulation [35, 39], but as yet, these aspects are not fully understood.

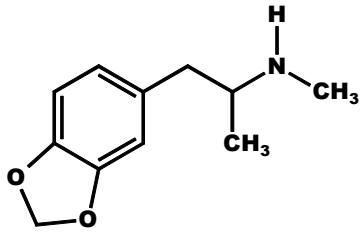

MDMA ("Ecstasy")

Figure 2-5: Molecular structure of MDMA

MDMA ("Ecstasy") is also an inhibitor of monoamine reuptake and known to release serotonin via the SERT [40]. However, this alone can not explain its particular "entactogenic" [41] effect and its neurotoxicity [15, 42], which has been shown in PET studies by McCann et al. [16] and Scheffel et al. [43]. Further research is needed, and PET investigations might be most useful here.

2.1.2 Structure

The monoamine transporters are members of a larger family of sodium dependent plasma membrane transporters [31, 44]. Progress in the monoamine transporter field had been impeded by the difficulties associated with purifying these membrane proteins. However, in 1991, Pacholczyk et al. [45] succeeded in cloning the human NET, thus allowing the rapid cloning of the DAT and the SERT. The transporter molecules consist of 617 to 630 amino acids [32]. Hydrophobicity analyses of the amino acid sequence suggest the presence of 12 putative transmembrane domains (TMs) with a large extracellular loop between TM3 and TM4, possessing two to four glycosylation sites [31]. A schematic representation of the putative secondary structure of a monoamine transporter can be seen in **Figure 2-6**.

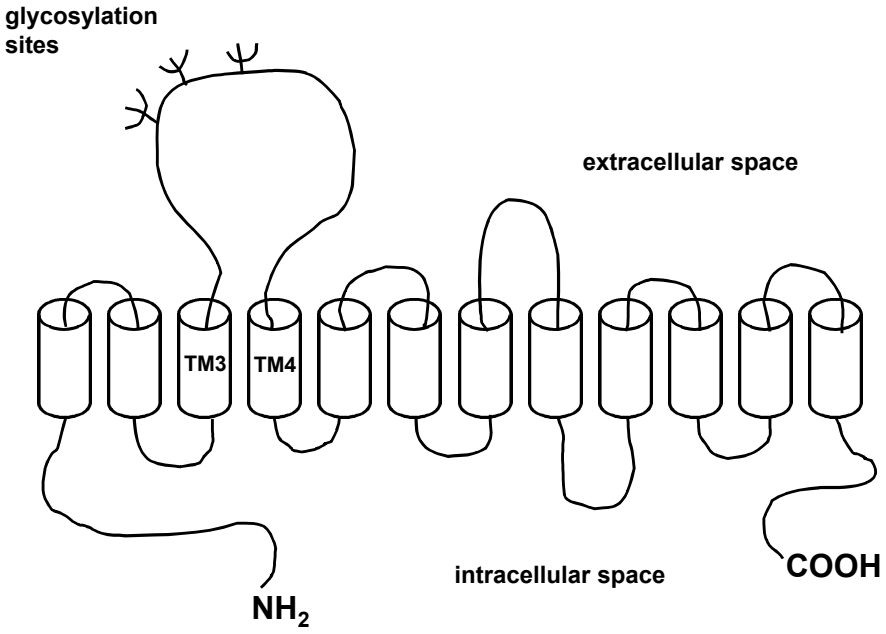

Figure 2-6: Schematic representation of the putative secondary structure of a monoamine transporter

Comparing the primary amino acid sequences reveals a homology of 80% between DAT and NET, and a homology of 69% between DAT and SERT. Preliminary structure-function analyses have provided some insight into which domains or specific amino acids are important for ligand binding. Details are given in [31] and [32]. However, as the three-dimensional structures of the monoamine transporters are presently not available, ligand binding domains can not be specified. Yet there are indications that for instance the SSRIs **citalopram**, **sertraline** and **paroxetine** share a common ligand binding domain at the SERT [46], as well as **citalopram**, **fluoxetine**, **imipramine** and **cocaine** [47], and that this domain corresponds to the binding site of serotonin itself [47].

2.1.3 Transport Mechanism

Transmitter reuptake is an energy demanding process involving conformational changes in the transporter. The energy required for the process is provided by Na^+/K^+-ATPase. The transmitter molecule is transported into the cell with one or two sodium ions and one chloride ion. In the case of the SERT, one potassium ion is simultaneously transported out of the cell [44]. Rudnick [44] provides a detailed description of transport mechanism.

2.2 Molecular Modelling

2.2.1 Definition

Molecular Modelling is the investigation of molecular structures and properties using computational chemistry and graphical visualisation techniques in order to provide a plausible three-dimensional representation under a given set of circumstances [48]. Molecular design is the application of such techniques leading to the discovery of new chemical entities with specific properties for the intended application [48]. Höltje and Folker´s book “Molecular Modeling” [49] provides a comprehensive overview of molecular modelling techniques including small molecule and protein modelling together with illustrations and examples.

2.2.2 Short History

The synthesis and screening of hundreds and thousands of potential drug candidates to find one active drug molecule is an extremely

expensive and laborious procedure. Although often guided by rational concepts, drug research generally has been, over decades, a mere trial-and-error search for new leads and active analogues [50]. More effective strategies are desirable and a rational alternative is the derivation of structure-activity hypotheses and their quantitative evaluation. Progress in drug design depends on the ability to understand the interactions of drugs with their biological target. In 1894, Fischer [51] introduced the principle of “lock-and-key” when describing the interaction of a ligand with its receptor. This theory was later extended by Koshland [52] hypothesising an induced fit, i.e. a conformational change of the receptor protein, upon ligand binding. These ideas led to a better understanding of the way drugs are working, and provided the basis for rational drug design. Different types of protein-ligand interactions exist. The most important are electrostatic interactions including hydrogen bonding and ionic effects, and hydrophobic interactions. Protein-ligand interactions are thoroughly explained in an individual chapter of the book “Wirkstoffdesign” (“Drug Design”) by Böhm, Klebe and Kubinyi [53]. The pharmacophore concept is a result of the “lock-and-key” principle. Binding to a protein within a series of compounds is attributed to a particular arrangement of common structural features. In 1964, the Hansch analysis [54] was introduced. Hansch and Fujita [54] correlated physicochemical properties with biological activity. In the same year, Free and Wilson [55] developed a model of additive group contributions to biological activity. These works are considered the beginning of quantitative structure-activity relationship (QSAR) investigations. However, the three-dimensionality of the physicochemical properties was not taken into account yet.

2.2.3 3D QSAR: CoMFA and CoMSIA

Three-dimensional quantitative structure-activity relationship (3D QSAR) involves the analysis of the quantitative relationship between the biological activity of a set of compounds and their three-dimensional properties using statistical correlation methods [48]. In 1988, Cramer et al. [56] first introduced the Comparative Molecular Field Analysis (CoMFA) method. This technique was based on the assumption that changes in binding affinities of ligands are related to changes in shape and strength of non-covalent interaction fields surrounding the molecules. These fields were of steric and electrostatic nature first, but were later extended by hydrophobic fields and hydrogen bond accepting and hydrogen bond donating fields. To compute the fields, the molecules are located in a cubic grid, and the interaction energies between each molecule and a specifically defined probe atom are calculated for each grid point. The molecules are thus represented by their field properties. To detect common regions within the fields of all molecules, multivariate statistics is applied. Within the CoMFA procedure, the Partial Least Squares (PLS) regression method [57-59] (cp. **Chapter 2.2.4**) is used. A QSAR in the form of a highly complex linear equation is computed. As every regression equation the QSAR is characterised by its correlation coefficient r^2 which is computed from the residuals of the least-squares fit. It is a measure of how well the model reproduces or fits the input data. Other parameters for estimating the quality of a regression are the standard error of estimate SE and the F-value which is the ratio of explained to unexplained variance. Each numerical regression coefficient maps directly to a location in space. Since each lattice point has a QSAR coefficient, the CoMFA QSAR equation is summarised graphically as a 3D contour map, showing those fields in which the lattice points are associated with extreme values. These correspond to the molecular

fields which are considered crucial for binding affinity. The QSAR CoMFA equation can also be used for predicting property values of new compounds provided that the structures being predicted are similar to those used for model derivation.

An important prerequisite for the CoMFA procedure is a suitable alignment of the set of molecules. Aligning the molecules means superimposing them by particular rules. This ensures that the molecular fields can be compared. The alignment can be achieved by pharmacophore identification [49], followed by superimposing the common pharmacophoric points of the molecules. Comprehensive overviews on CoMFA and its scope and limitations are given in [60-62].

However, a number of problems inherent to CoMFA are known, some of them directly connected with the field calculation method. For calculating the steric contributions, the Lennard-Jones potential is used, and for calculating the electrostatic contributions, the Coulomb potential is used. **Figure 2-7** shows the curves of these potentials.

One main difficulty are the cutoff values, whose application excludes very high field contributions near the molecular surface from analysis. Due to the sharp increase of the Lennard Jones potential, and a comparatively shallow increase of the Coulomb potential near the molecular surface, the application of cutoff values can be highly critical as important contributions might be dropped for some molecules [61]. Moreover, small shifts within the alignment can lead to dramatically altered results.

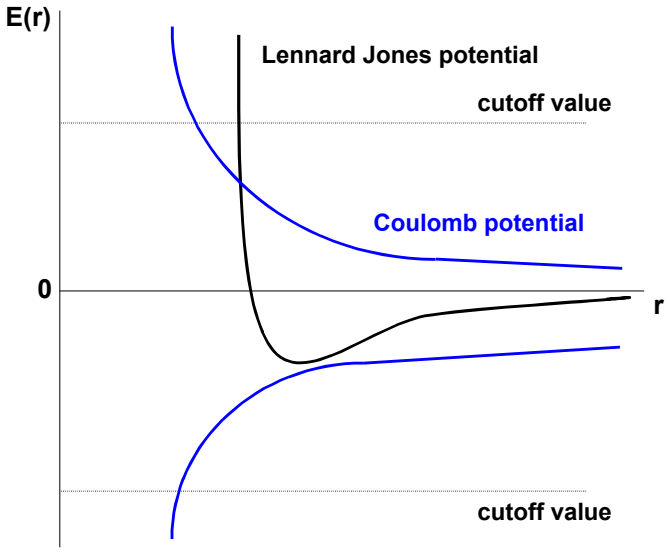

Figure 2-7: Schematic representation of the Lennard Jones and the Coulomb potential describing steric and electrostatic contributions to the CoMFA fields (adapted from [53]). The Lennard Jones potential is used to calculate interatomic interactions between two atoms without considering their charges. Negative values correspond to attractive forces, positive values correspond to repulsive forces. When the two atoms approach each other, the potential first reaches a minimum due to mutual polarisation, then increases sharply towards infinity due to repulsive forces. The Coulomb potential is used to calculate electrostatic interactions between two atoms. For atoms of the same charge, the repulsive forces become infinitely large with decreasing distance between them. For oppositely charged atoms, the attractive forces become infinitely large with decreasing distance. For the hyperbolic Coulomb potential, cutoff values are applied.

CoMSIA is an extension of the CoMFA methodology recently developed by Klebe et al. [63, 64]. Molecular similarity is compared in terms of similarity indices. Its advantages over the standard CoMFA technique are reported to be a greater robustness regarding both region shifts and small shifts within the alignment, and more intuitively interpretable contour maps [65]. This is a result of the application of similarity indices calculated by using a Gaussian-type distance dependence instead of the Lennard-Jones and the Coulomb potential

which makes the more or less arbitrary application of cutoff values unnecessary. This is demonstrated in **Figure 2-8**.

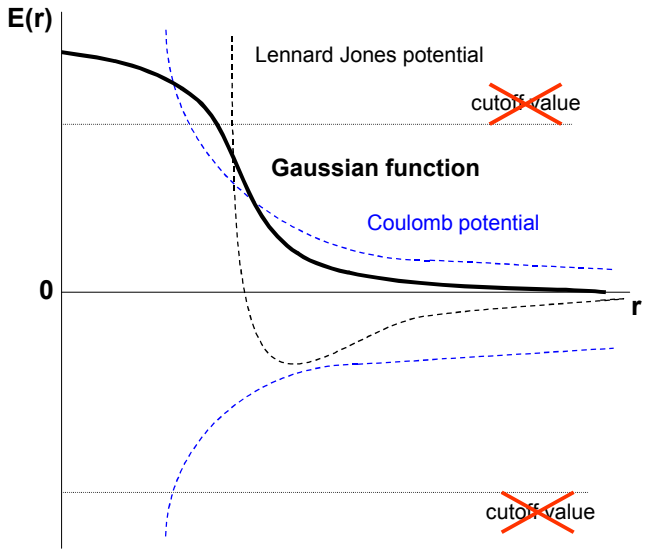

Figure 2-8: A Gaussian type function that slowly reaches its maximum with the distance between the probe atom and the molecule becoming smaller. For comparison see again the Lennard Jones and the Coulomb potential (adapted from [53]).

Moreover, not only steric and electrostatic fields are typically considered with the CoMSIA technique, but also hydrophobic fields and hydrogen bond donor and hydrogen bond acceptor fields.

2.2.4 Partial Least Squares (PLS)

When correlating the large amount of descriptor variables (X variables), i.e. the field contributions at the numerous grid points produced by CoMFA and CoMSIA, with the target variables (Y variables), i.e. the biological activity of the molecules, classical Multiple Linear Regression

(MLR) reaches its limits. Instead, Partial Least Squares (PLS) regression is used as data with strongly correlated and noisy X variables that clearly outnumber the Y variables can be handled. The structural descriptors are called the X matrix, the activity values constitute the Y matrix. The idea of PLS is based on the Principle Component Analysis (PCA). The X matrix is projected into vectors by extracting so-called Principle Components (PCs) from the matrix that explain the variance within the structural descriptors in relation to the target variables. The NIPALS (Nonlinear Iterative Partial Least Squares) algorithm is usually used as described in [57]. The PCs are also known as X scores. Strictly speaking, the term Principle Component is incorrect for PLS and instead, the term Latent Variable (LV) or PLS factor should be used. However, Principle Component is also commonly accepted. The X scores are linear combinations of the original variables and the weights of the coefficients needed for X matrix transformation. These weights are also known as loadings. Saying that a variable is highly “loaded” in a PC means that the PC has a high importance for the variable. Thus, the loadings are essential for understanding which X variables are important and which X variables provide the same information. The part of the data that is not explained by the model, i.e. the residuals, are of diagnostic interest. Large residuals of Y indicate that a model is poor. A residual plot of Y variables is useful for identifying outliers.

To estimate model complexity, i.e. the number of significant PLS components, cross-validation is used. One or more test compounds are removed from the data set and after model derivation with the remaining structures the target properties of these compounds are predicted. After deleting every object once, the sum of squared differences between predicted and observed target property is computed. This sum is called PRESS (Predictive Residual Sum of

Squares). Both the cross-validated correlation coefficient q^2 and the standard error of prediction s_{PRESS} are computed from PRESS. Thus, cross-validation estimates the predictive ability of a model which is an important criterion when investigating the number of significant model components.

The PLS method is thoroughly explained and exemplified by Geladi and Kowalski [57, 66], and Wold and co-workers [58, 59].

3 Methods

3.1 Hardware

All molecular modelling calculations were performed on a Silicon Graphics Octane (R 10 000) workstation with a main memory of 640 MB and a CPU of 175 MHz, running under the operating system IRIX 6.6.

3.2 Software

The molecular modelling software package *SYBYL* 6.6 [67] utilising the following *SYBYL* modules was employed for this work: *SYBYL*/Base, Advanced Computation, QSAR, Advanced CoMFA (including the Optimize QSAR interface) and GASP. The Tripos Force Field [68] was used for all calculations.

3.3 Biological Data

An important prerequisite for the quantitative investigation of SARs is a suitable data set. Affinity data should have been determined in just one laboratory using just one method to avoid systematic errors. For the present work a chemically heterogeneous data set taken from literature consisting of 13 antidepressants and 6 metabolites was used [34]. The molecular structures are shown in **Figure 3-1**.

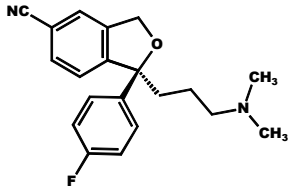

***(S)*-citalopram (m1)**

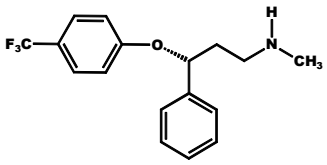

***(S)*-fluoxetine (m2)**

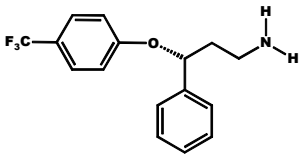

***(S)*-norfluoxetine (m3)**

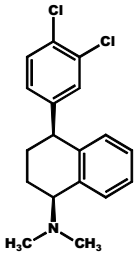

sertraline (m4)

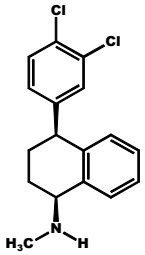

desmethylsertraline (m5)

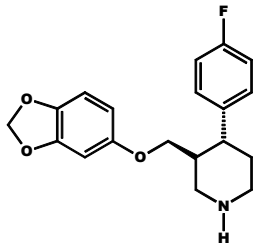

paroxetine (m6)

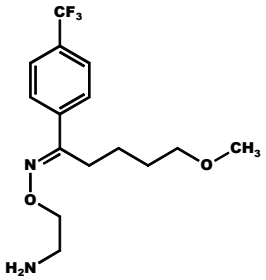

fluvoxamine (m7)

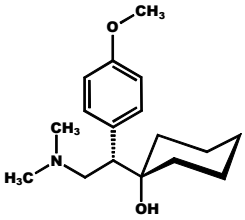

venlafaxine (m8)

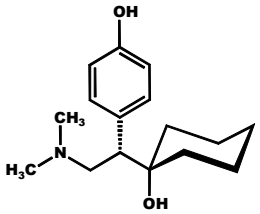

O-desmethylvenlafaxine (m9)

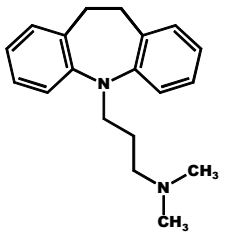

imipramine (m10)

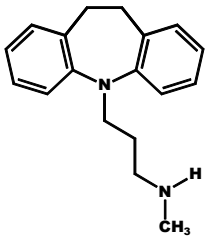

desipramine (m11)

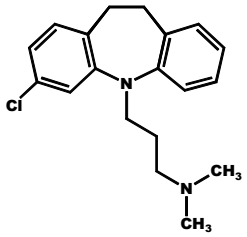

chloroimipramine (m12)

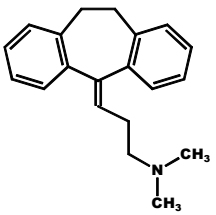

amitriptyline (m13)

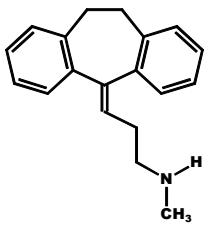

nortriptyline (m14)

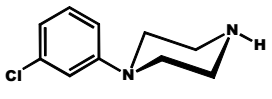

***m*-CPP (m15)**

Figure 3-1: Molecular structures of the serotonin reuptake inhibitors used for the QSAR studies (continued on the following page)

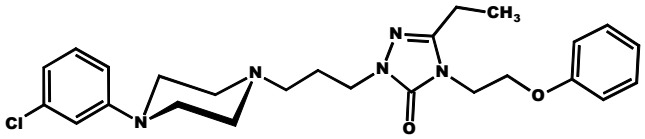

nefazodone (m16)

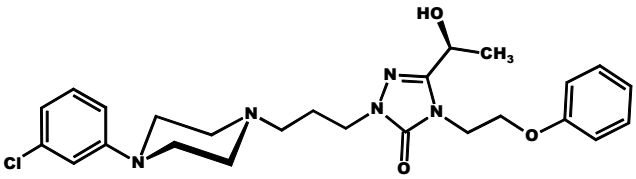

***(S)*-hydroxynefazodone (m17)**

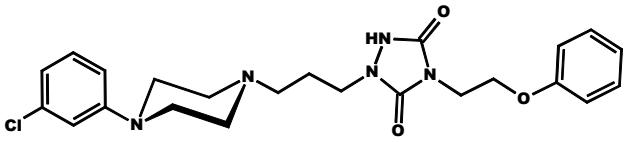

triazoledione (m18)

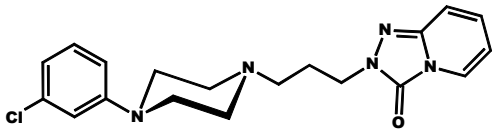

trazodone (m19)

The given binding data had been determined for both the SERT and the NET by competitive radioligand binding assays. Affinities had been obtained for the SERT from rat cortex using [^{3}H]citalopram, and from human transfected cells using both [^{3}H]citalopram and [^{3}H]serotonin. For the NET affinities had been obtained from rat cortex using [^{3}H]nisoxetine and from human transfected cells using both [^{3}H]nisoxetine and [^{3}H]norepinephrine. For this study, data from the human SERT and the human NET determined against [^{3}H]citalopram and [^{3}H]nisoxetine was chosen. The respective equilibrium inhibition constants (K_i) and their negative logarithms (pK_i) are given in **Table 3-1**.

Table 3-1: Experimental binding affinities [34] of the serotonin transporter ligands used for the QSAR studies, and affinity differences

	$K_{i\ exp.}$ ± SE (nM) [a]		$pK_{i\ exp.}$ (nM) [b]		$\Delta pK_{i\ exp.}$ [c]
Compound	**SERT**	**NET**	**SERT**	**NET**	
citalopram (**m1**)	1.5 ± 0.03	7 865 ± 304	8.82	5.10	3.72
fluoxetine (**m2**)	0.90 ± 0.06	777 ± 37	9.05	6.11	2.94
norfluoxetine (**m3**)	2.3 ± 0.10	3 947 ± 222	8.64	5.40	3.24
sertraline (**m4**)	0.15 ± 0.01	817 ± 80	9.82	6.09	3.73
desmethylsertraline (**m5**)	3.7 ± 0.26	811 ± 17	8.43	6.09	2.34
paroxetine (**m6**)	0.065 ± 0.006	85 ± 5	10.19	7.07	3.12
fluvoxamine (**m7**)	1.6 ± 0.1	2 950 ± 103	8.80	5.53	3.27
venlafaxine (**m8**)	7.5 ± 0.4	2 269 ± 84	8.12	5.64	2.48
O-desmethylvenlafaxine (**m9**)	7.7 ± 0.3	2 753 ± 114	8.11	5.56	2.55
imipramine (**m10**)	1.3 ± 0.04	20 ± 0.54	8.89	7.70	1.19
desipramine (**m11**)	22 ± 1	0.63 ± 0.03	7.66	9.20	-1.54
chloroimipramine (**m12**)	0.05 ± 0.001	n.d. [d]	10.30	-	-
amitriptyline (**m13**)	2.8 ± 0.1	19 ± 1	8.55	7.72	0.83
nortriptyline (**m14**)	15 ± 0.1	1.8 ± 0.07	7.82	8.74	-0.92
m-CPP (**m15**)	202 ± 9	1 940 ± 152	6.69	5.71	0.98
nefazodone (**m16**)	459 ± 28	618 ± 12	6.34	6.21	0.13
hydroxynefazodone (**m17**)	1 015 ± 27	664 ± 24	5.99	6.18	-0.19
triazoledione (**m18**)	34 527 ± 6 773	> 100 000	4.46	4.00	0.46
trazodone (**m19**)	252 ± 10	37 419 ± 1 433	6.60	4.43	2.17

[a] $K_{i\ exp.}$ ± SE = experimental equilibrium inhibition constant ± standard error [b] $pK_{i\ exp.}$ = negative logarithm of the experimental equilibrium inhibition constant
[c] $\Delta pK_{i\ exp.} = pK_{i\ exp.}$ (SERT) - $pK_{i\ exp.}$ (NET) [d] n.d. = not determined

The affinities towards both transporters are spread over a satisfactorily large range with seven logarithmic units for the SERT, and six logarithmic units for the NET. Consequently, the derivation of a statistically significant 3D QSAR model can be expected. Affinity data for the SERT and the NET are strongly correlated as shown by a high correlation coefficient of 0.93. For chloroimipramine, affinities are given for the SERT only, whereas for mazindol, affinities are given for the NET only. Therefore, chloroimipramine was considered in 3D QSAR studies on SERT affinities only. Mazindol was not considered at all. In cases in which the racemic mixture is usually used (citalopram and fluoxetine), the enantiomer which is known to be more potent was considered (in both cases the *(S)*-enantiomer) as no data about pure enantiomers were available. For the hydroxymetabolite of nefazodone,

the *(S)*-enantiomer was arbitrarily chosen. Naturally, a larger data set than the one used would be preferable for 3D QSAR studies. But no larger appropriate data collection obtained in only one laboratory was found in literature. So data consistency was preferred to the idea of a more comprehensive data set.

Binding affinity data of [^{11}C]DASB and its derivatives at the SERT and at the NET (cp. **Chapter 4.3.3**) was taken from literature [21, 26, 69]. K_i-values are given in **Table 4-3**.

3.4 Compound Generation

The compounds under investigation were either constructed from X-ray crystal structure [70-75] or using *SYBYL´s* fragment library. All molecules used for model derivation were generated in both their N-protonated and their non-protonated form. An initial geometry optimisation was performed *in vacuo* using the Tripos Force Field [68] and the following non-default settings: *Method:* Conjugate Gradient, *Termination Gradient:* 0.01 kcal/mol*Å, *Max. Iterations:* 10 000. The resulting structures were used as starting geometries for both Genetic Algorithm (GA) searches and Genetic Algorithm Similarity Program (GASP) alignments. GA searches were carried out for all substances in both their N-protonated and non-protonated forms in order to find low energy conformations and to compare them with the conformations found after the alignment procedure, and thus be able to judge how far the latter are away from a possible minimum conformation. The GA search method was selected as conformational search method as it is known to perform very well in finding lowest-energy conformations [76]. *(S)*-Citalopram (**m1**) was then chosen as a reference substance for the subsequent alignment. One of the suggested minimum conformations

derived from the GA search with N-protonated *(S)*-citalopram (**m1**) fitted into Gundertofte´s pharmacophore model [28] very well. This model was used as the basis for the alignment. The conformation was further minimized with non-default settings (*Method:* Conjugate Gradient, *Termination Gradient:* 0.01 kcal/mol*Å, *Max. Iterations:* 10 000). Conformations of most of the other structures were obtained as a result of the alignment. When constructing the TCAs, the flexibility of the ethylene bridged ring system at room temperature [77] needed to be considered. The conformation of the ring system of chloroimipramine (**m12**) seen in its crystal structure [78] is different from the conformations of the ring systems of imipramine (**m10**) [74] and amitriptyline (**m13**) [72]. However, in accordance with the idea of flexibility, the same ring system conformation was used for all TCAs. Imipramine (**m10**) was taken from the GA search, and chloroimipramine (**m12**) was constructed from imipramine (**m10**). Trazodone (**m19**), triazoledione (**m18**) and *(S)*-hydroxynefazodone (**m17**) were constructed from nefazodone (**m16**) using *SYBYL´s* fragment library. Metabolites of any other molecules (*(S)*-norfluoxetine (**m3**), desmethylsertraline (**m5**), O-desmethylvenlafaxine (**m9**), desipramine (**m11**), and nortriptyline (**m14**)) were constructed from their respective parent compound.

DASB was constructed using *SYBYL´s* fragment library. It was generated both in its N-protonated and non-protonated form. An initial geometry optimisation was performed *in vacuo* using the Tripos Force Field [68] and the following non-default settings: *Method:* Conjugate Gradient, *Termination Gradient:* 0.01 kcal/mol*Å, *Max. Iterations:* 10 000. The resulting structure was used as starting geometry for the alignment and for a conformational GA search. Any DASB derivatives were constructed from their respective parent compound using *SYBYL´s* fragment library. They were minimized using the following

non-default settings: *Method:* Conjugate Gradient, *Termination Gradient:* 0.01 kcal/mol*Å, *Max. Iterations:* 100.

3.5 Alignment Procedure

GASP (Genetic Algorithm Similarity Program) [67] served as alignment tool. It is a genetic algorithm developed for the superimposition of sets of flexible molecules [79]. Molecules are represented by a chromosome that encodes conformational information and intermolecular mappings between important structural features that may be required for activity [76]. The fitness of the alignment is determined by the number and similarity of the overlaid features, by the volume overlap of the alignment and the internal van der Waals energy of the molecular conformations [76]. Default settings were used and ten alignments were generated during each GASP run. All conformations generated by GASP and chosen for CoMFA and CoMSIA analysis were further minimized *in vacuo* using the Tripos Force Field [68] and the following non-default settings: *Method:* Conjugate Gradient, *Termination Gradient:* 0.01 kcal/mol*Å, *Max. Iterations:* 1000.

3.6 3D QSAR

3.6.1 CoMFA

Steric and electrostatic CoMFA fields were calculated using the Lennard Jones potential and the Coulomb potential [56]. Default parameters (Tripos standard field, dielectric distance $1/r^2$, steric and electrostatic cutoff 30 kcal/mol, positively charged sp^3 hybridised

carbon atom as probe atom, grid spacing 2 Å) were used unless stated otherwise. Partial atomic charges were calculated using the Gasteiger-Hueckel method. All CoMFA calculations were done with the Tripos Advanced CoMFA module [67]. To investigate the influence of different parameter settings on the CoMFA analysis, various steric and electrostatic cutoffs were explored as well as different grid spacings and column filtering, and various energy levels. The procedure was guided by suggestions made by Cramer et al. [61] and Folkers et al. [60]. To check the statistical significance of the models, cross-validation was done by means of the "Leave One Out" (LOO) procedure using the SAMPLS method [80]. The models were assessed by their cross-validated correlation coefficient q^2, by their optimal number of components and by their standard error of prediction s_{PRESS}. Usually, the optimal number of components is determined by selecting the highest q^2-value, which most often corresponds to the smallest s_{PRESS} value. In the CoMFA and CoMSIA studies at the SERT, the "*Fraction_of_Variance"* was likewise examined. Whenever the last added component improved the "*Fraction_of_Variance"* by less than about 5%, the less complex model was chosen. This optimal number of components was subsequently used to derive the final QSAR models. CoMFA standard scaling was applied to all PLS analyses. The whole validation procedure, also including cross-validation in groups and data scrambling as described in **Chapter 4.2.1**, was done following recommendations by Wold and Eriksson [81] and Thibaut et al. [82].

3.6.2 CoMSIA

CoMSIA fields were calculated using standard parameters (probe atom with radius 1, charge +1, hydrophobicity +1, hydrogen bond donating +1, hydrogen bond accepting +1, attenuation factor α of 0.3, grid

spacing 2 Å). Partial atomic charges were calculated by using the Gasteiger-Hueckel method. Cross-validation and PLS analyses were done in analogy to the CoMFA analyses as described above.

3.6.3 Region Focusing

Region focusing is the application of weights to the lattice points in a CoMFA region to enhance or attenuate the contribution of those points to subsequent analyses [76]. The PLS regression method is modified by a dimension-wise interactive variable selection (IVS) approach [83, 84]. It is usually applied in order to enhance the predictability of a CoMFA study. *"StDev*Coefficient"* values were used as weights, and different weighting factors were applied of which 0.5 was found to be most appropriate.

3.6.4 Selectivity Analysis

To elucidate the selectivity-discriminating criteria between SERT and NET ligands, a method was used that was first described by Wong et al. [85], and was later successfully applied by Matter et al. [86] and Böhm et al. [65]. The differences between the negative logarithms of each ligand´s affinities at the SERT and at the NET were applied as dependent properties in both CoMFA and CoMSIA analyses. The difference data spread over more than five orders of magnitude as shown in **Table 3-1**.

3.6.5 Prediction of Novel Compounds

The CoMFA and CoMSIA models served as starting point for the virtual development of new substances. For the prediction of the binding

affinities at the SERT and at the NET, the CoMFA PLS analysis considering sterics and electrostatics, and the CoMSIA PLS analysis considering sterics, electrostatics and hydrophobics (**Table 4-1**) were used. These models were chosen as they predict the binding affinity of **DASB** both at the SERT and at the NET in the correct order of magnitude (**Table 4-3**). All CoMFA calculations were carried out with the Tripos Advanced CoMFA Module [67]. **DASB** served as lead structure. The Optimize QSAR interface [67] can be used to build a series of analogues and make a preliminary survey of their expected activities against a known QSAR [76]. In this study, the N,N-dimethyl-2-phenylsulfanyl-benzylamine core structure of **DASB** and its derivatives was provided as molecular scaffold, and S^1 and S^2 were specified as interchangeable substituents (**Figure 4-19**). New structures are automatically suggested by screening a database of possible substituents. The following default settings were used: *Configuration Options:* Standard (*Conformational Refinement:* All-trans, *Computation of Charges:* Gasteiger-Hueckel), *Method:* Random, *Cycles:* 100. The 12 best hits were retrieved. The CoMFA PLS analysis considering sterics and electrostatics for the SERT was used (**Table 4-1**).

Predictions of target properties are most reliable if extrapolation with respect to topologies and functionalities does not occur, but small extrapolations of descriptors that make only a small contribution to the model are not a cause of particular concern. Extrapolation is described by the total contribution made to the prediction by the out-of-range descriptors [76]. In predicting biological activity on a common log scale any extrapolation below 0.3 log units is probably acceptable [76]. This is the case for most CoMFA predictions. Some CoMSIA predictions, however, do not comply with this requirement, and are indicated with an asterisk in **Table 4-3** to **Table 4-6**.

4 Results and Discussion

4.1 Pharmacophore Model and Alignment

4.1.1 Pharmacophore Models of SERT Ligands

The crucial step of every CoMFA and CoMSIA study is the alignment of the substances of the data set. Every alignment is usually based on a pharmacophore hypothesis. Only a small number of pharmacophoric models of SERT ligands have been published to date [28, 29, 87-90]. Whereas in most cases only one aromatic moiety (R1) had been included in the pharmacophore building process and this aromatic moiety had been placed at a distance from the basic nitrogen comparable to the distance in serotonin itself [29, 87-90], Gundertofte et al. [28] described a secondary phenyl ring (R2) as an additional pharmacophoric feature. This stereoselective pharmacophoric model was based on low-energy conformations of *(S)*-citalopram (**m1**), *(S)*-fluoxetine (**m2**), paroxetine (**m6**) and sertraline (**m4**). As pharmacophoric features, the centres of the two aromatic rings R1 and R2 mentioned above and a site point (Sp) at a distance of 2,8 Å from the basic nitrogen in the direction of the lone pair had been defined [28]. The latter point had been used to simulate an interaction with a hypothetical acidic residue, presumed to be the primary recognition site in the transporter molecule. The distance between the aromatic rings R1 and R2 is confined to a narrow range from 4.6 Å to 5.2 Å. The distance between R1 and Sp is in the range of 7.4 Å and 8.3 Å, and the distance between R2 and Sp is in the range of 6.2 Å and 6.9 Å. The

two pharmacophoric aromatic rings are perpendicular to each other. **Figure 4-1** illustrates the pharmacophoric features exemplified by *(S)*-citalopram (**m1**).

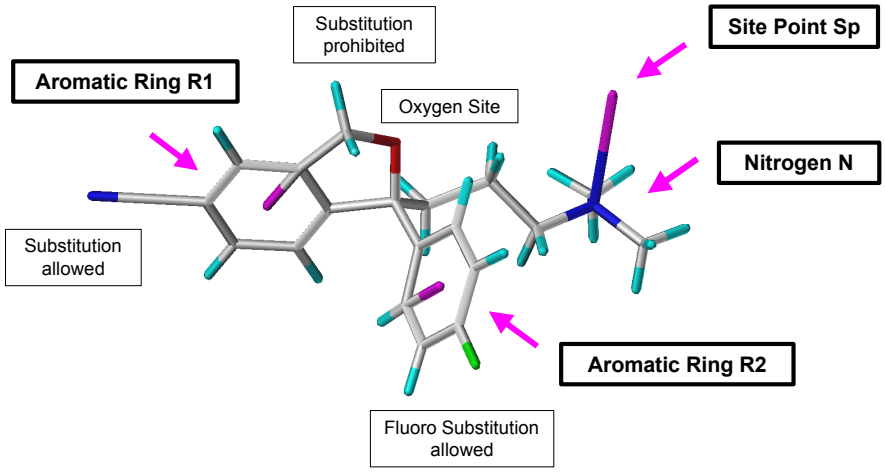

Figure 4-1: Pharmacophore model of serotonin transporter ligands [28]. Pink dummy atoms illustrate the pharmacophoric points: the centres of the two aromatic rings R1 and R2 and the site point Sp.

Additionally, Gundertofte et al. [28] found that the substituents at the primary ring R1 of *(S)*-citalopram (**m1**), *(S)*-fluoxetine (**m2**), paroxetine (**m6**) and sertraline (**m4**) occupy the same region in space. Thus, substitution is allowed in this position. The fluoro substituents of *(S)*-citalopram and paroxetine at the secondary ring R2 also point to the same region in space. Moreover, another region was detected which is occupied by many selective NET inhibitors. Substitution is prohibited here for high SERT affinity, whereas norepinephrine reuptake inhibition is enhanced when this area is occupied by substituents. In addition, a possible extra pharmacophoric element in terms of an oxygen atom was detected. A similar observation had earlier been made by Rupp et

al. [29] who suggested a favourable interaction in this position between an oxygen atom and the transporter. The pharmacophore model of Gundertofte et al. [28] was used as the basis for the present work.

4.1.2 Alignment Procedure and Discussion

The molecules of the chosen data set [34] are a chemically heterogeneous group. A conformational search followed by an atom-based superposition of minimum conformations did not lead to satisfying results. As GASP was able to reproduce the suggested alignment of the SSRIs *(S)*-citalopram (**m1**), *(S)*-fluoxetine (**m2**), paroxetine (**m6**) and sertraline (**m4**) in a way similar to the outcome seen in the work of Gundertofte et al. [28], it was considered to be an appropriate alignment tool. A stepwise alignment procedure was applied because GASP can only handle up to six or seven molecules simultaneously [76]. The suggested alignments were assessed by visual inspection following prior knowledge about the likely pharmacophore model. The attempt to apply the same superposition rules to all molecules did not result in a satisfactory alignment, and consequently different ways were tried for each molecule until a reasonable solution in every single case was found. In the following, the final alignment procedure is detailed.

(S)-Citalopram (**m1**) obtained from the conformational GA search served as template for most superpositions. It was selected because it is not only a potent and highly selective inhibitor of the SERT [32], but it can also be regarded as a ring-opened analogue of the first generation TCAs and so it serves well as a “connecting link” between these different groups of SERT ligands. To superimpose the SSRIs, a GASP run with *(S)*-citalopram (**m1**) as template, *(S)*-fluoxetine (**m2**), paroxetine (**m6**), sertraline (**m4**) and *m*-CPP (**m15**) was carried out. An

appropriate solution in which all substances met the requirements of the Gundertofte model [28] was found. As *m*-CPP (**m15**) possesses only one aromatic moiety, the question of whether this is to be aligned with the pharmacophoric feature R1 or R2 of *(S)*-citalopram (**m1**) needed to be addressed. Both possibilities seem reasonable, but as GASP suggested only the superposition onto R1, this solution was used for further studies. The resulting and further minimized conformation of *(S)*-fluoxetine (**m2**) was then used as a template in a subsequent GASP run with fluvoxamine (**m7**), and in most alignment suggestions, the aromatic moiety of fluvoxamine (**m7**) was superimposed onto R1 of *(S)*-fluoxetine (**m2**). This solution was selected for the final alignment. Analogously, venlafaxine (**m8**) was superimposed onto paroxetine (**m6**) as template by using GASP. Paroxetine (**m6**) was chosen here as a template as only this yielded a conformation of venlafaxine (**m8**) consistent with the distance requirements of the Gundertofte model [28]. GASP superimposed the aromatic moiety of venlafaxine (**m8**) onto R1 of paroxetine (**m6**). The resulting alignments with *(S)*-citalopram (**m1**) are shown in **Figure 4-2**.

When aligning the TCAs, the question arose as to which way round the TCAs should be superimposed upon *(S)*-citalopram (**m1**) concerning R1 and R2. GASP suggested both a superposition of the TCAs´ R1 onto *(S)*-citalopram´s (**m1**) R1 and R2. In accordance with a pharmacophore study of Rupp et al. [29], a superposition of R1 with R1 and R2 with R2 was finally used for the alignment. As GASP did not prove useful for the alignment of imipramine (**m10**), a low-energy conformation that complied with the distance requirements of the Gundertofte model [28] was taken from the GA search. Imipramine (**m10**) was superimposed onto *(S)*-citalopram (**m1**) by a four-point fit considering R1, R2, N and Sp. Amitriptyline (**m13**) was fitted onto imipramine (**m10**) by using GASP.

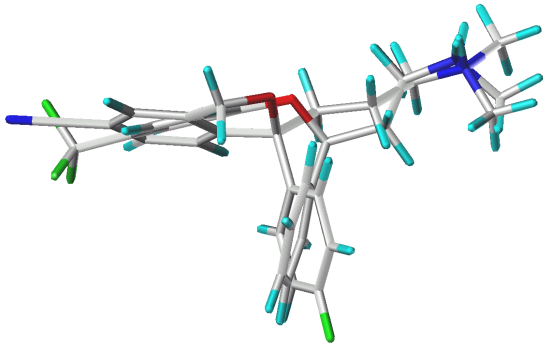

***(S)*-citalopram and *(S)*-fluoxetine**

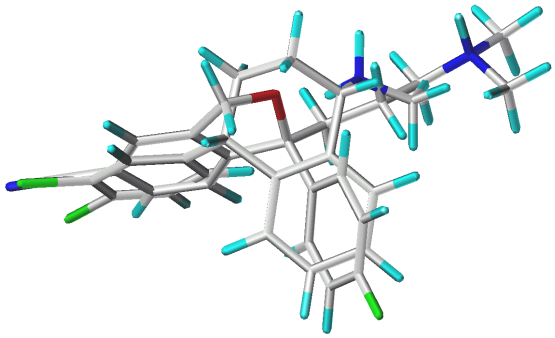

***(S)*-citalopram and sertraline**

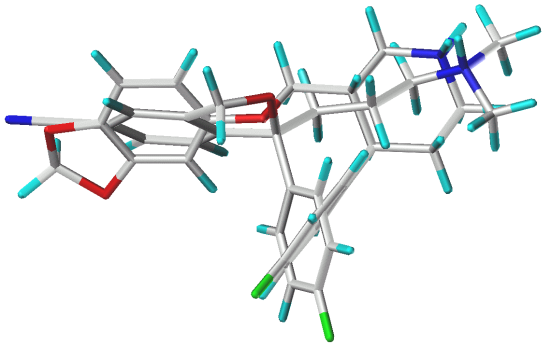

***(S)*-citalopram and paroxetine**

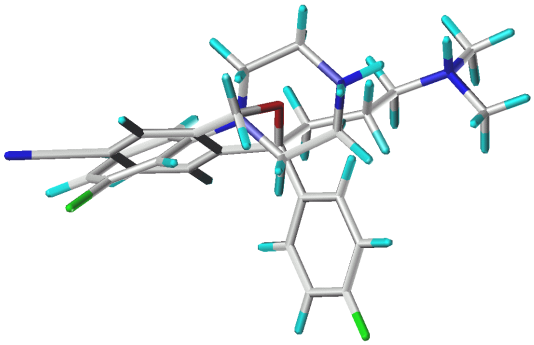

***(S)*-citalopram and *m*-CPP**

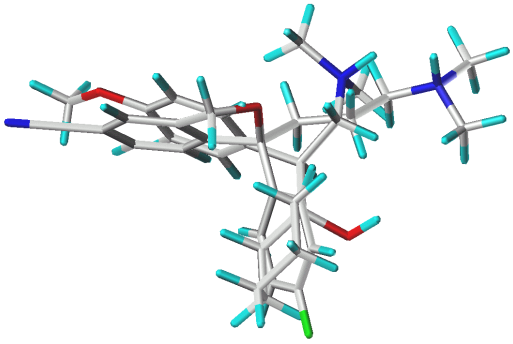

***(S)*-citalopram and venlafaxine**

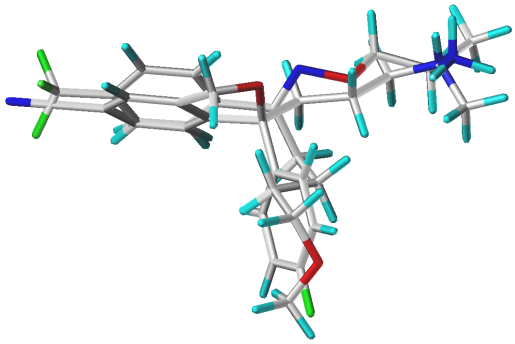

***(S)*-citalopram and fluvoxamine**

Figure 4-2: Alignment of *(S)*-citalopram and *(S)*-fluoxetine, sertraline, paroxetine, *m*-CPP, venlafaxine and fluvoxamine

The alignment of the phenylpiperazines was most challenging as this class of SERT ligands is chemically very different from the SSRIs or the TCAs. At first the question was addressed of whether to superimpose just one aromatic moiety or two aromatic moieties of the phenylpiperazines onto the pharmacophoric features of the Gundertofte model [28]. Using GASP did not lead to satisfying results

as the phenylpiperazines are highly flexible molecules, and too many potential solutions were given, many of them quite unlikely. Finally, the minimized crystal structure of nefazodone (**m16**) [73] was used for superimposition. The function of a pharmacophoric feature was ascribed only to the phenyl ring of the phenylpiperazine partial structure. This concept is in agreement with an early study on 5-HT_{1A}-receptor agonists in which phenylpiperazines are aligned in a similar way with aminotetralins and indolalkylamines [91]. A direct alignment of nefazodone **(m16**) onto *m*-CPP (**m15**) was not possible, as in the case of *m*-CPP (**m15**), the equatorial hydrogen atom is directed towards the pharmacophoric point Sp, whereas in the case of nefazodone (**m16**), the equatorial position is occupied by a substituent. However, an atom-to-atom fit of nefazodone (**m16**) onto *(S)*-citalopram (**m1**) considering all six ring atoms of the phenyl moieties of R1, in addition to the pharmacophoric features N and Sp, resulted in a satisfying superposition.

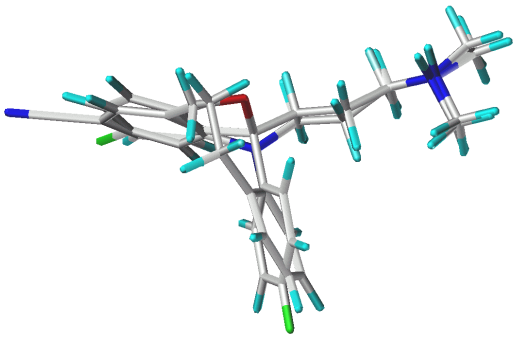

***(S)*-citalopram and chloroimipramine**

Figure 4-3: Alignment of *(S)*-citalopram and chloroimipramine

The resulting alignment of the TCAs is exemplified by chloroimipramine as shown in **Figure 4-3**. The resulting alignment of the

phenylpiperazines is illustrated by nefazodone (**m16**) as shown in **Figure 4-4**.

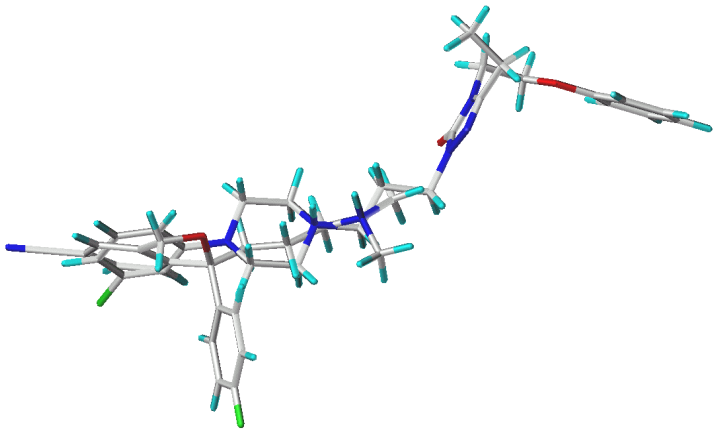

Figure 4-4: Alignment of *(S)*-citalopram and nefazodone

The same alignment was used for both the SERT and the NET although it is not necessarily the case that all ligands bind in the same manner to both transporters. However, this makes direct comparison of the different physico-chemical requirements for high binding affinity at the SERT and at the NET possible. Moreover, using the same alignment is a necessary prerequisite for the selectivity analysis.

4.1.3 Alignment of DASB

To modify the N,N-dimethyl-2-phenylsulfanyl-benzylamine core structure and to predict the binding affinity of new diphenyl sulphides by using the CoMFA and CoMSIA models, these structures needed to be fitted into the present alignment. As the same alignment was assumed for all diphenyl sulphides, the superposition was carried out

for one structure only. **DASB** was chosen for this purpose as a satisfying superimposition resulted. Analogously to the alignment procedure used for model derivation, *(S)*-citalopram (**m1**) was used as template onto which **DASB** was superimposed together with *(S)*-fluoxetine (**m2**), paroxetine (**m6**) and sertraline (**m4**). The conformation used for the alignment was chosen by visual inspection. This conformation fitted well into the Gundertofte model [28] and was found among the ten lowest-energy conformations from the GA search, confirming that the choice was a sensible one. The resulting alignment of *(S)*-citalopram (**m1**) and **DASB** is shown in **Figure 4-5**.

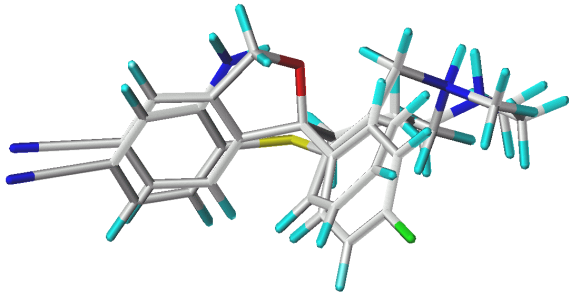

***(S)*-citalopram and DASB**

Figure 4-5: Alignment of *(S)*-citalopram and DASB

4.2 CoMFA and CoMSIA Models

4.2.1 CoMFA Models for the SERT and the NET

Statistically significant and chemically meaningful CoMFA models were developed for both the SERT and the NET. **Table 4-1** summarises the results of the CoMFA studies.

For both CoMFA and CoMSIA studies non-protonated structures were used because statistical results proved better than with N-protonated structures. Additional reasons for using non-protonated structures were the relative influence of steric and electrostatic fields upon the final models. When deriving CoMFA models with the protonated structures, the PLS analysis revealed a contribution of over 80% of the steric field. This seems quite unlikely and might well be due to known problems in connection with the electrostatic field itself as detailed in [61]. With the shallow distance dependence of the Coulomb potential, the electrostatic field may in fact be dominated by the influence of distant but highly charged atoms, in this case, the protonated nitrogen atoms. Different recommendations to overcome this problem are given in literature [61, 92], for instance the use of different probe atoms and various cutoff values. Several suggestions were tried, but finally non-protonated structures were used to minimize the influence of highly charged atoms. Moreover, the parameter of never dropping electrostatics at sterically unfavourable points (as opposed to dropping electrostatics within the steric cutoff for each row) was applied as recommended in [60] and [93]. This resulted in CoMFA models that were not any longer dominated by steric contribution, but showed a contribution of sterics and electrostatics comparable to the contribution in the respective CoMSIA studies. Apart from never dropping electrostatics, default parameter settings were appropriate for the data set, which is in agreement with the suggestion of Folkers et al. [60] to use CoMFA with its default settings only, because of the complex interdependence of the parameters.

A 3D QSAR model is considered statistically significant if its q^2-value is above 0.3 [94, 95] although a q^2-value above 0.4 to 0.5 [53] is naturally preferable. The CoMFA model for the SERT is consequently a clearly statistically significant model showing a q^2-value of 0.538 at 3

components. Experimental binding affinities and the residuals of the final non cross-validated models are shown in **Table 4-2**. The correlation plot of $pK_{i\ fit}$ versus $pK_{i\ exp.}$ is shown in **Figure 4-6**.

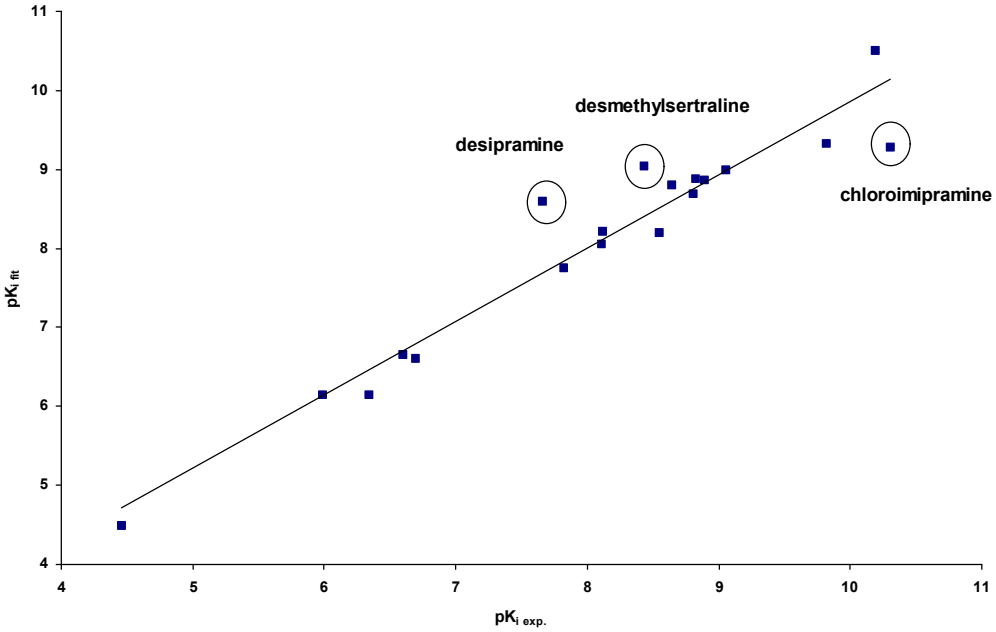

Figure 4-6: Non cross-validated CoMFA analysis at the SERT: correlation plot of $pK_{i\ fit}$ versus $pK_{i\ exp.}$ with r^2 = 0.929, SE = 0.437, F = 65.80. The fit for chloroimipramine, desipramine and desmethylsertraline is deviating by more than one order of magnitude.

Three compounds, namely chloroimipramine (**m12**), desipramine (**m11**) and desmethylsertraline (**m5**) are incorrectly predicted by about one order of magnitude. This problem disappears when more components are added to the model. However, due to the risk of overtraining the system the less complex model was chosen, accepting a less perfect correlation. Furthermore the contour map for the model with only three components is much more conclusive.

Table 4-1: Summary of CoMFA and CoMSIA analyses results

								Fraction in %		
Biological Target	Model	q^2	s_{PRESS}	N_{PC} [h]	r^2	SE	F	steric	electrostatic	hydrophobic
SERT	CoMFA	0.538	1.118	3	0.929	0.437	65.80	0.355	0.645	-
	CoMFA+RF [a]	0.674	0.940	3	0.932	0.430	68.13	0.435	0.565	-
	CoMSIAse [b], [c]	0.531	1.127	3	0.916	0.478	54.28	0.293	0.761	-
	CoMSIAs [b]	0.637	0.991	3	0.860	0.615	30.78	1.000	-	-
	CoMSIAe [c]	0.547	1.040	1	0.736	0.793	47.47	-	1.000	-
	CoMSIAh [d]	0.508	1.083	1	0.727	0.807	44.29	-	-	1.000
	CoMSIAda [e], [f]	0.354	1.242	1	0.645	0.920	30.93	-	-	-
	CoMSIAseh [b], [c], [d]	0.529	1.129	3	0.920	0.464	57.75	0.174	0.527	0.299
	CoMSIAall [g]	0.456	1.213	3	0.957	0.341	111.45	0.101	0.278	0.165
NET	CoMFA	0.445	1.028	2	0.829	0.571	33.85	0.322	0.678	-
	CoMSIAse [b], [c]	0.502	0.973	2	0.785	0.639	25.61	0.184	0.816	-
	CoMSIAh [d]	0.322	1.179	3	0.873	0.510	29.85	-	-	1.000
	CoMSIAseh [b], [c], [d]	0.505	1.007	3	0.887	0.482	33.89	0.125	0.549	0.326
Affinity	CoMFA	0.279	1.495	2	0.782	0.822	25.09	0.341	0.659	-
Differences	CoMFA+RF [a]	0.453	1.303	2	0.826	0.735	33.13	0.533	0.467	
	CoMSIAse [b], [c]	0.289	1.485	2	0.704	0.958	16.63	0.210	0.790	-

[a] RF = Region Focusing [b] s = sterics [c] e = electrostatics [d] h = hydrophobics [e] d = hydrogen-donating [f] a = hydogen-accepting [g] all = sehda [h] N_{PC} = number of Principal Components

Table 4-2: Experimental binding affinities, affinity differences, and residuals of fitted binding affinities

	Biological Data			Serotonin Transporter (SERT)			Norepinephrine Transporter (NET)		Selectivity Analysis		
	$pK_{i\,exp.}$ [a]		$\Delta pK_{i\,exp.}$ [c]	$pK_{i\,exp.}$ [a] - $pK_{i\,fit}$ [b]			$pK_{i\,exp.}$ [a] - $pK_{i\,fit}$ [b]		$\Delta pK_{i\,exp.}$ [c] - $\Delta pK_{i\,fit}$ [d]		
compound	SERT	NET		CoMFA	CoMFA+RF[e]	CoMSIAse[f],[g]	CoMFA	CoMSIAse[f],[g]	CoMFA	CoMFA+RF[e]	CoMSIAse[f],[g]
citalopram **(m1)**	8.82	5.10	3.72	-0.06	-0.28	0.02	-0.31	0.15	0.19	0.17	-0.32
fluoxetine **(m2)**	9.05	6.11	2.94	0.05	-0.03	-0.11	0.76	0.69	-0.59	0.09	-0.59
norfluoxetine **(m3)**	8.64	5.40	3.24	-0.17	0.02	-0.37	0.09	0.07	-0.25	0.31	-0.30
sertraline **(m4)**	9.82	6.09	3.73	0.49	0.80	0.76	0.07	-0.10	0.81	0.75	1.39
desmethylsertraline **(m5)**	8.43	6.09	2.34	-0.61	-0.29	-0.46	0.17	-0.14	-0.49	-0.47	0.11
paroxetine **(m6)**	10.19	7.07	3.12	-0.31	-0.45	0.03	0.09	0.02	0.52	-0.40	0.85
fluvoxamine **(m7)**	8.80	5.53	3.27	0.09	0.08	-0.08	-0.01	0.71	0.03	-0.03	-0.62
venlafaxine **(m8)**	8.12	5.64	2.48	-0.09	0.05	0.04	-0.09	-0.63	0.08	-0.68	0.80
O-desmethylvenlafaxine **(m9)**	8.11	5.56	2.55	0.06	0.23	-0.04	-0.29	-0.62	0.38	-0.02	0.73
imipramine **(m10)**	8.89	7.70	1.19	0.01	-0.25	-0.02	-0.43	-0.57	0.91	1.22	0.96
desipramine **(m11)**	7.66	9.20	-1.54	-0.93	-0.93	-1.04	1.02	1.01	-1.67	-1.31	-1.76
chloroimipramine **(m12)**	10.30	n.d.[h]	-	1.02	0.64	1.07	-	-	-	-	-
amitriptyline **(m13)**	8.55	7.72	0.83	0.35	0.30	0.34	-0.93	-0.50	1.39	0.78	0.86
nortriptyline **(m14)**	7.82	8.74	-0.92	0.07	0.11	-0.12	0.43	0.80	-0.48	-0.57	-1.01
m-CPP **(m15)**	6.69	5.71	0.98	0.09	0.25	0.10	0.18	0.01	-0.75	-0.28	-0.79
nefazodone **(m16)**	6.34	6.21	0.13	0.19	0.19	0.00	0.25	0.26	-0.37	-0.24	-0.54
hydroxynefazodone **(m17)**	5.99	6.18	-0.19	-0.16	-0.11	-0.11	0.16	0.09	-0.63	-0.52	-0.71
triazoledione **(m18)**	4.46	4.00	0.46	-0.04	-0.40	0.23	-	-	-	-	-
trazodone **(m19)**	6.60	4.43	2.17	-0.07	0.10	-0.22	-1.16	-1.26	0.92	1.21	0.95

[a] $pK_{i\,exp.}$ = negative logarithm of the experimental equilibrium inhibition constant [b] $pK_{i\,fit}$ = negative logarithm of the fitted equilibrium inhibition constant [c] $\Delta pK_{i\,exp.} = pK_{i\,exp.}(SERT) - pK_{i\,exp.}(NET)$ [d] $\Delta pK_{i\,fit} = pK_{i\,fit}(SERT) - pK_{i\,fit}(NET)$ [e] RF = Region Focusing
[f] s = sterics [g] e = electrostatics [h] n.d.= not determined

Helpful in this respect was also the X loading contour diagram which is retrievable from QSAR analysis by the *"XLoadings_from_PLS"* field. The fields show the loadings on each PLS component and can also be used to identify the meaning of each component. Up to the third component new descriptors are added whereas only redundancy and inconsistent results were observed from the forth components onwards, indicating that merely noise had been modelled. This confirms that the choice of using only three components for the model is appropriate. The X loading contour diagrams for each of the three components of the CoMFA model for the SERT are shown and discussed in **Chapter 4.2.3**.

For the CoMFA model derived from affinity data at the NET, triazoledione (**m18**) was excluded from the training series. As triazoledione (**m18**) proved to be inactive in biological testing (K_i given as > 100 μmol/l in [34]) but was predicted to be active in the 10 μmol/l range by CoMFA (data not shown), a detrimental bias on model statistics can be expected. As a result of excluding triazoledione (**m18**), the q^2-value for the NET model increased from 0.364 at 2 components (data not shown) to 0.445 at 2 components.

In addition to LOO cross-validation, cross-validation in groups was carried out for affinity data at the SERT. The training set was divided into four equally sized groups and the compounds were randomly assigned to one of these groups. One group was dropped when deriving the model and used for prediction. For reasons of computing time, column filtering (2 kcal/mol) was applied and the procedure was repeated ten times. This resulted in similar q^2-values compared to the corresponding LOO results. The q^2-values ranged from 0.436 to 0.635.

Scrambling the biological data and performing a cross-validation afterwards is commonly used to check the consistency of the model as

this allows detection of possible chance correlations. After randomising the data several times only negative or very small positive q^2-values were observed for both the SERT and the NET, showing model consistency. The q^2-values ranged from -1.269 to 0.044 for scrambled SERT data and from -0.764 to 0.169 for scrambled NET data.

To improve the predictability of the models region focusing was tried. According to [84], a model improvement should only be trusted if the q^2-value increases by at least 10%. In the present work, this was the case for the SERT model only. Whereas the q^2-value for the SERT increased from 0.538 to 0.674 at 3 components, there was only a small increase from 0.445 to 0.457 at 2 components for the NET. Thus, a final non cross-validated model using region focusing was only derived for the SERT. The same number of components as in the original model was used so that the results were directly comparable. Additional application of tightened grid spacing and column filtering as suggested in [76] did not markedly improve the results. However, applying region focusing to clearly senseless models derived from scrambled data also considerably increased q^2-values, now ranging from -0.416 to 0.102 for scrambled SERT data. Thus, improved statistics as a result of region focusing need to be handled with care.

The external predictive power of a 3D QSAR model is ideally checked by means of an appropriate test set but the chosen training set of 19 compounds was too small to spare any structures for a reasonable test set. Instead, affinity data of several SERT ligands measured in test systems different from the one used for the training set were predicted in the correct order of magnitude for both the SERT and the NET as detailed in **Chapter 4.3.3**.

4.2.2 CoMSIA Models for the SERT and the NET

Statistical data of the CoMSIA models for the SERT and for the NET is summarised in **Table 4-1**. Experimental binding affinities and the residuals of the final non cross-validated models are shown in **Table 4-2**.

Applying CoMFA and CoMSIA to the same datasets usually results in models of similar statistical significance as demonstrated by Klebe et al. [64]. The present work confirms these findings when comparing the q^2-value of 0.538 for CoMFA and 0.531 for CoMSIA for the SERT considering only sterics and electrostatics. Again, cross-validation in groups was performed in addition to LOO cross-validation for affinity data at the SERT, yielding q^2-values ranging from 0.456 to 0.630.

Various CoMSIA studies experimenting with different combinations of steric and electrostatic fields, hydrophobic fields and hydrogen bond donor and acceptor fields were carried out. Almost all combinations yielded similar q^2-values, supporting the finding of Böhm et al. [65] that there must be more or less the same information hidden in the different fields regarding the quantitative explanation of binding affinity, and thus, no improvement of model statistics is to be expected. For the SERT, the best q^2-value of 0.637 was obtained when applying steric fields only, the second best q^2-value of 0.547 when applying electrostatic fields only. Applying sterics and electrostatics, or sterics, electrostatics and hydrophobics together yielded comparable q^2-values of 0.531 and 0.529. The q^2-value decreased when combining all five field types (q^2 = 0.456). It has to be noted, though, that CoMSIA studies considering hydrogen bonding fields alone were done with the protonated structures as the protonated nitrogen is supposed to be of importance in ligand binding [28]. This is supported by the fact that considering hydrogen donating properties with the non-protonated

structures yielded very poor q^2-values. The correlation plot of $pK_{i\ fit}$ versus $pK_{i\ exp.}$ of the final non cross-validated CoMSIA model considering sterics and electrostatics is shown in **Figure 4-7**.

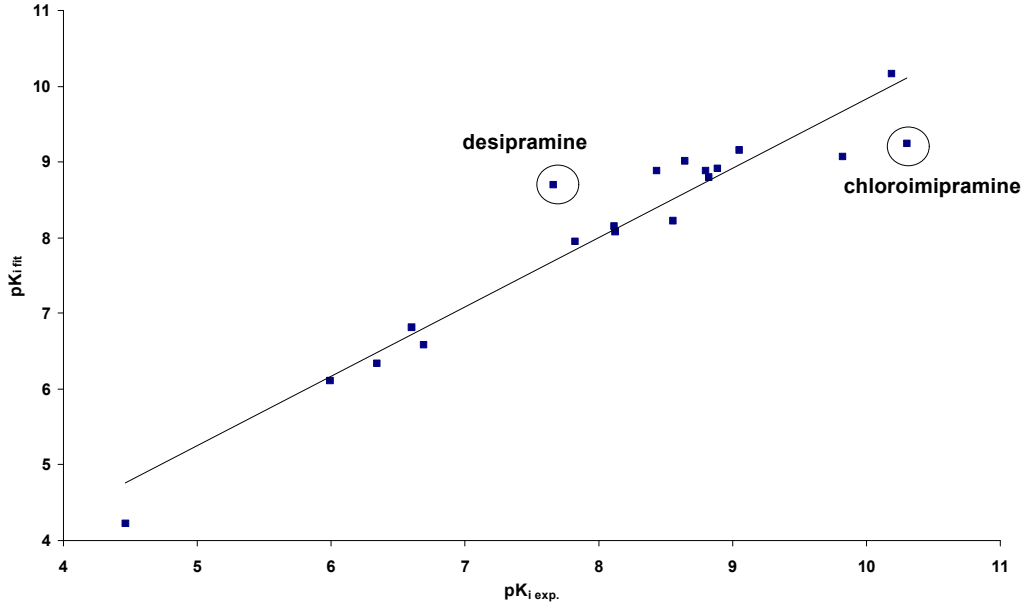

Figure 4-7: Non cross-validated CoMSIA analysis considering sterics and electrostatics at the SERT: correlation plot of $pK_{i\ fit}$ versus $pK_{i\ exp.}$ with r^2 = 0.916, SE = 0.478, F = 54.28. The fit for chloroimipramine and desipramine is deviating by more than one order of magnitude.

The CoMSIA analysis for the NET considering sterics and electrostatics yielded a q^2-value of 0.502. The CoMSIA analysis for the NET using hydrophobics yielded a q^2-value of 0.322. The CoMSIA analysis of hydrogen bonding properties yielded a rather poor q^2-value, and is thus discounted and not discussed further.

4.2.3 Discussion of the Contour Plots

CoMFA and CoMSIA results were graphically interpreted by field contribution maps. Coefficient contour maps using the field type *"StDev*Coeff"* were generated. To select the appropriate contour levels for each feature, the respective histograms of actual field values were analysed. Contour levels that produced chemically meaningful contour maps were chosen. Whereas the contour maps of CoMFA models highlight those regions in space where the aligned molecules would favourably or unfavourably interact with a possible environment, the contribution maps obtained by the CoMSIA approach denote those areas within the region occupied by the ligands that ´favour´ or ´dislike´ the presence of a group with a particular physico-chemical property [64]. The latter is said to be a much more intuitive guide when designing new ligands. Only CoMSIA plots for hydrogen bonding properties are contoured in a way similar to the CoMFA maps, denoting areas where donor or acceptor groups should be located within the putative receptor. Contour diagrams of the CoMFA and CoMSIA models considering sterics and electrostatics are shown for the SERT in **Figure 4-8**, and for the NET in **Figure 4-9**. Added to the maps are *(S)*-citalopram (**m1**) and desipramine (**m11**) as examples for substances displaying high affinity and high selectivity for the respective transporter. As the contour diagrams derived from CoMFA and CoMSIA are very much alike they will be discussed together.

Analysing the contour plots for the SERT reveals three regions in the CoMFA plot where steric bulk enhances affinity. This is the green area around the substituent at the primary aromatic moiety R1, the green area around the aromatic moiety R2, and the green area into which the methyl group of many N-methylated substances with high affinity to the

SERT is orientated. The latter finding is clearly alignment-dependent as the orientation of the N-methyl groups of the various substances was carefully contemplated when actually doing the alignment.

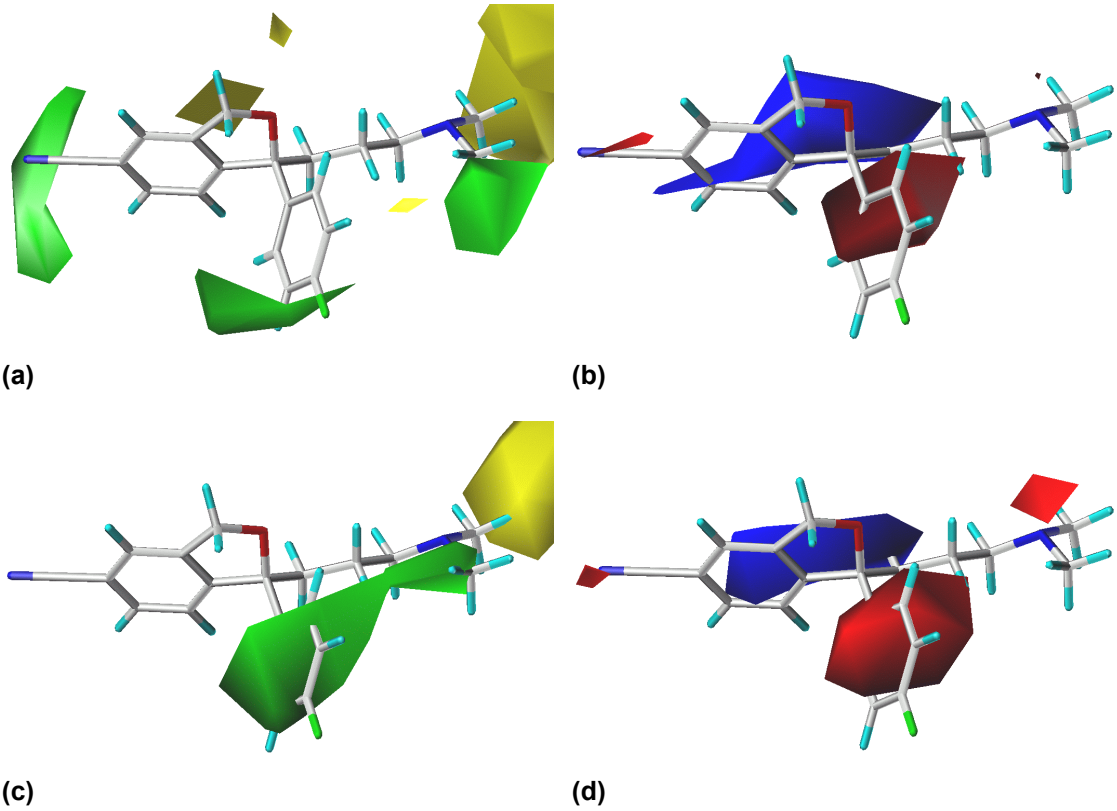

Figure 4-8: CoMFA (**(a)**, **(b)**) and CoMSIA (**(c)**, **(d)**) *"StDev*Coeff"* plots for the serotonin transporter denoting steric (**(a)**, **(c)**) and electrostatic (**(b)**, **(d)**) features. The contour levels were derived by examining the field value histograms. *(S)*-Citalopram is shown within the fields. **(a), (c)** Green areas indicate regions where steric bulk favourably effects binding affinity. Yellow regions denote areas in which sterically demanding groups have got a detrimental effect on binding affinity. **(b), (d)** Blue contours enclose areas where more positive charges increase binding affinity, whereas in the regions enclosed by red contours, more negative charges are favoured.

The CoMSIA contour plot for the SERT also shows a large green region spanning from R2 to the N-methyl group, but unexplicably does not reveal any green region at R1. The areas indicated by yellow contours should be sterically avoided, otherwise reduced affinity can be

expected. The large yellow region visible in both the CoMFA and the CoMSIA plot extending far beyond the alkyl side chain (not completely shown in **Figure 4-8**) can be attributed to the phenylpiperazines; these are aligned in a way that their long residues attached to the phenylpiperazine moiety are pointing to that region. The model ascribes their low affinity at the SERT to this long residue by which they can be clearly differentiated from any other SERT ligands. Obviously, this is also alignment-dependent.

Blue areas represent regions where electron-deficiency is advantageous. One large blue region can be seen in both plots for the SERT around the primary aromatic moiety R1. This can be attributed to ring substituents with a strong electron-withdrawing effect as for instance the cyano group in *(S)*-citalopram (**m1**). Interestingly, this area is only visible when working with non-protonated compounds as opposed to N-protonated compounds. A possible explanation is the influence of the highly charged protonated nitrogen that obscures other important electrostatic contributions. The red contoured area between R1 and R2 shows that partial negative charge is important at this part of the molecules for high binding affinity. Another red region can be detected around the ring substituent at R1, which consequently, should be an electronegative substituent if high affinity is desired. This finding is in agreement with the work of Rupp et al. [29]. The red region near the pharmacophoric nitrogen of *(S)*-citalopram (**m1**) needs to be handled with care, of course, as one must consider the fact that it is most likely that the compounds bind to the SERT in their N-protonated state and not in their non-protonated state as assumed in this model for the reasons outlined in **Chapter 4.2.1**. Surprisingly, no red area is found near the oxygen in *(S)*-citalopram´s (**m1**) dihydrofuran ring, although both *(S)*-fluoxetine (**m2**) and paroxetine (**m6**) also orientate their oxygen atoms into that area and an oxygen in this region is

considered to be of some importance in high affinity binding at the SERT [28].

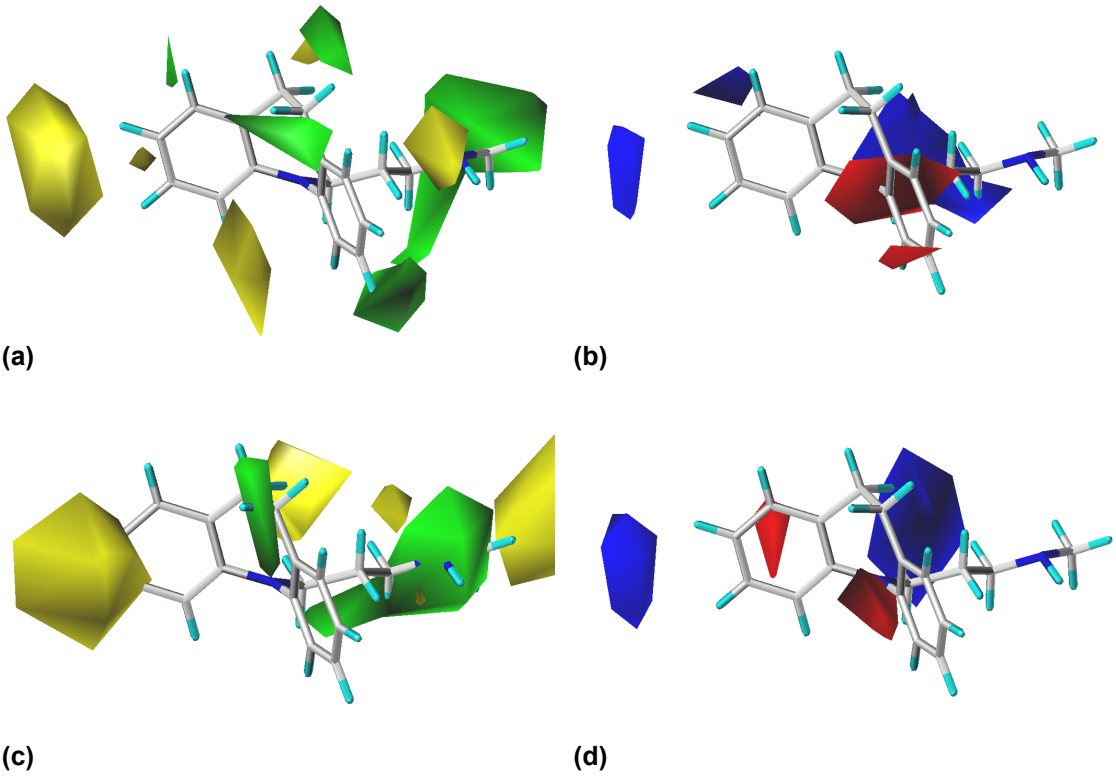

Figure 4-9: CoMFA (**(a)**, **(b)**) and CoMSIA (**(c)**, **(d)**) *"StDev*Coeff"* plots for the norepinephrine transporter denoting steric (**(a)**, **(c)**) and electrostatic (**(b)**, **(d)**) features. The contour levels were derived by examining the field value histograms. Desipramine is shown within the fields. **(a), (c)** Green areas highlight those regions where steric bulk enhances binding affinity, whereas yellow regions denote those areas where steric bulk has got a detrimental effect on binding affinity. **(b), (d)** Blue contoured areas show regions where more positive charges are favourable for binding affinity, whereas within the red areas more negative charges are favoured.

When analysing the contour plots for NET ligands, three distinct green regions were observed in the CoMFA plot where steric bulk is favourable for binding affinity. The first is the area in which the methyl group of many ligands with high affinity to the NET is located as demonstrated by desipramine (**m11**) in **Figure 4-9**. This is also

alignment-dependent as discussed above for SERT ligands. The second (consisting of two separated areas in the CoMFA plot) is a region occupied by the ethylene bridge connecting the two aromatic moieties of the TCAs. This region corresponds to the area found by Gundertofte et al. [28], in which substitution is prohibited for high SERT binding affinity, and whose occupation enhances norepinephrine reuptake inhibition. The third green region is an area around the secondary aromatic moiety R2. However, it is not typical for NET ligands only, as the presence of a secondary aromatic moiety or a bulky substituent is also a necessary prerequisite for high affinity binding at the SERT. In accordance with this, no green region around R2 is visible in the CoMSIA plot. Various yellow regions that should be sterically avoided can be seen. One of them clearly shows that large substituents at R1 should be avoided for high affinity at the NET. The regions encompassed by red contours show areas where partial negative charges are favourable for binding affinity. A red region around the primary aromatic moiety R1 indicates that the aromat should be electron-rich for high binding affinity at the NET. This is an important distinguishing feature from high affinity SERT ligands as these require an electron-deficient aromat in this position. Another red area can be seen in the CoMFA plot around the secondary aromatic moiety, indicating that a partial negative charge is favourable here. A third red area is the region that is occupied by a nitrogen or an sp_2-hybridized atom in the case of the TCAs.

A CoMFA plot was derived for the SERT model that had been submitted to region focusing (not shown here). When the weights are *“StDev*Coefficient”* values, the process is exactly equivalent to image enhancement [76]. As expected, the focused fields appear much more sparse. Surprisingly, the green region related to R2 is suppressed in the SERT model submitted to region focusing. Any other fields

discussed above can still be seen, showing their importance for high affinity binding.

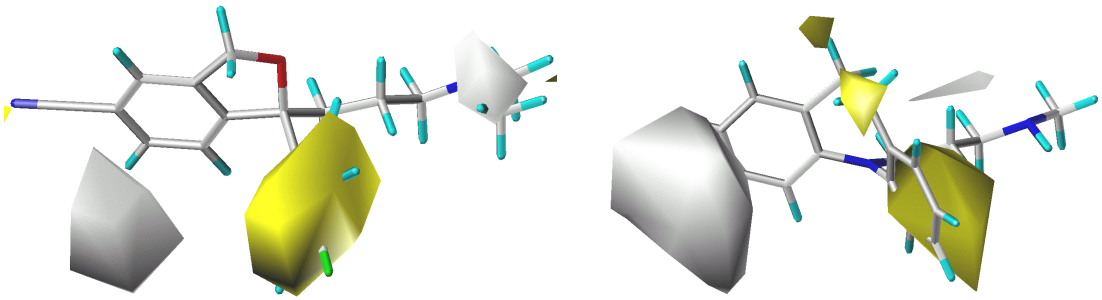

(a) **(b)**

Figure 4-10: CoMSIA *"StDev*Coeff"* contour plots illustrating hydrophobic features at the serotonin transporter (**(a)**) and at the norepinephrine transporter (**(b)**). *(S)*-Citalopram and desipramine are shown within the fields. Yellow contoured regions show areas in which hydrophobic groups favourably effect binding affinity, whereas in white contoured regions hydrophobic groups have got an unfavourable effect on binding affinity.

Figure 4-10 shows the hydrophobic plots for the SERT and the NET derived from the CoMSIA models considering hydrophobics only. The yellow areas denote regions in which hydrophobic groups are favourable for high affinity binding, whereas the light grey areas highlight regions in which such groups have got a detrimental effect on binding affinity. The CoMSIA map for the SERT reveals that the substituent at the primary aromatic moiety R1 should be hydrophobic as should be those parts of the molecule located at the R2 site. The CoMSIA plot for the NET also shows a large yellow region at the R2 site, indicating that lipophilic partial structures are favourable here. Another yellow region can be seen in the area in which the ethylene bridge of the TCAs is located.

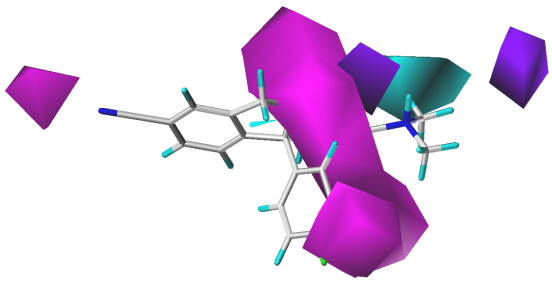

Figure 4-11: CoMSIA *"StDev*Coeff"* contour plot showing hydrogen bond donor and hydrogen bond acceptor properties at the serotonin transporter. *(S)*-Citalopram is shown within the fields. In the magenta contoured areas, hydrogen bond donors would be favourably located in a hypothetical receptor, i.e. hydrogen bond accepting groups in the aligned molecules would favourably point towards these areas. Cyan contoured areas highlight those regions in space in which hydrogen bond acceptors would be favourably located in a putative receptor. Purple contoured areas show regions that are unfavourable for hydrogen bond accepting groups in a putative receptor.

Figure 4-11 shows the map for hydrogen bonding properties for the SERT derived from the N-protonated structures. Cyan contours highlight areas in which hydrogen-bond acceptors would be favourably located in a putative receptor. Paroxetine (**m6**) and *(S)*-fluoxetine (**m2**) are directing one of their nitrogen protons towards this area. For *(S)*-citalopram (**m1**) this is actually not the case as can be seen in the figure. Obviously this is compensated by the combination of other favourable features. In the magenta contoured areas, hydrogen bond donors would be favourably located in a putative receptor. The cyano group in *(S)*-citalopram (**m1**) for instance could act as such a hydrogen bond accepting group. Another feature displaying hydrogen bond accepting properties is the oxygen atom present in paroxetine (**m6**), *(S)*-fluoxetine (**m2**) and *(S)*-citalopram (**m1**) to which had been ascribed a pharmacophoric function [28] as discussed before. However, the magenta region around R2 is difficult to explain and seems less convincing.

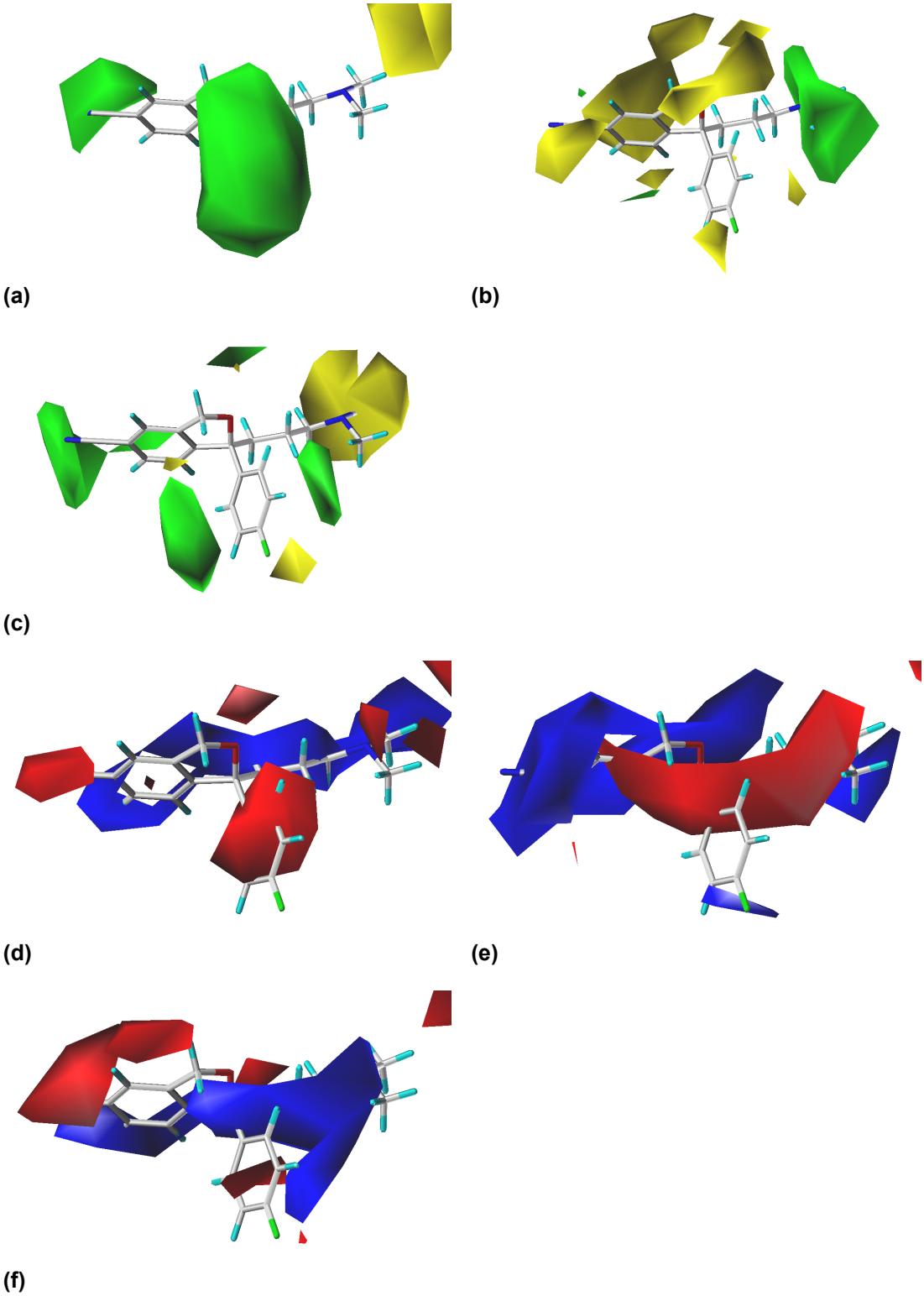

Figure 4-12: CoMFA *"XLoadings_from_PLS"* contour plots for the SERT, denoting those steric (**(a)**, **(b)**, **(c)**) and electrostatic (**(d)**, **(e)**, **(f)**) variables that are "loaded" on each of the three PLS components (PC1: **(a)** and **(d)**, PC2: **(b)** and **(e)**, PC3: **(c)** and **(f)**). *(S)*-citalopram is shown within the fields.

As described in **Chapter 4.2.1**, X loading contour diagrams for both the CoMFA and the CoMSIA models for the SERT were derived by retrieving the *"XLoadings_from_PLS"* fields. As the diagrams were similar for CoMFA and CoMSIA, only the X loadings for the CoMFA analysis are shown in **Figure 4-12**. When comparing the individual contour diagrams one realises that many of the important features necessary for high SERT binding affinity that were discussed earlier can be found on the first PLS component. For instance, sterically demanding groups with partial negative charges are favourable as substituents at R1, and the presence of R2 is important. Some other features are added with the second and third component. The presence of one of the methyl groups at the pharmacophoric nitrogen is favourable for high SERT binding affinity whereas the presence of the other one seems to be unfavourable. Thus, additional important information is disclosed.

4.2.4 Selectivity Analysis

To better explain the selectivity-discriminating criteria, a selectivity analysis was performed as described in **Chapter 3.6.4**. Since triazoledione (**m18**) had been removed from the training set for the NET model, it consequently was not considered in the selectivity analysis. Applying both the CoMFA and the CoMSIA method yielded comparable q^2-values of 0.279 and 0.289. Statistical data of the selectivity CoMSIA models is summarised in **Table 4-1**. Experimental binding affinities and the residuals of the final non cross-validated models are shown in **Table 4-2**. Obviously, statistics are not expected to be as good as for the SERT and the NET model alone, because the affinity differences are associated with a higher experimental uncertainty due to error propagation [65]. However, model statistics

could be improved by applying region focusing to the CoMFA model, resulting in a statistically significant model with a q^2-value of 0.453. One clear shortcoming of the selectivity model is the poor fitted prediction of desipramine (**m11**). Whereas desipramine (**m11**) is a clearly NET selective substance, it is predicted by the CoMFA and CoMSIA final non cross-validated models as being SERT selective. Only the CoMFA model enhanced by region focusing predicts desipramine (**m11**) as being NET selective, but still in a wrong order of magnitude. Apart from this the selectivity analysis led to reasonable and well interpretable results. The outcome of the CoMFA and the CoMSIA plots is very similar, and for this reason, the results for the CoMSIA study are discussed only. The CoMSIA contour plot is shown in **Figure 4-13**. The contour plot clearly reveals those steric and electrostatic features that are important for selectivity at the SERT over the NET. One of the green regions, which require sterically demanding groups, is stretching out from R2 towards one of the N-methyl groups as observed before in the CoMSIA plot for the SERT, although in the selectivity plot, the methyl group is not actually included in the green contoured area. Thus, occupation of this area is obviously not a necessary criterion for SERT selectivity. This becomes clear when thinking of sertraline (**m4**), which, in the present alignment, does not fill this particular space, although it displays high selectivity for the SERT. The other green contoured region is found at a position into which substituents at the primary aromatic moiety R1 of selective SERT ligands extend, like the cyano group of *(S)*-citalopram (**m1**). It can be concluded that the presence of such a substituent is a necessary requirement for SERT selectivity. Moreover, this substituent needs to be electronegative as indicated by the red contoured region. This inevitably results in an electron-deficient aromatic moiety R1, which is highlighted by blue contours. Thus, these latter features are not only

important for high affinity at the SERT, but also for high selectivity at the SERT over the NET. Interestingly, another red region indicating negative charge to be favourable can be seen just above the oxygen atom of the dihydrofuran ring of *(S)*-citalopram (**m1**). This was expected to be seen earlier as discussed for the SERT CoMFA model. So obviously the presence of a group or atom possessing partial negative charges, as for instance the oxygen in paroxetine (**m6**) or *(S)*-fluoxetine (**m2**), is important when discussing selectivity criteria.

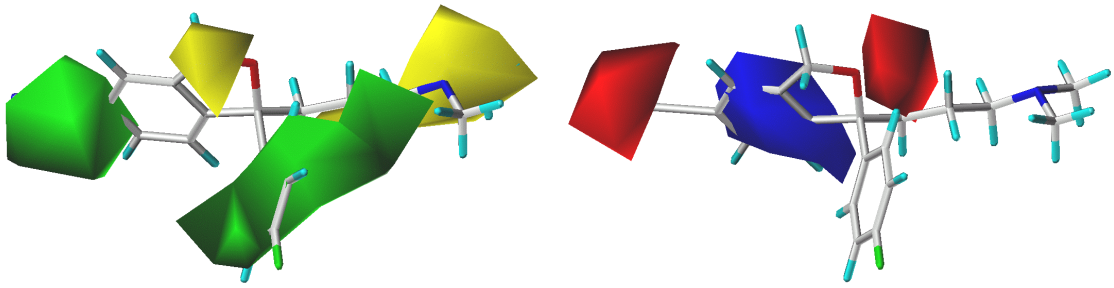

(a) **(b)**

Figure 4-13: CoMSIA *"StDev*Coeff"* contour plot illustrating steric (**(a)**) and electrostatic (**(b)**) selectivity features derived from the affinity differences between the serotonin transporter (SERT) and the norepinephrine transporter (NET). *(S)*-Citalopram is shown as an example of a highly SERT selective compound. **(a)** Areas enclosed by green contours show regions where steric bulk enhances selectivity at the SERT over the NET, whereas sterically demanding groups within yellow regions decrease selectivity. **(b)** More positive charges are favourable for SERT selectivity in blue contoured regions. Red areas denote regions where more negatively charged groups have got a favourable effect on SERT selectivity.

Two areas are highlighted by yellow contours. One of them is the region into which the methyl group extends that was found earlier to be of importance in high affinity binding at the NET. Clearly, the occupancy of this region with bulky substituents has got a detrimental effect on SERT selectivity. Equally, occupancy of the region in which the ethylene group that is bridging the two aromatic rings in the TCAs

is found, has a negative effect on SERT selectivity as indicated by the second yellow region in **Figure 4-13**.

Hydrophobicity was not considered in the selectivity analysis as the hydrophobicity contour plots for the SERT and for the NET were very similar. Thus, no reasonable selectivity analysis was to be expected. Hydrogen bonding properties were not considered in the selectivity analysis as no conclusive models for the NET had been developed, and thus analysing selectivity using these properties would not be meaningful.

4.3 Design and Prediction of Novel Compounds

4.3.1 General Approach

As various N,N-dimethyl-2-phenylsulfanyl-benzylamines had turned out to be promising PET ligands for the SERT, the endeavour was to find even more suitable substances of this type. To structurally modify the lead compound **DASB** (**Figure 1-3**), knowledge on SARs of serotonin transporter ligands derived from the CoMFA and CoMSIA models was employed. It should be noted at this point that the phenyl rings of these diphenyl sulphides are termed ring A and ring B according to Sindelar et al. [96] and Emond et al. [25]. Ring B corresponds to R1 of the Gundertofte model [28], and ring A corresponds to R2. In **Figure 4-14**, **DASB** is shown within the steric and electrostatic CoMFA fields for the SERT. The three green regions reveal those areas where steric bulk enhances affinity. The substituent in **DASB**´s position 4´ at ring B and the area around ring A are located here, as well as the area into which one of **DASB**´s N-methyl groups is orientated. The areas indicated by

yellow contours should be sterically avoided, otherwise reduced affinity can be expected. **DASB** does not occupy these areas.

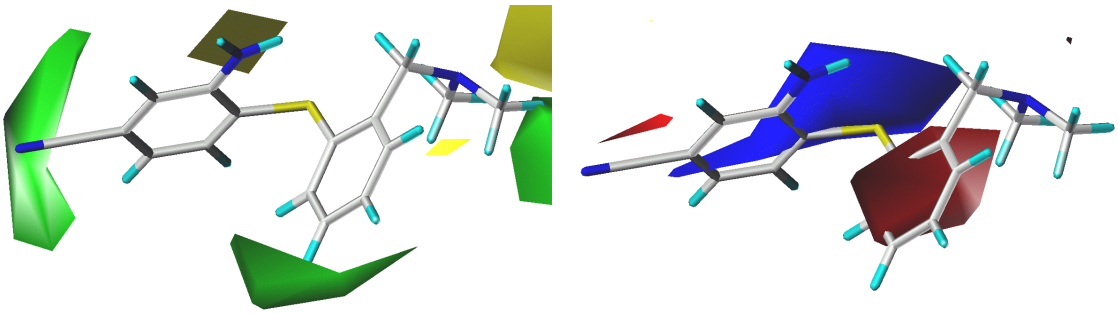

(a) **(b)**

Figure 4-14: DASB within the steric **(a)** and electrostatic **(b)** *"StDev*Coeff"* CoMFA fields for the SERT. Green regions show areas where steric bulk enhances binding affinity, whereas steric bulk has got a detrimental effect on binding affinity in yellow regions. Partial positive charges are favourable in blue regions, and partial negative charges are favourable in red regions.

A blue area, which represents a region where electron-deficiency is advantageous, can be seen around ring B. This can be attributed to ring substituents with a strong electron withdrawing effect as for instance the cyano group in **DASB**. In regions enclosed by red areas, more negative charges are favoured. One red area is found at ring A, another red area is seen around **DASB**´s cyano group, showing that an electronegative substituent is favourable here. The fact that **DASB** is a compound displaying high affinity at the SERT is well illustrated by the CoMFA contour map. Therefore the contour diagrams prove useful when designing new SERT ligands from the N,N-dimethyl-2-phenylsulfanyl-benzylamine scaffold. Moreover, known SARs of these diphenyl sulphides were considered during structural modification, as well as the concept of bioisosterism in drug design. Additionally, structures were automatically suggested by using *SYBYL´s* Optimize QSAR module [67] (cp. **Chapter 3.6.5**).

Table 4-3: Experimental and predicted binding affinities of diphenyl sulphides

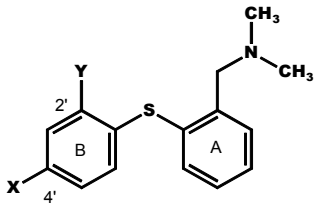

			SERT			NET		
Compound	**X**	**Y**	**$K_{i\ pred.}$ CoMFA (nM)**	**$K_{i\ pred.}$ CoMSIA (nM)**	**$K_{i\ exp.}$ (nM)**	**$K_{i\ pred.}$ CoMFA (nM)**	**$K_{i\ pred.}$ CoMSIA (nM)**	**$K_{i\ exp.}$ (nM)**
DASB	NC-	NH_2-	1.34	1.65	1.1 [a)]	3715	2188*	1350 [a)]
ADAM	I-	NH_2-	2.25	1.23*	0.40 [b)]	1259	288	683 [d)]
s2	Br-	NH_2-	2.47	1.56*	0.37 [c)]	1122	282	107 [d)]
s3	Cl-	NH_2-	2.50	1.74*	0.27 [a)]	1148	316	230 [a)]
s4	F-	NH_2-	2.07	1.82	4.8 [b)]	1514	550	137 [b)]
MADAM	H_3C-	NH_2-	2.82	2.34	0.43 [c)] (1.65 [d)])	102	468	325 [d)]
s5	H_3CO-	NH_2-	1.54	1.70*	1.89 [a)]	794	288	1992 [a)]
s6	F_3C-	NH_2-	0.57	0.97	0.33 [a)]	8318	4365	1205 [a)]
s7	FCH_2-	NH_2-	1.66	1.45	1.8 [b)]	1000	209	97 [b)]
s8	CH_3CH_2-	NH_2-	2.60	1.99*	0.17 [c)]	661	117	367 [c)]
s9	FCH_2CH_2-	NH_2-	2.60	2.72	3.4 [b)]	562	126	809 [b)]
s10	CH_2=CH_2-	NH_2-	3.29	1.77*	2.74 [c)]	759	219	-
s11	$FCH_2CH_2CH_2$-	NH_2-	3.30	2.48	11.0 [c)]	575	81	219 [c)]
IDAM	I-	$HOCH_2$-	0.98	0.79*	0.98 [d)]	513	240	12.8 [d)]
s12	I-	CH_3OCH_2-	2.54	1.89*	2.50 [d)]	2239	537	212 [d)]
s13	Br-	CH_3OCH_2-	2.61	2.49	2.75 [d)]	2089	513	326 [d)]
s14	I-	FCH_2-	1.13	0.69	(0.003 [e)]) [h)]	759	537	-
s15	I-	F-	1.12	0.58*	(0.22 [e)]) [h)]	1862	1096	-
s16	Br-	F-	1.26	0.76	(0.12 [e)]) [h)]	1585	1047	-
s17	Cl-	F-	1.20	0.82	(0.33 [e)]) [h)]	1698	1202	-
ODAM	-	-	1.03	1.75*	2.8 [f)]	759	437	(20.0 [f)])
s18	-	-	1.42	1.98	> 1000 [g)]	1096	229	-

[a)] Wilson AA et al., J Med Chem 43, 3103-10 (2000) [b)] Huang Y et al., J Labelled Cpd Radiopharm 44 (1 Suppl), S18 (2001) [c)] Jarkas N et al., J Labelled Cpd Radiopharm 44 (1 Suppl), S204 (2001) [d)] Emond P et al., J Med Chem 45, 1253-58 (2002) [e)] Oya S et al., J Labelled Cpd Radiopharm 44 (1 Suppl), S15-16 (2001) [f)] Zhuang Z-P et al., J Labelled Cpd Radiopharm 42 (1 Suppl), S357-358 (1999) [g)] Oya S et al., J Labelled Cpd Radiopharm 82 (1 Suppl), S57 (1999) [h)] SERT expressed in LLC-PK_1 cells. $K_{i\ exp.}$ (IDAM): 0.097 nM, $K_{i\ exp.}$ (ADAM): 0.013 nM. Direct comparison of K_i-values seems questionable here.

* extrapolation > 0.3 log unit

4.3.2 SARs of Diphenyl Sulphides

SARs of various diphenyl sulphides as potential antidepressants were first described by Sindelar et al. [22, 96]. Whereas structure **s1** shows high binding affinity at both the SERT and the NET, **moxifetin**, additionally bearing a hydroxy group in position 3´, is SERT selective [97, 98]. Any further modifications at the moxifetin scaffold made by Sindelar et al. [22, 96] resulted in compounds possessing a substituent in position 3´. This changes with Ferris et al. [23] describing **403U76** as a new potential antidepressant inhibiting both the serotonin and norepinephrine reuptake. The 2´, 4´-substitution pattern seen in **403U76** was maintained throughout further ligand optimisation for SPECT and PET applications.

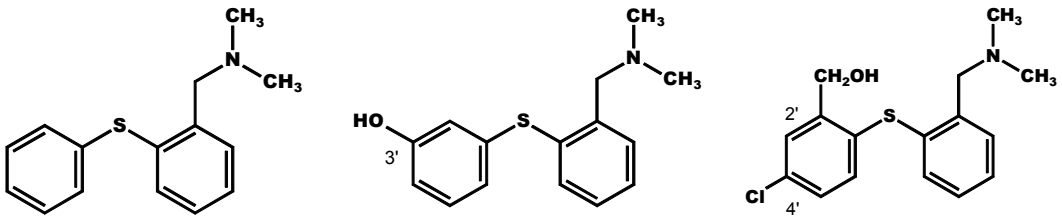

s1 **moxifetin** **403U76**

Figure 4-15: Molecular structures of s1, moxifetin and 403U76

A comprehensive overview of the SARs of 2´, 4´-substituted diphenyl sulphides is given by Emond et al. [25]. **Table 4-3** shows a collection of binding affinity data of diphenyl sulphides from literature.

The dimethylaminomethyl group in position 2 of ring A seems to be optimal although a monomethylaminomethyl group is also tolerated. At position 2´ of ring B, the SERT binding site tolerates quite a broad

range of functional groups containing a heteroatom, such as alcohol, ether, ester, nitro and amine functions. The nature of this group seems to be important for SERT selectivity. Whereas compounds containing a hydroxymethyl group in position 2´ (**IDAM**) display high binding affinity at both the SERT and the NET, compounds substituted with an amino group (**ADAM**) or a methoxymethyl group (**s12**, **s13**) in position 2´ are SERT selective [25]. Oya et al. [99] recently reported a new compound substituted with a fluorine-18 labelled fluoromethyl group in position 2´ (**s14)** displaying very high binding affinity at the SERT and also showing promising characteristics as a possible PET ligand. As no affinity data for the NET or the DAT is given, no conclusions about SERT selectivity can be drawn. Choi et al. [100] reported that a fluoro substitution is also tolerated in position 2´ (**s15**, **s16**, **s17**)**.** It was further reported that arylation and acylation of the amino group in position 2´ in most cases resulted in reduced binding affinity at the SERT. Regarding the 4´ position of ring B, Emond et al. [25] concluded that the nature of the substituent only slightly influences the SERT binding affinity, as for instance a fluorine, a bromine and a iodine atom seem to be interchangeable in this position. This is supported by the findings of Wilson et al. [21] showing that also a chlorine (**s3**), a trifluoromethyl (**s6**), a methoxy (**s5**) and a cyano (**DASB**) group in position 4´ display high SERT binding affinity. However, not all substituents are favourable as PET ligands. The trifluoromethyl group, for instance, is much too lipophilic, thus displaying a clearance from the cerebellum too slow for favourable pharmacokinetics in human PET studies [21]. According to Emond et al. [25], sterically demanding groups in position 4´ markedly decrease binding affinity at the SERT. However, Jarkas et al. [69] found that both an ethyl (**s8**) and an ethenyl (**s10**) group in position 4´ display good binding affinity at the SERT. Huang et al. [26] reported that a 2-fluoroethyl group in position 4´ (**s9**)

also displays a good binding affinity at the SERT but additionally, a moderate binding affinity at the NET.

Zhuang et al. [101] prepared an analogue of **IDAM** called **ODAM** with an oxygen instead of a sulphur bridge between the two phenyl rings as this was thought to be metabolically more stable.

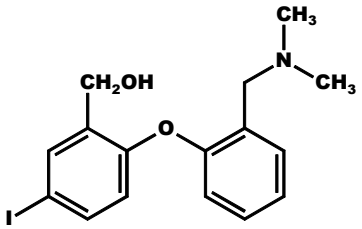

ODAM

Figure 4-16: Molecular structure of ODAM

ODAM showed high binding affinity at the SERT and moderate binding affinity at both the NET and the DAT. However, Acton et al. [102] concluded that, although **ODAM** seems to have a higher brain uptake than **IDAM** and indeed a slower metabolism, it also exhibits higher nonspecific binding than **IDAM,** which makes it less suitable as a PET ligand.

4.3.3 Comparison of Predicted and Experimental Binding Affinity

To check whether the CoMFA and CoMSIA models are suitable to predict SERT binding affinity of new diphenyl sulphides, the K_i-values of several diphenyl sulphides already synthesised and biologically tested were predicted. Predicted and experimental K_i-values for both the SERT and the NET are shown in **Table 4-3**. Additionally, predicted versus experimental pK_i values for the diphenyl sulphides are shown within the correlation plot of the CoMFA analysis for the SERT (**Figure 4-17**).

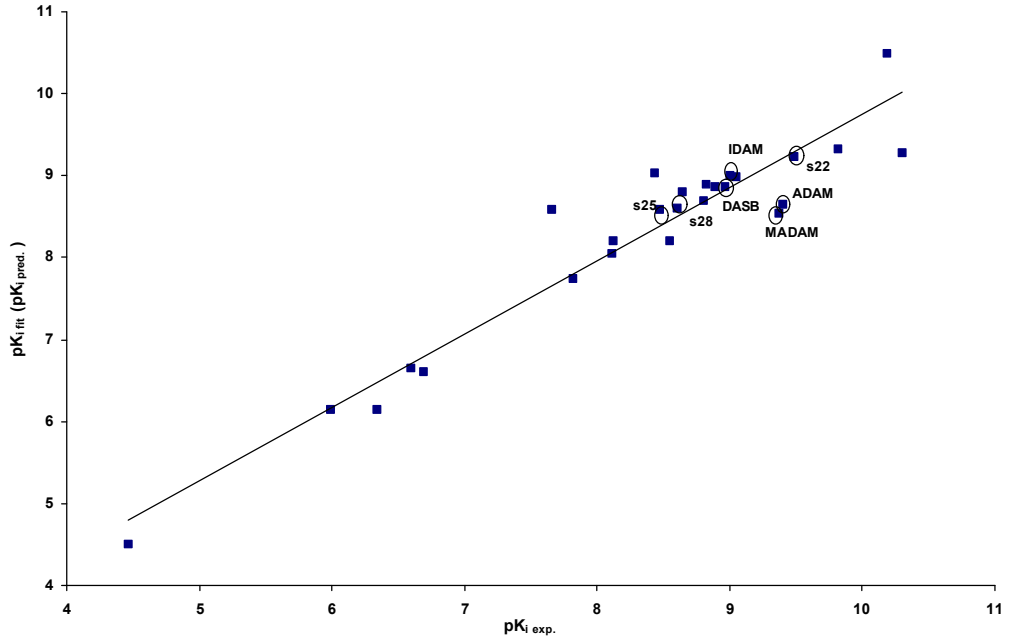

Figure 4-17: Predicted versus experimental pK_i values of seven diphenyl sulphides within the correlation plot of the non cross-validated CoMFA analysis for the serotonin transporter. ADAM and MADAM are predicted in the wrong order of magnitude, whereas DASB, IDAM, s22, s25 and s28 are correctly predicted.

Clearly, one has to be careful with comparison of data across laboratories. However, the comparison of K_i-values seems permissible as the K_i-value is an absolute value for a compound and is independent of the specific radioligand used and the concentration of radioligand in the assay [34]. For **DASB**, a K_i-value of 1.1 nM at the SERT and of 1350 nM at the NET was experimentally determined [21], showing that **DASB** is highly selective for the SERT. This is correctly predicted by the CoMFA and CoMSIA analyses, the predicted K_i-values being within the same order of magnitude as the experimentally determined ones with 1.34 nM (CoMFA) and 1.65 nM (CoMSIA) for the SERT, and 3715 nM (CoMFA) and 2188 nM (CoMSIA) for the NET. The K_i-values of compound **s9,** bearing a 2-fluoroethyl group in position 4´, are also predicted within the correct order of magnitude for both the SERT and the NET. This is of particular interest, as the 2-fluoroethly group is suitable for fluorine-18 labelling. This was shown only recently by Huang et al. [103] who prepared fluorine-18 labelled **s9**. However, judging from binding affinity data given in [26], compound **s9** is less SERT selective than **DASB**. This probably makes it less suitable as a PET radiotracer, although Huang et al. [103] were able to demonstrate high specificity during PET studies in rats and baboons. The binding affinity of **IDAM**, possessing a hydroxymethyl group in position 2´ and a iodine atom in position 4´, is correctly predicted as being in the sub-nanomolar range at the SERT, whereas the binding affinity at the NET seems to be underestimated by one order of magnitude. CoMSIA analysis appears to be performing better when looking at the K_i-values of **ADAM** and its fluorine (**s4**), bromine (**s2**) and chlorine (**s3**) analogues. The K_i-values for the NET are predicted in the correct order of magnitude by CoMSIA. However, binding affinity at the SERT seems to be underestimated by one order of magnitude by both CoMFA and CoMSIA. Compound **s14**, possessing a fluoromethyl group in position

2´ and a iodine atom in position 4´, is correctly predicted as displaying high binding affinity at the SERT, although binding affinity seems to be slightly underestimated. Compound **s14** is of particular interest as fluorine-18 labelling of the fluoromethyl group proved to be possible [99]. Binding affinity at the SERT of **ODAM**, differing from the other compounds by the oxygen which bridges the two phenyl rings, is also predicted in the correct order of magnitude by both CoMFA and CoMSIA. Nevertheless, SERT selectivity seems to be slightly overestimated by both models. Binding affinity at the SERT of the pyridinyl compound **s18**, for which Oya et al. [104] reported only weak binding affinity at the SERT, seems to be wrongly predicted by several orders of magnitude. This is, clearly, a shortcoming of the models.

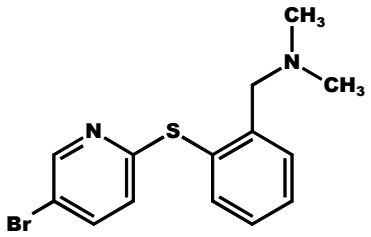

s18

Figure 4-18: Molecular structure of s18

Yet most of the tested diphenyl sulphides are correctly predicted by both CoMFA and CoMSIA, thus making the models suitable for the estimation of binding affinities for novel diphenyl sulphide structures. This also becomes clear from the correlation plot in **Figure 4-17**, showing the quality of the predictions.

4.3.4 Bioisosterism

The principle of bioisosteric replacement of functional groups is considered to be a successful optimisation strategy. Langmuir [105] introduced the concept of isosterism in 1919. Isosterism was at that time used to describe the similarity of molecules or ions which have the same number of atoms and valence electrons. This concept was extended by Grimm´s hydride displacement law [106], describing the similarity between groups of atoms which have the same number of valence electrons, but a different numbers of hydrogen atoms. For instance some similarities are present within the sequence F, OH, NH_2, and CH_3. Grimm [106] termed such groups “pseudoatoms”. However, hydrogen bonding was not yet understood. Friedman [107] introduced the term bioisosterism. Bioisosteres are groups or molecules which are structurally similar and show the same type of biological activity. Comprehensive overviews of isosterism and bioisosterism in drug design are documented in the publications [108-112]. The concept of bioisosterism was used when designing new diphenyl sulphide derivatives.

Table 4-4: Predicted binding affinities of novel diphenyl sulfides

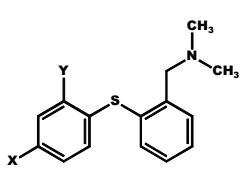

(a)

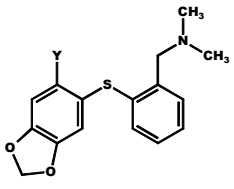

(b)

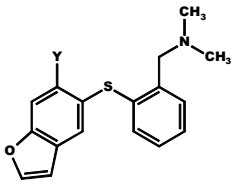

(c)

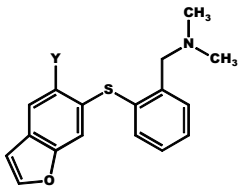

(d)

Compound	Scaffold	X	Y	$K_{i\ pred.}$ SERT (nM)		$K_{i\ pred.}$ NET (nM)	
				CoMFA	CoMSIA	CoMFA	CoMSIA
n1	(a)	H_3CO-C(O)-	NH_2-	1.18	1.67*	2344	1230*
n2	(a)	H_3C-CH_2O-C(O)-	NH_2-	1.24	1.60*	2239	1230
n3	(a)	FCH_2O-C(O)-	NH_2-	1.18	1.44	2239	759
n4	(a)	FCH_2-CH_2O-C(O)-	NH_2-	1.23	1.43*	2239	891
n5	(a)	H_3CS-	NH_2-	2.77	2.79	708	219
n6	(a)	F_3CS-	NH_2-	2.48	1.10*	851	135
n7	(a)	FH_2CS-	NH_2-	2.54	2.48	871	191
n8	(a)	NCO-	NH_2-	1.34	1.77	1413	537
n9	(a)	NCS-	NH_2-	2.24	1.88	794	200
n10	(a)	NC-	H_3CO-	1.28	1.27	3548	3236*
n11	(a)	FCH_2CH_2-	NO_2-	1.51	1.29	1698	912
n12	(a)	NC-	FCH_2-	0.78	0.81*	2692	4169*
n13	(a)	H_3CO-C(O)-	FCH_2-	0.70	0.88*	1778	2344*
n14	(a)	NO_2-CH=CH-	FCH_2-	1.18	4.15*	363	117*
n15	(a)	NC-	H_3CO-C(O)-	0.52	1.13*	7943	7586*
n16	(a)	FCH_2CH_2-	H_3CO-C(O)-	1.06	1.84	1514	513
n17	(a)	NC-	FH_2CO-C(O)-	0.44	1.01*	9120	8511*
n18	(a)	NC-	FH_2C-C(O)-	0.46	0.68*	6607	4074*
n19	(a)	H_3C-NH-$S(O)_2$-	NH_2-	0.90	2.10	2818	1259
n20	(a)	H_3C-NH-$S(O)_2$-	FCH_2-	0.45	1.09	1862	2042
n21	(a)	H_3C-$S(O)_2$-	NH_2-	1.13	3.78	1549	776
n22	(a)	H_3C-$S(O)_2$-	FCH_2-	0.55	1.91	1096	1230*
n23	(a)	H_3C-S(O)-	NH_2-	1.63	3.15	1122	550
n24	(a)	H_3C-S(O)-	FCH_2-	0.81	1.61*	776	832
n25	(a)	H_3C-NHC(O)-	NH_2-	0.76	1.79*	2630	1445*
n26	(a)	H_3C-NHC(O)-	FCH_2-	0.41	0.93*	2042	2630*
n27	(a)	FCH_2-CH_2-C(O)-	NH_2-	0.88	0.90*	1622	537
n28	(a)	FCH_2-CH_2-C(S)-	NH_2-	1.16	0.98*	1349	380
n29	(a)	FCH_2-CH_2O-C(S)-	NH_2-	1.52	1.51*	1905	646
n30	(a)	FCH_2-CH_2S-C(O)-	NH_2-	0.87	0.87*	2239	871
n31	(a)	FCH_2CH_2-	HC(O)-	0.91	1.47*	1445	309
n32	(a)	FCH_2CH_2-	HON=CH-	1.66	2.75	692	200
n33	(a)	FCH_2CH_2-	HN=CH-	1.04	1.91	1072	195
n34	(a)	FCH_2CH_2-	H_3CN=CH-	0.99	1.78	955	162
n35	(a)	FCH_2CH_2-	Phe-C(O)-	2.37*	3.62*	1072	550*
n36	(a)	FCH_2-CH_2O-C(O)-	HC(O)-	0.36	0.74*	6026	2399
n37	(a)	FCH_2-CH_2O-C(O)-	HON=CH-	0.59	1.42*	3020	1589
n38	(a)	FCH_2-CH_2O-C(O)-	HN=CH-	0.40	0.96*	4571	1514
n39	(a)	FCH_2-CH_2O-C(O)-	H_3CN=CH-	0.38	0.89*	3890	1259
n40	(a)	FCH_2-CH_2O-C(O)-	Phe-C(O)-	0.64	2.16*	5623	4898
n41	(a)	Phe-	FCH_2-	1.09	0.97*	724	724
n42	(a)	FCH_2-phe-	NH_2-	2.32	1.69*	871	355
n43	(b)	-	NH_2-	0.64	0.82*	851	316
n44	(b)	-	FCH_2-	0.32*	0.42*	603	575
n45	(c)	-	NH_2-	1.22	1.17*	871	347
n46	(c)	-	FCH_2-	0.67	0.60*	631	589
n47	(d)	-	NH_2-	0.96	1.00*	603	174
n48	(d)	-	FCH_2-	0.50	0.51*	437*	302

*extrapolation > 0.3 log units

Table 4-5: Predicted binding affinities of novel phenyl-pyridinyl sulphides and phenyl-thienyl sulphides

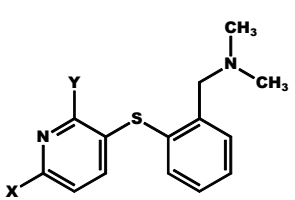

(a)

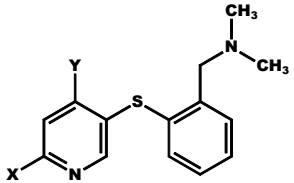

(b)

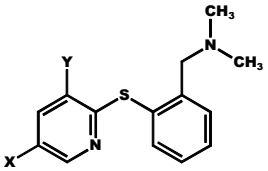

(c)

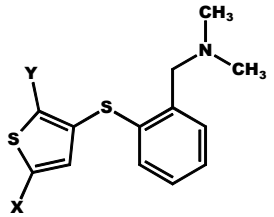

(d)

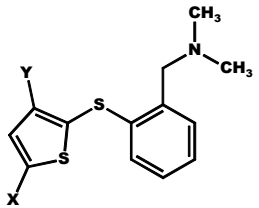

(e)

				SERT		NET	
Compound	**Scaffold**	**X**	**Y**	**$K_{i\ pred.}$ CoMFA (nM)**	**$K_{i\ pred.}$ CoMSIA (nM)**	**$K_{i\ pred.}$ CoMFA (nM)**	**$K_{i\ pred.}$ CoMSIA (nM)**
n49	(a)	NC-	NH_2-	0.74	1.38	3467	1698*
n50	(a)	FCH_2CH_2-	NH_2-	1.33	2.59	813	91*
n51	(a)	FCH_2O-C(O)-	NH_2-	0.59	1.35	2818	562
n52	(a)	FCH_2CH_2O-C(O)-	NH_2-	0.54	1.30	2630	661
n53	(a)	FCH_2CH_2C(O)-	NH_2-	0.50	0.85	2042	355*
n54	(a)	H_3CO-C(O)-	FCH_2-	0.36	0.72*	1862	1585
n55	(b)	NC-	NH_2-	1.17	1.54	3631	2089
n56	(b)	FCH_2CH_2-	NH_2-	1.71	2.63	759	126*
n57	(b)	FCH_2O-C(O)-	NH_2-	1.16	1.29*	2344	724
n58	(b)	FCH_2CH_2O-C(O)-	NH_2-	1.15	1.32*	2455	813
n59	(b)	FCH_2CH_2C(O)-	NH_2-	0.87	0.80*	1698	537
n60	(b)	H_3CO-C(O)-	FCH_2-	0.67	0.78*	1738	2188*
n61	(c)	NC-	NH_2-	2.58	3.11	2291	1660*
n62	(c)	FCH_2CH_2-	NH_2-	2.83	4.61	550	102*
n63	(c)	FCH_2O-C(O)-	NH_2-	1.81	2.54	1778	562
n64	(c)	FCH_2CH_2O-C(O)-	NH_2-	2.61	1.75	1820	617
n65	(c)	FCH_2CH_2C(O)-	NH_2-	1.27	1.59*	1230	437
n66	(c)	H_3CO-C(O)-	FCH_2-	1.09	1.52*	1230	1698*
n67	(d)	NC-	NH_2-	1.79	2.64	3631	4898*
n68	(d)	FCH_2CH_2-	NH_2-	2.68	3.31	692	182
n69	(d)	FCH_2CH_2O-C(O)-	NH_2-	1.15	2.20	1479	1514*
n70	(e)	NC-	NH_2-	0.84	1.21	4467	3802*
n71	(e)	FCH_2CH_2-	NH_2-	1.66	1.85	692	132
n72	(e)	FCH_2CH_2O-C(O)-	NH_2-	0.81*	0.78*	2291	1047

*extrapolation > 0.3 log unit

Table 4-6: Predicted binding affinities of novel compounds with different diphenyl bridging

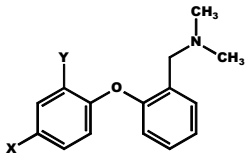

(a)

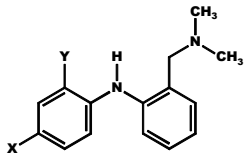

(b)

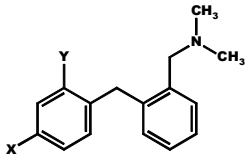

(c)

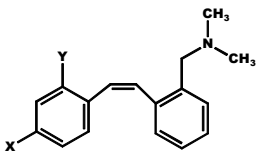

(d)

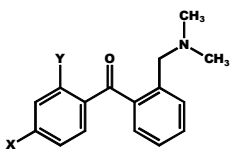

(e)

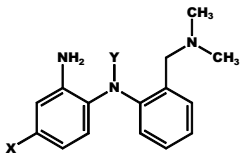

(f)

				SERT		NET	
Compound	**Scaffold**	**X**	**Y**	**$K_{i\ pred.}$ CoMFA (nM)**	**$K_{i\ pred.}$ CoMSIA (nM)**	**$K_{i\ pred.}$ CoMFA (nM)**	**$K_{i\ pred.}$ CoMSIA (nM)**
n73	(a)	NC-	NH_2-	1.32	1.95	3631	3890*
n74	(a)	FCH_2CH_2-	NH_2-	3.55	2.65	603	295
n75	(a)	FCH_2CH_2O-C(O)-	NH_2-	0.96	1.45*	2570	2630*
n76	(a)	FCH_2CH_2-C(O)-	NH_2-	1.12	1.15*	2089	2239*
n77	(b)	NC-	NH_2-	0.77	0.75	1698	933*
n78	(b)	FCH_2CH_2-	NH_2-	2.37	1.11	174	59
n79	(b)	FCH_2CH_2O-C(O)-	NH_2-	0.79	0.68	1122	575
n80	(b)	FCH_2CH_2-C(O)-	NH_2-	0.67	0.44*	676	389*
n81	(c)	NC-	NH_2-	0.47	0.88	1514	617
n82	(c)	FCH_2CH_2-	NH_2-	0.94	1.37*	550	204
n83	(c)	FCH_2CH_2O-C(O)-	NH_2-	0.38	0.73*	891	324
n84	(c)	FCH_2CH_2-C(O)-	NH_2-	0.37	0.47*	550	204
n85	(d)	NC-	NH_2-	2.35	3.84	794	617
n86	(d)	FCH_2CH_2-	NH_2-	4.01*	4.80	219*	55
n87	(d)	FCH_2CH_2O-C(O)-	NH_2-	4.39	3.37	407	229
n88	(d)	FCH_2CH_2-C(O)-	NH_2-	2.99*	2.22	550	204
n89	(e)	NC-	NH_2-	3.40	3.39	14 125*	17 378*
n90	(e)	FCH_2CH_2-	NH_2-	6.35	5.07	1950	1698*
n91	(e)	FCH_2CH_2O-C(O)-	NH_2-	2.81	3.04	8128	12 589*
n92	(e)	FCH_2CH_2-C(O)-	NH_2-	2.17	2.72	7413	11 482*
n93	(f)	NC-	NC-	1.00	1.44*	7079*	10 715*
n94	(f)	NC-	H_3C-	1.35	0.76*	933	546*
n95	(f)	NC-	FCH_2-	1.30	0.58*	871	479
n96	(f)	NC-	H_3C-CH_2-	1.17	0.86	871	575
n97	(f)	NC-	FCH_2CH_2-	1.60	0.89*	1148	602
n98	(f)	FCH_2CH_2-	NC-	2.17	2.23	1202	661*
n99	(f)	FCH_2CH_2O-C(O)-	NC-	0.88	1.29*	4786	5370*
n100	(f)	FCH_2CH_2-C(O)-	NC-	0.73	0.74*	3236	3020*

*extrapolation > 0.3 log units

4.3.5 Novel Compounds and Discussion

Table 4-4 to **Table 4-6** summarise the molecular structures of the newly designed compounds and their predicted binding affinities at the SERT and at the NET. Very high binding affinity of a radioligand in combination with a comparatively slow clearance from tissue can restrict its usefulness for PET, because the rate-limiting step of tracer retention may become the delivery instead of the binding process [1]. A consequence of this would be to only consider substances whose K_i-values are found within a particular range, for instance, between 0.5 and 10 nM as suggested by Lassen et al. [113] for benzodiazepine receptor tracers. However, as the used CoMFA and CoMSIA models cannot predict PET kinetics, and thus no optimum K_i-value for any one compound can be estimated, all substances were considered which were estimated as displaying high binding affinity in a nanomolar or subnanomolar range at the SERT and low binding affinity at the NET. Another aspect during molecular design was to obtain structures that could easily be radiolabelled with either carbon-11 or preferably fluorine-18. Carbon-11 labelling of one of the N-methyl groups as seen in [^{11}C]**DASB** seems not necessarily suitable as the N-methyl groups are susceptible to metabolism. Therefore it seems difficult to quantify radiolabelled metabolites that cross the blood brain barrier and need to be considered during evaluation of a PET study. These considerations seem to contrast with the findings of Halldin et al. [114] who labelled **MADAM** with carbon-11 in two different positions (at the methyl group of the phenyl ring and at one methyl group of the tertiary amino group) and measured metabolism in monkey brain. They found no significant difference with regard to brain kinetics and metabolism, indicating that no radioactive metabolites entered the brain.

When modifying the N,N-dimethyl-2-phenylsulfanyl-benzylamine scaffold, four structural features were focused upon. These were the substituents in position 2´ and 4´ of ring B, the aromatic ring B itself, and the sulphur bridge between ring A and ring B as shown in **Figure 4-19**.

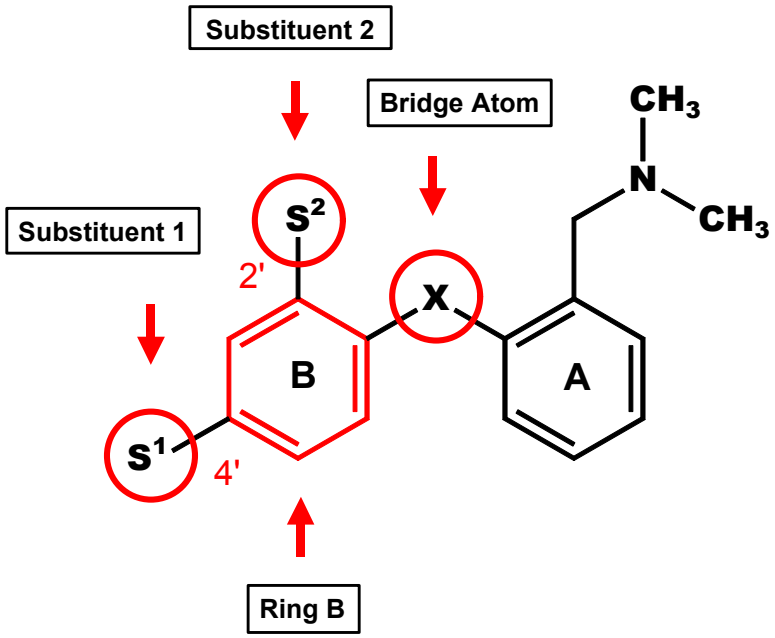

Figure 4-19: Positions of possible modifications at the former N,N-dimethyl-2-phenylsulfanyl-benzylamine scaffold. Substituents in position 2´ and 4´ were exchanged as well as the aromatic ring B and the atom bridging ring A and ring B.

From the CoMFA and CoMSIA models it became clear that the substituent in position 4´ should preferably display electron-withdrawing characteristics which is particularly required for high SERT selectivity. Obviously, a fluoroethyl group in position 4´ as seen in structure **s9** does not meet this requirement which explains its selectivity loss compared to **DASB** [26]. Therefore, the replacement of the fluoroethyl group with a fluoroethyl-oxycarbonyl group (ester) seems promising as the possibility of fluorine-18 labelling is maintained. The estimated K_i -

values of compound **n4** are 1.23 nM (CoMFA) and 1.43 nM (CoMSIA) for the SERT, and 2239 nM (CoMFA) and 891 nM (CoMSIA) for the NET. Substitution of the fluoroethyl group by a fluoroethyl-carbonyl group (ketone) seems also most promising, since compound **n27** was predicted to have K_i-values around 0.88 nM (CoMFA) and 0.90 nM (CoMSIA) for the SERT, and around 1622 nM (CoMFA) and 537 nM (CoMSIA) for the NET.

To further improve binding affinity at the SERT, replacement of ring B with an electron-deficient pyridine ring seemed reasonable. Depending on the position of the nitrogen atom in the pyridine ring, binding affinity at the SERT is estimated as slightly decreased compared to **n4** for compound **n64,** and as about the same for compound **n58**, whereas a markedly improved binding affinity at the SERT (K_i = 0.54 nM) is estimated for compound **n52** by CoMFA analysis. Moreover, SERT selectivity seems to be retained, as for compound **n52** a K_i-value of 2630 nM at the NET is estimated by using CoMFA. Substitution with a fluoroethyl group in position 4´ as in compounds **n50**, **n56**, and **n62** appears to result in decreased selectivity, whereas binding affinity at the SERT is predicted in a nanomolar range suitable for a PET ligand. Substitution in position 4´ by a fluoroethyl-carbonyl group as in compounds **n53**, **n59** and **n65** results in clearly selective substances. This is demonstrated by **Figure 4-20**, showing compound **n53** within the SERT CoMFA fields and within the CoMSIA selectivity fields. The electron deficient pyridine ring is located in the blue region, which shows that partial positive charges are favourable for high binding affinity at the SERT and for SERT selectivity at this site. Moreover, the fluoroethyl-carbonyl substituent is directed towards the green region. This region denotes areas in which steric bulk enhances binding affinity and SERT selectivity. The oxygen atom of the carbonyl group is directed towards the red region visible in both the SERT CoMFA plot

and the CoMSIA selectivity plot. Thus, partial negative charge is located in the red region as required. Furthermore, this may confirm the choice of the conformation of the fluoroethyl-carbonyl substituent.

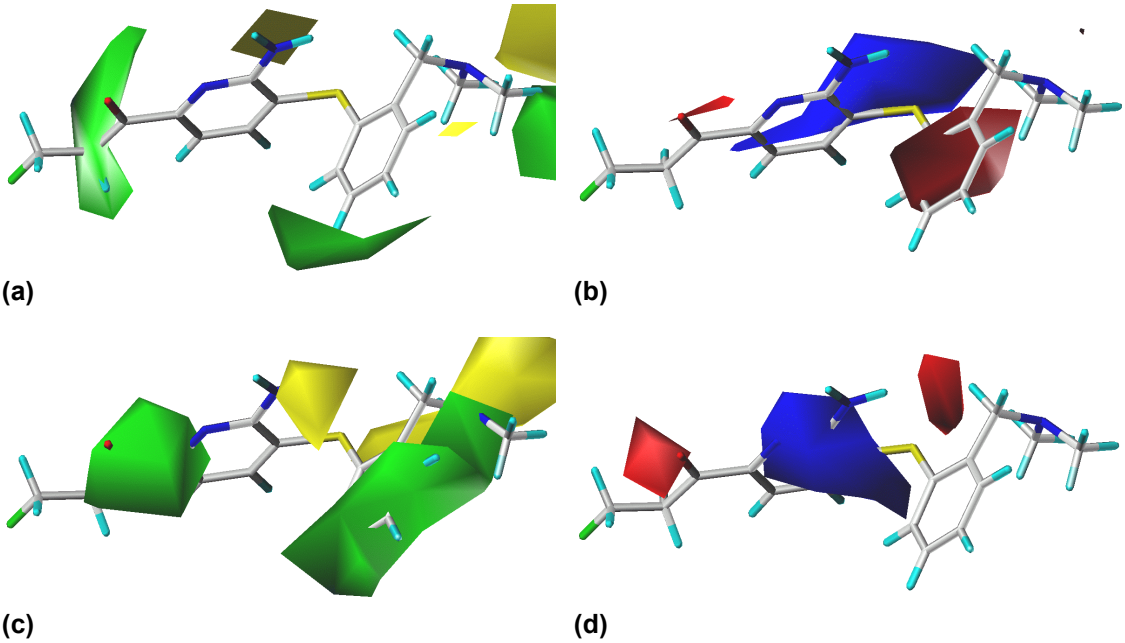

Figure 4-20: Compound **n53** within the steric **(a)** and electrostatic **(b)** SERT *"StDev*Coeff"* CoMFA fields, and within the steric **(c)** and electrostatic **(d)** *"StDev*Coeff"* CoMSIA fields from the selectivity analysis. Green regions denote those areas in which steric bulk is favourable for high binding affinity at the SERT and for high SERT selectivity. Yellow regions denote those areas where steric bulk has got a detrimental effect on SERT binding affinity and SERT selectivity. Binding affinity and SERT selectivity is enhanced by partial positive charges in blue regions, and by partial negative charges in red regions.

As thiophene is considered a classical bioisostere of benzene [108, 112], the exchange of ring B for thiophene was attempted. Good results were obtained for compound **n67** and compound **n70**, differing from each other in the position of the sulphur atom in the thiophene ring. Both compounds were predicted as displaying high binding affinity at the SERT and low binding affinity at the NET, thus being highly selective. To make fluorine-18 labelling possible, the cyano group was

exchanged for the above mentioned fluoroethyl-oxycarbonyl group, resulting in compounds **n69** and **n72**, which are predicted as also showing high binding affinity at the SERT, and as being SERT selective. The only congeneric compounds found in literature with ring B being replaced with thiophene had been prepared and tested by Sindelar et al. [22]. These two compounds displayed only moderate affinity at the SERT. Probably this can be attributed to a different substitution pattern.

As suggested by Oya et al. [99] for compound **s30**, the amino group in position 2´ can be replaced with a fluoromethyl group without affinity loss and, moreover, this provides a good possibility for fluorine-18 labelling. Affinity and selectivity seem to be retained for compound **n12**, possessing an electron-withdrawing cyano group in position 4´, or for the pyridine compounds **n54** and **n60**. Another electron withdrawing group is the methylsulfonyl group which Burger [108] suggested to be bioisosteric to the trifluoromethyl group. As Wilson et al. [21] found that a trifluoromethyl group in position 4´ makes compound **s22** much too lipophilic to display favourable PET kinetics, substitution of position 4´ with a methylsulfonyl group is probably advantageous for a PET ligand. Both compound **n21**, possessing an amino group in position 2´, and compound **n22**, possessing a fluoromethyl group in position 2´, are predicted to be highly selective SERT ligands. Compound **n21** could possibly be carbon-11 labelled at the methylsulfonyl group, whereas compound **n22** can obviously be fluorine-18 labelled. Other possible electron-withdrawing substituents in position 4´, probably resulting in highly selective SERT ligands, are a methylamino-carbonyl group (**n25**, **n26**), a methylsulfoxide group (**n23**, **n24**), a methylamino-sulfonyl group (**n19**, **n20**), a fluoroethyl-thiocarbonyl group (**n28**), a fluoroethyl-oxythiocarbonyl group (**n29**), a fluoroethyl-sulfanylcarbonyl group (**n30**), and a cyanato group (**n8**). These groups were suggested as a

result of an Optimize QSAR run. Only moderately selective substances seem to result from a thiocyanato group (**n9**), a methylsulfanyl group (**n5**) or a trifluoromethylsulfanyl group (**n6**) in position 4´. A nitroethenyl group in position 4´ (**n14**) also does not seem to be favourable, although it is suggested to be bioisosteric to halogens or the trifluoromethyl group [112]. The idea of placing an additional electron withdrawing group in position 2´ resulted in the suggestion of compounds **n15** – **n17**, all possessing an ester function in position 2´. These compounds are predicted as being highly selective for the SERT. Considering known SARs, these suggestions seem reasonable, which is confirmed by Emond et al. [25] stating that ester functions are generally tolerated in position 2´. Whereas compound **n15** can only be carbon-11 labelled, fluorine-18 labelling seems possible for compounds **n16** and **n17** at either the fluoroethyl group in position 4´, or the fluoromethyl-oxycarbonly group in position 2´. Substitution of position 2´ with a fluoromethyl-carbonyl group resulted in compound **n18** which is predicted to be a particularly selective high affinity SERT ligand as can be concluded from the estimated K_i-values of 0.46 nM (CoMFA) and 0.68 nM (CoMSIA) for the SERT, and 6607 nM (CoMFA) and 4074 nM (CoMSIA) for the NET. Moreover, fluorine-18 labelling seems possible. Another idea was to link position 4´ and 5´ with a methylenedioxy group (**n43** and **n44**) in analogy to the SSRI **paroxetine**, or with a furano ring (**n45** – **n48**). Compounds **n44**, **n46** and **n48**, possessing a fluoromethyl group in position 2´, are predicted as being as selective as their respective amino analogues **n43**, **n45** and **n47**. Substitution of position 2´ with a formyl group (aldehyde) (**n31** and **n36**), and their corresponding oximes (**n32** and **n37**), imines (**n33** and **n38**), and methylimines (**n34** and **n39**), was a result of using the Optimize QSAR module. To provide a possibility for fluorine-18 labelling, position 4´ was substituted with either a fluoroethyl group,

which in the case of the aldehyde (**n31**) and the imine (**n33**) still seems to result in comparatively SERT selective substances, or with a fluoroethyl-oxycarbonly group, which in all cases seems to result in highly SERT selective compounds. This series of compounds also appears to be quite convenient for synthesis planning as the oxime, the imine and the methylimine can easily be prepared from the aldehyde. Substitution of position 2´ with a benzoyl rest (**n35** and **n40**), which was also found as a result of an Optimize QSAR run, seems arguable in some ways. Although it was found by Choi et al. [100] that sometimes quite large substituents are tolerated in position 2´, as for instance a fluorophenyl-carbonylamino group, such sterically demanding substituents are probably too lipophilic to finally display favourable PET characteristics. Another suggestion derived from an Optimize QSAR run is the substitution of position 4´ with a phenyl rest as seen in compound **n41** and **n42**. On the one hand, Emond et al. [25] concluded that sterically demanding groups in position 4´ have got a detrimental effect on binding affinity at the SERT, but on the other hand, such groups at ring B are considered favourable for high SERT affinity and high SERT selectivity by the CoMFA and CoMSIA models. The phenyl ring in compound **n42** is further substituted by a fluoromethyl group which could possibly be fluorine-18 labelled.

Starting from the finding of Zhuang et al. [101] that **ODAM** is binding with high affinity at the SERT, a series of additional structures were suggested in which the sulphur bridge was replaced with bioisosteric groups or atoms. Classical bioisosteres of divalent sulphur (-S-) are a methylene group (-CH_2-), divalent oxygen (-O-), and amine functions (-NH- or -NR-) [108, 112]. Less typical, but also known as bioisosteric to divalent sulphur, are a cyanamide (-NCN-) [108, 111, 112, 115] and an ethene group (-CH=CH-) [108, 111, 112]. Binding affinity at the SERT is predicted to move towards the sub-nanomolar range for the

DASB analogues **n77** and **n81** in which the sulphur bridge was substituted by either an amine function or a methylene bridge. Binding affinity at the NET seems to increase only slightly and is still in the same order of magnitude as for **DASB**. Thus, selective SERT ligands can probably be obtained by replacing the sulphur bridge with a methylene bridge or an amine function. DASB analogue **n73**, in which the sulphur bridge is exchanged by an oxygen bridge, seems to show similar binding characteristics as **DASB** itself. This is in close agreement with the suggestion of Burger [108] that it is often the steric rather than the electronic properties of the oxygen or sulphur bridge that are the determinants of pharmacological activity. The replacement of the sulphur atom with a *(Z)*-configurated carbon-carbon double bond results in compound **n85**, which still seems to show affinity at the SERT in the same order of magnitude as **DASB** itself, but is predicted to be markedly less SERT selective. The cyanamide **n93** is believed to be highly SERT selective with predicted K_i-values at the SERT of 1.00 nM (CoMFA) and 1.44 nM (CoMSIA), and at the NET of 7079 nM (CoMFA) and 10 715 nM (CoMSIA). These values strongly qualify this compound for inclusion as a possible PET ligand. Moreover, carbon-11 labelling seems possible at the cyanamide group as has been reported for diphenyl[^{11}C]cyanamide [116]. Another particularly interesting structure for possible application as a PET tracer is compound **n97**. The amine function bridging the two phenyl rings has been further substituted with a fluoroethyl group which could possibly be fluorine-18 labelled. Just as its ethyl, methyl and fluoromethyl analogues (**n96**, **n94** and **n95**), compound **n97** is predicted to be highly SERT selective. The benzophenone derivative **n89** is also predicted to be a highly SERT selective substance with remarkably low affinity at the NET and so are its fluoroethyl-oxycarbonyl analogue **n91** and its fluoroethyl-carbonyl analogue **n92**. However, binding affinity at the SERT also seems to be

lower than for the respective sulphur bridged analogues. Surely, any modifications at the 2´ and 4´ position suggested earlier can be also be transferred to the DASB analogues in which the sulphur bridge is replaced by other bioisosteric atoms or groups. This can be interesting for synthesis planning.

5 Conclusion

Structure-activity relationships of SERT ligands were quantitatively investigated at both the SERT and the NET by applying 3D QSAR techniques. After carefully aligning the model compounds from the structurally heterogeneous data set, statistically significant CoMFA and CoMSIA models were obtained. Structural requirements for SERT selectivity were elucidated. An electron-deficient primary aromatic moiety with an electronegative substituent, and the presence of another sterically demanding moiety as for instance a secondary aromatic ring are necessary selectivity criteria. The 3D QSAR models provide a rational basis for the development and optimisation of potential new PET ligands displaying SERT selectivity. Highly comparable results were obtained from the CoMFA and CoMSIA models, indicating that both field types are equally well suited if discontinuous and predominating electrostatic field variables are avoided. The latter was ensured by disregarding the protonation state, and by never dropping electrostatics at sterically unfavourable points. The results of this methodological comparison may be generalised to a certain extent.

In recent PET literature, diphenyl sulphides such as [^{11}C]**DASB** are described to be promising PET ligands for the SERT. However, as yet, no optimal PET ligand had been found among them. The diphenyl sulphide scaffold seems suitable for fine tuning. Many existing diphenyl sulphides were correctly predicted by both the CoMFA and the CoMSIA models. Therefore their N,N-dimethyl-2-phenylsulfanyl-benzylamine scaffold was used in the present work as lead structure. A series of 100 potential new and selective PET radiotracers for the SERT were designed by modifying this N,N-dimethyl-2-phenylsulfanyl-

benzylamine scaffold. Many of the newly designed compounds possessing a fluoroethyl-oxycarbonyl group in position 4´ are predicted to be selective high affinity ligands at the SERT and are of particular interest for possible fluorine-18 labelling. The same holds true for compounds possessing a fluoroethyl-carbonly group in position 4´. Fluorine-18 labelling seems also possible for substances possessing a fluoroethyl group in position 4´, combined with an electron withdrawing group in position 2´ as it is the case for the aldehyde **n31** and its corresponding oxime **n32**, imine **n33** and methylimine **n34**. The oxim, the imin, and the methylimin should be easily accessible from the aldehyd. Compound **n18**, possessing a flouromethyl-carbonyl group in position 2´, provides another new possibility for fluorine-18 labelling. Compound **n93** is predicted as highly SERT selective and the cyanamide substructure may be an alternative for carbon-11 labelling. Compound **n97**, possessing a tertiary fluoroethyl amine substructure, provides another new option for fluorine-18 labelling.

Although most compounds are predicted as being SERT selective it has to be acknowledged that only data on SERT and NET affinity had been available when generating the models, whereas data on DAT affinity had been lacking.

Future studies might include synthesis and biological testing of the compounds to verify the predictions. Combinatorial chemistry seems suitable as all new structures possess similar scaffolds. Moreover, the 3D QSAR models might serve as queries for 3D database searching in order to find new leads. Another idea to continue the ligand based 3D QSAR studies is pseudoreceptor modelling. No 3D structure of the target site is required. Instead, a receptor model is constructed from single isolated amino acids [49, 117]. The CoMFA and CoMSIA fields can be of valuable help when choosing the amino acids. With the developing practice of NMR spectroscopy and X-ray crystallography,

the 3D structure of the SERT might be available soon. This will provide new options for molecular modelling. The application of receptor based techniques including docking studies and *de-novo* design will be possible.

The present work presents a fairly unique combination of PET ligand design and molecular modelling. Yet the models do not provide any information concerning PET kinetics. Screening for suitability of the novel compounds as PET ligands is needed. Following this, the derivation of models predicting PET kinetics seems conceivable. First approaches in this direction have been made by Abrunhosa et al. [118, 119]. A model has been developed correlating the *in vivo* behaviour of a series of PET ligands with their calculated physico-chemical characteristics [118]. Further optimisation of PET ligands for the SERT can possibly be achieved by considering kinetic aspects during molecular modelling. As kinetic shortcomings are the main reason for PET ligand failing, this will dramatically facilitate PET ligand development.

6 References

[1] Halldin C, Gulyas B, Langer O, Farde L (2001). Brain radioligands - state of the art and new trends. Q J Nucl Med; 45 (2): 139-152.

[2] Scheffel U, Dannals RF, Suehiro M, Ricaurte GA, Carroll FI, Kuhar MJ, Wagner HN, Jr. (1994). Development of PET/SPECT ligands for the serotonin transporter. NIDA Res Monogr; 138: 111-130.

[3] Oh SJ, Ha H-J, Chi DY, Lee HK (2001). Serotonin receptor and transporter ligands - current status. Curr Med Chem; 8: 999-1034.

[4] Laakso A, Hietala J (2000). PET studies of brain monoamine transporters. Curr Pharm Design; 6: 1611-1623.

[5] Hume SP, Lammertsma AA, Bench CJ, Pike VW, Pascali C, Cremer JE, Dolan RJ (1992). Evaluation of S-[^{11}C]citalopram as a radioligand for in vivo labeling of 5-hydroxytryptamine uptake sites. Nucl Med Biol; 19: 851-855.

[6] Lasne MC, Pike VW, Turton DR (1989). The radiosynthesis of [N-methyl-^{11}C]-sertraline. Appl Radiat Isot; 40: 147-151.

[7] Shiue C-Y, Shiue GG, Cornish KG, O'Rourke MF (1995). PET study of the distribution of [^{11}C]fluoxetine in a monkey brain. Nucl Med Biol; 22: 613-616.

[8] Smith DF, Jensen PN, Gee AD, Hansen SB, Danielsen E, Andersen F, Saiz PA, Gjedde A (1997). PET neuroimaging with [^{11}C]venlafaxine: serotonin uptake inhibition, biodistribution and binding in living pig brain. Eur Neuropsychopharmacol; 7: 195-200.

[9] Bergstrom KA, Halldin C, Hall H, Lundkvist C, Ginovart N, Swahn CG, Farde L (1997). In vitro and in vivo characterisation of nor-beta-CIT: a potential radioligand for visualisation of the serotonin transporter in the brain. Eur J Nucl Med; 24 (6): 596-601.

[10] Farde L, Halldin C, Mueller L, Suhara T, Karlsson P, Hall H (1994). PET study of [^{11}C]-beta-CIT binding to monoamine transporters in the monkey and human brain. Synapse (N Y); 16: 93-103.

[11] Chen P, Kilts CD, Galt JR, Ely TD, Camp VM, Malveaux EJ, Goodman MM (2000). Synthesis, characterization and SPECT imaging of serotonin transporter (SERT) with [^{123}I]ZIENT: A new high affinity and selective SERT imaging agent. J Nucl Med; 41 (5 Suppl): 39.

[12] Goodman MM, Chen P, Kilts C, Ely T, Hoffman JM, Votaw J, Camp V (1999). Radiolabeled 2-β-carbomethoxy-3-β-(4-(2-fluoroethyl)-3-iodophenyl)-nortropane (FEINT): Synthesis, characterization and in vitro audiography of a potential radioligand for mapping serotonin transporter sites by both PET and SPECT. J Nucl Med; 40 (5 Suppl): 306.

[13] Szabo Z, Kao PF, Scheffel U, Suehiro M, Mathews WB, Ravert HT, Musachio JL, Marenco S, Kim SE, Ricaurte GA, et al. (1995). Positron emission tomography imaging of serotonin transporters in the human brain using [^{11}C](+)McN5652. Synapse; 20: 37-43.

[14] Szabo Z, Scheffel U, Suehiro M, Dannals RF, Kim SE, Ravert HT, Ricaurte GA, Wagner HN, Jr. (1995). Positron emission tomography of 5-HT transporter sites in the baboon brain with [^{11}C]McN5652. J Cereb Blood Flow Metab; 15: 798-805.

[15] McCann UD, Eligulashvili V, Ricaurte GA (2000). (+/-)-3,4-Methylenedioxymethamphetamine ('Ecstasy')-induced serotonin neurotoxicity: Clinical studies. Neuropsychobiology; 42: 11-16.

[16] McCann UD, Szabo Z, Scheffel U, Dannals R, Ricaurte GA (1999). Positron emission tomographic evidence of toxic effect of MDMA ("Ecstasy") on brain serotonin neurons in human beings. The Lancet; 352: 1433-1437.

[17] Oya S, Kung M-P, Acton PD, Mu M, Hou C, Kung HF (1999). A New Single-Photon Emission Computed Tomography Imaging Agent for Serotonin Transporters: [^{123}I]IDAM, 5-Iodo-2-((2-((dimethyl-amino)methyl)-phenyl)thio)benzyl Alcohol. J Med Chem; 42: 333-335.

[18] Oya S, Choi SR, Hou C, Mu M, Kung MP, Acton PD, Siciliano M, Kung HF (2000). 2-((2-((dimethylamino)methyl)phenyl)thio)-5-iodophenyl-amine (ADAM): an improved serotonin transporter ligand. Nucl Med and Biol; 27: 249-254.

[19] Tarkiainen J, Vercouillie J, Guilloteau D, Gulyas B, Sovago J, Cselenyi Z, Emond P, Chalon S, Sandell J, Hiltunen J, Farde L, Halldin C (2001). Carbon-11 Labelling of MADAM in Two Different Postions: A Highly Selective PET Radioligand for the Serotonin Transporter. J Labelled Cpd Radiopharm; 44 (1 Suppl): S193-S195.

[20] Wilson AA, Houle S (2000). 2-(Phenylthio)benzylamines as PET serotonin transporter ligands: Synthesis with ^{11}C and evaluation in vivo. J Nucl Med; 41 (5 Suppl): 38-39.

[21] Wilson AA, Ginovart N, Schmidt M, Meyer JH, Threlkeld PG, Houle S (2000). Novel radiotracers for imaging the serotonin transporter by positron emission tomography: synthesis, radiosynthesis, and in vitro and ex vivo evaluation of ^{11}C-labeled 2-(phenylthio)araalkylamines. J Med Chem; 43: 3103-3110.

[22] Sindelar K, Pomykacek J, Valchar M, Dobrovsky K, Metysova J, Polivka Z (1991). Potential antidepressants and inhibitors of 5-hydroxytryptamine and noradrenaline re-uptake in the brain: N,N-dimethyl(arylthio)thenylamines and N,N-dimethyl-2-(thienylthio)-benzylamines. Collect Czech Chem Commun; 56: 449-458.

[23] Ferris RM, Brieaddy L, Mehta N, Hollingsworth E, Rigdon G, Wang C, Soroko F, Wastila W, Cooper B (1995). Pharmacological properties of 403U76, a new chemical class of 5-hydroxytryptamine- and noradrenaline-reuptake inhibitor. J Pharm Pharmacol; 47: 775-781.

[24] Houle S, Ginovart N, Hussey D, Meyer JH, Wilson AA (2000). Imaging the serotonin transporter with positron emission tomography: Initial human studies with [^{11}C]DAPP and [^{11}C]DASB. Eur J Nucl Med; 27: 1719-1722.

[25] Emond P, Vercouillie J, Innis R, Chalon S, Mavel S, Frangin Y, Halldin C, Besnard J-C, Guilloteau D (2002). Substituted Diphenyl Sulfides as Selective Serotonin Transporter Ligands: Synthesis and In Vitro Evaluation. J Med Chem; 45: 1253-1258.

[26] Huang Y, Bae SA, Zhu Z, Guo N, Hwang DR, Laruelle M (2001). Fluorinated Analogues of ADAM as New PET Radioligands for the Serotonin Transporter: Synthesis and Pharmacological Evaluation. J Labelled Cpd Radiopharm; 44 (1 Suppl): S18-S20.

[27] Muszynski IC, Scapozza L, Kovar K-A, Folkers G (1999). Quantitative structure-activity relationships of phenyltropanes as inhibitors of three monoamine transporters: Classical and CoMFA studies. Quant Struct-Act Relat; 18: 342-353.

[28] Gundertofte K, Liljefors T, Bogeso KP (1997). A stereoselective pharmacophoric model of the serotonin reuptake site. In: van de Waterbeemd H, Testa B, Folkers G (Ed.). Computer-assisted lead finding and optimization. Verlag Helvetica Chimica Acta (VHCA), Basel: pp. 443-459.

[29] Rupp A, Kovar KA, Beuerle G, Ruf C, Folkers G (1994). A new pharmophoric model for 5-HT reuptake-inhibitors: differentiation of amphetamine analogues. Pharm Acta Helv; 68: 235-244.

[30] Hansch C, Caldwell J (1991). The structure-activity relationship of inhibitors of serotonin uptake and receptor binding. J Comput-Aided Mol Des; 5: 441-453.

[31] Povlock SL, Amara SG (1997). The structure and function of norepinephrine, dopamine, and serotonin transporters. In: Reith MEA (Ed.). Neurotransmitter transporters: Structure, function and regulation. Humana Press, Totowa, New Jersey: pp. 1-28.

[32] Olivier B, Soudijn W, van Wijngaarden I (2000). Serotonin, dopamine and norepinephrine transporters in the central nervous system and their inhibitors. Prog Drug Res; 54: 59-119.

[33] Schloss P, Williams DC (1998). The serotonin transporter: A primary target for antidepressant drugs. J Psychopharmacol; 12: 115-121.

[34] Owens MJ, Morgan WN, Plott SJ, Nemeroff CB (1997). Neurotransmitter receptor and transporter binding profile of antidepressants and their metabolites. J Pharmacol Exp Ther; 283: 1305-1322.

[35] Julien RM (1997). Drogen und Psychopharmaka. Spektrum Akademischer Verlag GmbH, Heidelberg, Berlin, Oxford.

[36] Ritz MC, Lamb RJ, Goldberg SR, Kuhar MJ (1987). Cocaine receptors on dopamine transporters are related to self-administration of cocaine. Science; 237: 1219-1223.

[37] Berke JD, Hyman SE (2000). Addiction, dopamine, and the molecular mechanisms of memory. Neuron; 25: 515-532.

[38] Nestler EJ (2001). Perspectives: Neurobiology: Total recall-the memory of addiction. Science (Washington, DC, United States); 292: 2266-2267.

[39] Muszynski IC (1999). Quantitative Struktur-Wirkungsbeziehungen (QSAR) an der Kokain-Bindungsstelle der Monoamintransporter: Klassische und CoMFA-Studien. Dissertation. Tübingen: Eberhard-Karls-Universität.

[40] Rudnick G, Wall SC (1992). The molecular mechanism of "ecstasy" [3,4-methylenedioxymethamphetamine (MDMA)]: serotonin transporters are targets for MDMA-induced serotonin release. Proc Natl Acad Sci USA; 89: 1817-1821.

[41] Nichols DE (1986). Differences between the mechanism of action of MDMA, MBDB, and the classic hallucinogens. Identification of a new therapeutic class: entactogens. J Psychoact Drugs; 18: 305-313.

[42] White SR, Obradovic T, Imel KM, Wheaton MJ (1996). The effects of methylenedioxymethamphetamine (MDMA, "Ecstasy") on monoaminergic neurotransmission in the central nervous system. Prog Neurobiol; 49: 455-479.

[43] Scheffel U, Szabo Z, Mathews WB, Finley PA, Dannals RF, Ravert HT, Szabo K, Yuan J, Ricaurte GA (1998). In vivo detection of short- and long-term MDMA neurotoxicity-a positron emission tomography study in the living baboon brain. Synapse (New York); 29: 183-192.

[44] Rudnick G (1997). Mechanisms of biogenic amine neurotransmitter transporters. In: Reith MEA (Ed.). Neurotransmitter transporters: Structure, function and regulation. Humana Press, Totowa, New Jersey: pp. 73-100.

[45] Pacholczyk T, Blakely RD, Amara SG (1991). Expression cloning of a cocaine- and antidepressant-sensitive human noradrenaline transporter. Nature; 350: 350-354.

[46] Scheffel U, Ricaurte GA (1990). Paroxetine as an in vivo indicator of 3,4-methylenedioxymethamphetamine neurotoxicity: a presynaptic serotoninergic positron emission tomography ligand? Brain Res; 527: 89-95.

[47] Graham D, Esnaud H, Habert E, Langer SZ (1989). A common binding site for tricyclic and nontricyclic 5-hydroxytryptamine uptake inhibitors at the substrate recognition site of the neuronal sodium-dependent 5-hydroxytryptamine transporter. Biochem Pharmacol; 38: 3819-3826.

[48] Van de Waterbeemd H, Carter RE, Grassy G, Kubinyi H, Martin YC, Tute MS, Willett P (1997). Glossary of terms used in computational drug design. Pure Appl Chem; 69: 1137-1152.

[49] Hoeltje HD, Folkers G (1996). Molecular Modeling - Basic Principles and Applications.

[50] Kubinyi H (1993). The third dimension in QSAR: an introduction. In: Kubinyi H (Ed.). 3D QSAR Drug Design, Theory, Methods and Applications. ESCOM, Leiden; Volume 1: pp. 3-10.

[51] Fischer E (1894). Einfluß der Configuration auf die Wirkung der Enzyme. Ber Dtsch Chem Ges; 27: 2985-2993.

[52] Koshland DE, Jr., Nemethy G, Filmer D (1966). Comparison of experimental binding data and theoretical models in proteins containing subunits. Biochemistry; 5: 365-85.

[53] Böhm H-J, Klebe G, Kubinyi H (1996). Wirkstoffdesign. Spektrum Akademischer Verlag, Heidelberg, Berlin, Oxford.

[54] Hansch C, Fujita T (1964). ρ-σ-π Analysis; method for the correlation of biological activity and chemical structure. J Am Chem Soc; 86: 1616-1626.

[55] Free SM, Jr., Wilson JW (1964). A mathematical contribution to structure-activity studies. J Med Chem; 7: 395-399.

[56] Cramer RD, Patterson DE, Bunce JD (1988). Comparative molecular field analysis (CoMFA). 1. Effect of shape on binding of steroids to carrier proteins. J Am Chem Soc; 110: 5959-5967.

[57] Geladi P, Kowalski BR (1986). Partial least-squares regression: a tutorial. Anal Chim Acta; 185: 1-17.

[58] Wold S, Johansson E, Cocchi M (1993). PLS - Partial Least-Squares Projections to Latent Structures. In: Kubinyi H (Ed.). 3D QSAR in Drug Design, Theory, Methods and Applications. ESCOM, Leiden; Volume 1: pp. 523-550.

[59] Wold S (1995). PLS for Multivariate Linear Modeling. In: Van de Waterbeemd H (Ed.). Chemometric Methods in Molecular Design. VCH, Weinheim, New York, Basel, Cambridge, Tokyo; Volume 2: pp. 195-218.

[60] Folkers G, Merz A, Rognan D (1993). CoMFA: Scope and limitations. In: Kubinyi H (Ed.). 3D QSAR in drug design, Theory methods and applications. ESCOM, Leiden: pp. 583-618.

[61] Cramer RD, DePriest SA, Patterson DE, Hecht P (1993). The developing practice of comparative molecular field analysis. In: Kubinyi H (Ed.). 3D QSAR in drug design, Theory methods and applications. ESCOM, Leiden: pp. 443-485.

[62] Kim KH (1995). Comparative molecular field analysis (CoMFA). Mol Similarity Drug Des: 291-331.

[63] Klebe G, Abraham U, Mietzner T (1994). Molecular similarity indices in a comparative analysis (CoMSIA) of drug molecules to correlate and predict their biological activity. J Med Chem; 37: 4130-4146.

[64] Klebe G (1998). Comparative molecular similarity indices analysis: CoMSIA. In: Kubinyi H, Folkers G, Martin YC (Ed.). 3D QSAR in Drug Design: Recent Advances. KLUWER / ESCOM, Dordrecht / Boston / London; 3: pp. 87-104.

[65] Böhm M, Stürzebecher J, Klebe G (1999). Three-dimensional quantitative structure-activity relationship analyses using comparative molecular field analysis and comparative molecular similarity indices analysis to elucidate selectivity differences of inhibitors binding to trypsin, thrombin, and factor Xa. J Med Chem; 42: 458-477.

[66] Geladi P, Kowalski BR (1986). An example of 2-block predictive partial least-squares regression with simulated data. Anal Chim Acta; 185: 19-32.

[67] SYBYL molecular modeling software. Version 6.6. Tripos Inc.,1699 South Hanley Rd, Suite 303, St. Louis, MO 63144

[68] Clark M, Cramer RD, III, Van Opdenbosch N (1989). Validation of the general purpose Tripos 5.2 Force Field. J Comput Chem; 10: 982-1012.

[69] Jarkas N, McConathy J, Ely T, Kilts CD, Votaw J, Goodman MM (2001). Synthesis and Radiolabeling of New Derivatives of ADAM, Potential Candidates as SERT Imaging Agents for PET. J Labelled Cpd Radiopharm; 44 (1 Suppl): S204-S206.

[70] Caruso F, Besmer A, Rossi M (1999). The absolute configuration of sertraline (Zoloft) hydrochloride. Acta Crystallogr, Sect C: Cryst Struct Commun; C55: 1712-1714.

[71] Ibers JA (1999). Paroxetine hydrochloride hemihydrate. Acta Crystallogr, Sect C: Cryst Struct Commun; C55: 432-434.

[72] Klein CL, Lear J, O'Rourke S, Williams S, Liang L (1994). Crystal and molecular structures of tricyclic neuroleptics. J Pharm Sci; 83: 1253-1256.

[73] Madding GD, Smith DW, Sheldon RI, Lee B (1985). Synthesis and X-ray crystal structure of a 2,4,5-trisubstituted 1,2,4-triazolin-3-one. J Heterocycl Chem; 22: 1121-1126.

[74] Post ML, Kennard O, Horn AS (1975). Tricyclic antidepressants. Imipramine hydrochloride. Crystal and molecular structure of 5-(3-dimethylaminopropyl)-10,11-dihydro-5H-dibenz[b,f]azepine-hydrochloride. Acta Crystallogr, Sect B; B31: 1008-1013.

[75] Yardley JP, Husbands GE, Stack G, Butch J, Bicksler J, Moyer JA, Muth EA, Andree T, Fletcher H, 3rd, James MN (1990). 2-Phenyl-2-(1-hydroxycycloalkyl)ethylamine derivatives: Synthesis and antidepressant activity. J Med Chem; 33: 2899-2905.

[76] SYBYL molecular modeling software. Version 6.6. Theory Manual. Tripos Inc.,1699 South Hanley Rd, Suite 303, St. Louis, MO 63144

[77] Rupp AJ (1991). Pharmakophormodell für selektive 5-HT-Reuptake-Hemmer: Abgrenzung der Entactogene von stimulierenden und halluzinogenen Arylalkanaminen. Dissertation. Tübingen: Eberhard-Karls-Universität.

[78] Post ML, Horn AS (1977). The crystal and molecular structure of the tricyclic antidepressant chlorimipramine hydrochloride: 3-chloro-5-(3-dimethylaminopropyl)-10,11-dihydro-5H-dibenz[b,f]azepine-hydrochloride. Acta Crystallogr, Sect B; B33: 2590-2595.

[79] Jones G, Willett P, Glen RC (1995). A genetic algorithm for flexible molecular overlay and pharmacophore elucidation. J Comput-Aided Mol Des; 9: 532-549.

[80] Bush BL, Nachbar RB, Jr. (1993). Sample-distance Partial Least Squares: PLS optimized for many variables, with application to CoMFA. J Comput-Aided Mol Des; 7: 587-619.

[81] Wold S, Eriksson L (1995). Statistical Validation of QSAR Results: Validation Tools. In: Van de Waterbeemd H (Ed.). Chemometric Methods in Molecular Design. VCH, Weinheim, New York, Basel, Cambridge, Tokyo; Volume 2: pp. 309-318.

[82] Thibaut U, Folkers G, Klebe G, Kubinyi H, Merz A, Rognan D (1993). Appendix A. Recommendations for CoMFA studies and 3D QSAR publications. 3D QSAR Drug Des: 711-16.

[83] Lindgren F, Geladi P, Berglund A, Sjöström M, Wold S (1995). Interactive variable selection (IVS) for PLS. Part 2. Chemical applications. J Chemometrics; 9: 331-342.

[84] Lindgren F, Geladi P, Rännar S, Wold S (1994). Interactive variable selection (IVS) for PLS. Part 1. Theory and algorithms. J Chemometrics; 8: 349-362.

[85] Wong G, Koehler KF, Skolnick P, Gu ZQ, Ananthan S, Schonholzer P, Hunkeler W, Zhang W, Cook JM (1993). Synthetic and computer-assisted analysis of the structural requirements for selective, high-affinity ligand binding to diazepam-insensitive benzodiazepine receptors. J Med Chem; 36: 1820-1830.

[86] Matter H, Schwab W (1999). Affinity and selectivity of matrix metalloproteinase inhibitors: A chemometrical study from the perspective of ligands and proteins. J Med Chem; 42: 4506-4523.

[87] Humber LG, Lee D, Rakhit S, Treasurywala AM (1985). Computer-assisted investigation of structure-activity relationships in serotonin-uptake blockers. J Mol Graphics; 3: 84-89, 98-99.

[88] Lindberg UH, Thorberg SO, Bengtsson S, Renyi AL, Ross SB, Ogren SO (1978). Inhibitors of neuronal monoamine uptake. 2. Selective inhibition of 5-hydroxytryptamine uptake by alpha-amino acid esters of phenethyl alcohols. J Med Chem; 21: 448-456.

[89] Chang AS, Chang SM, Starnes DM (1993). Structure-activity relationships of serotonin transport: Relevance to nontricyclic antidepressant interactions. Eur J Pharmacol; 247: 239-248.

[90] Smith DF (1986). The stereoselectivity of serotonin uptake in brain tissue and blood platelets: The topography of the serotonin uptake area. Neurosci Biobehav Rev; 10: 37-46.

[91] El-Bermawy MA, Lotter H, Glennon RA (1992). Comparative molecular field analysis of the binding of arylpiperazines at the 5-HT_{1A} serotonin receptor. Med Chem Res; 2: 290-297.

[92] Thibaut U (1993). Applications of CoMFA and related 3D QSAR approaches. In: Kubinyi H (Ed.). 3D QSAR in drug design, Theory methods and applications. ESCOM, Leiden: pp. 661-696.

[93] Kim KH, Greco G, Novellino E (1998). A critical review of recent CoMFA applications. Perspect Drug Discovery Des; 12/13/14: 257-315.

[94] Clark M, Cramer RD, Jones DM, Patterson DE, Simeroth PE (1990). Comparative molecular field analysis (CoMFA). 2. Towards its use with 3D structural databases. Tetrahedron Comput Methodol; 3: 47-59.

[95] Clark RD, Sprous DG, Leonard JM (2001). Validating models based on large data sets. 13th European Symposium on Quantitative Structure-Activity Relationships: Rational approaches to drug design: 475-485.

[96] Sindelar K, Pomykacek J, Holubek J, Svatek E, Valchar M, Dobrovsky K, Metysova J, Polivka Z (1991). Potential antidepressants and selective inhibitors of 5-hydroxytryptamine re-uptake in the brain: synthesis of several potential metabolites of moxifetin and of two A-ring fluorinated analogs. Collect Czech Chem Commun; 56: 459-477.

[97] Jilek J, Sindelar K, Pomykacek J, Kmonicek V, Sedivy Z, Hrubantova M, Holubek J, Svatek E, Ryska M, et al. (1989). Potential antidepressants: 2-(methoxy- and hydroxyphenylthio)benzylamines as selective inhibitors of 5-hydroxytryptamine re-uptake in the brain. Collect Czech Chem Commun; 54: 3294-338.

[98] Jilek J, Urban J, Taufmann P, Holubek J, Dlabac A, Valchar M, Protiva M (1989). Potential antidepressants. 2-(Phenylthio)aralkylamines. Collect Czech Chem Commun; 54: 1995-2008.

[99] Oya S, Choi S-R, Hou C, Kung M-P, Acton PD, Shiue CY, Kung HF (2001). Synthesis and Characterization of ^{18}F-IDAM as a PET Imaging Agent for Serotonin Transporters. J Labelled Cpd Radiopharm; 44 (1 Suppl): S15-S17.

[100] Choi S-R, Oya S, Hou C, Kung HF (2001). Structure-Activity Relationship of Analogs of ADAM as Ligands for Serotonin Transporters. J Labelled Cpd Radiopharm; 44 (1 Suppl): S190-S192.

[101] Zhuang Z-P, Choi S-R, Hou C, Kung HF (1999). Synthesis of [^{123}I]ODAM as a Serotonin Transporter Imaging Agent. J Labelled Cpd Radiopharm; 42 (1 Suppl): S357-S359.

[102] Acton PD, Mu M, Plossl K, Hou C, Siciliano M, Zhuang Z-P, Oya S, Choi S-R, Kung HF (1999). Single-photon emission tomography imaging of serotonin transporters in the nonhuman primate brain with [^{123}I]ODAM. Eur J Nucl Med; 26: 1359-1362.

[103] Huang Y, Bae SA, Zhu Z, Hwang DR, Narendran R, Talbot PS, Hacket E, Kegeles LS, Laruelle M (2002). Radiosynthesis and evaluation of [^{18}F]AFM, a selective PET tracer for the serotonin transporter. J Nucl Med; 43 (5 Suppl): 358P.

[104] Oya S, Kung M-P, Hou C, Acton PD, Mu M, Kung HF (1999). Structure-Activity Relationships of IDAM and its Derivatives as Serotonin Transporter Imaging Agents. J Labelled Cpd Radiopharm; 42 (1 Suppl): S57-S59.

[105] Langmuir I (1919). Isomorphism, isosterism and covalence. J Am Chem Soc; 41: 1543-1559.

[106] Grimm HG (1925). Structure and size of the non-metallic hydrides. Z Elektrochem; 31: 474-480.

[107] Friedman HL (1951). Influence of Isosteric Replacement upon Biological Activity. National Academy of Sciences - National Research Council Publication No 206, Washington D.C.: pp. 295.

[108] Burger A (1991). Isosterism and bioisosterism in drug design. Prog Drug Res; 37: 287-371.

[109] Burger A (1963). A reappraisal of bioisosterism. Pharm Acta Helv; 38: 705-709.

[110] Hansch C (1974). Bioisosterism. Intra-Science Chem Rept; 8 (4): 17-25.

[111] Lipinski CA (1986). Bioisosterism in drug design. Annu Rep Med Chem; 21: 283-291.

[112] Thornber CW (1979). Isosterism and molecular modification in drug design. Chem Soc Rev; 8: 563-580.

[113] Lassen NA (1992). Neuroreceptor quantitation in vivo by the steady-state principle using constant infusion or bolus injection of radioactive tracers. J Cereb Blood Flow Metab; 12 (5): 709-716.

[114] Halldin C, Tarkiainen J, Sovago J, Vercouillie J, Gulyas B, Guilloteau D, Emond P, Chalon S, Hiltunen J, Farde L (2002). A PET-comparison in monkey brain of ^{11}C-MADAM labeled in two different positions - selective for the serotonin transporter. J Nucl Med; 43 (5 Suppl): 164P.

[115] Chiu W-H, Klein TH, Wolff ME (1979). Apparent bioisosteric replacement of -S- by NCN: synthesis of N-cyano-2-aza-A-nor-5-alpha-androstan-17-beta-ol acetate, an azasteroid androgen. J Med Chem; 22: 119-120.

[116] Westerberg G, Laangstroem B (1993). Synthesis of [^{11}C]- and [^{13}C]cyanogen bromide, useful electrophilic labeling precursors. Acta Chem Scand; 47: 974-978.

[117] Snyder JP, Rao SN, Koehler KF, Pellicciari R (1992). Drug modeling at cell membrane receptors: The concept of pseudoreceptors. Pharmacochem Libr; 18: 367-403.

[118] Abrunhosa AJ, Brady F, Luthra S, De Lima JJ, Jones T (2001). Preliminary studies of computer aided ligand design for PET. Physiological Imaging of the Brain with PET: 51-56.

[119] Abrunhosa AJ, Brady F, Luthra SK, Morris H, De Lima JJ, Jones T (1998). Use of Information Technology in the Search for New PET Tracers. In: Carson RE, Daube-Witherspoon ME, Herscovitch P (Ed.). Quantitative Functional Brain Imaging with Positron Emission Tomography. Academic Press, San Diego, CA: pp. 267-271.

Meine akademischen Lehrer neben Herrn Prof. Dr. K.-A. Kovar waren die Damen und Herren Professoren und Dozenten:

P. Dilg, A. Fahr, T. Gillmann, M. Haake, H. Häberlein, W. Hanefeld, K. Hartke, J. Hölzl, P. Imming, T. Kissel, S. Klumpp, F. Krafft, J. Krieglstein, K. Kuschinsky, H.-J. Machulla, R. Matusch, K. Radsak, M. Schlitzer, G. Seitz, M. Wichtl